IDENTIFYING NOVEL SUBSTRATES OF UBIQUITIN-SPECIFIC PROTEASE 7 (USP7) AND SPECKLE-TYPE POZ (POX VIRUS AND ZINC FINGER) PROTEIN (SPOP)

SUKHDEEP SINGH

A THESIS SUBMITTED TO THE FACULTY OF GRADUATE STUDIES IN

PARTIAL FULFILLMENT OF THE REQUIREMENTS FOR THE DEGREE OF

MASTER OF SCIENCE

GRADUATE PROGRAM IN BIOLOGY

YORK UNIVERSITY

TORONTO, ONTARIO

JANUARY 2022

ABSTRACT

Speckle-type POZ protein (SPOP), an E3 ubiquitin ligase adaptor protein, and ubiquitin-specific protease 7 (USP7), a deubiquitinating enzyme, have previously been implicated in prostate cancer pathogenesis. The objective of this project was to identify novel substrates of SPOP and USP7 to provide insight on the molecular mechanisms contributing to prostate cancer. Employing biochemical and cellular biology techniques, we identified, murine double minute 2 (MDM2), an E3 ubiquitin ligase, as a potential substrate of SPOP. We demonstrated that SPOP interacts with MDM2 through its MATH domain in vitro and negatively regulates its stability in vivo. Moreover, we identified sirtuin 2 (SIRT2), an NAD^+-dependent deacetylase, as a novel substrate of USP7. We demonstrated that USP7 interacts and regulates the stability of SIRT2 in vivo. Collectively, our results suggest that SPOP and USP7 through the regulation of MDM2 and SIRT2, may contribute to prostate cancer, however further studies are required to verify this.

ACKNOWLEDGMENTS

First and foremost, I would like to express my sincere gratitude to my supervisor Dr. Vivian Saridakis for accepting me as your student and giving me the opportunity to join your lab. I am forever grateful for everything I have learned in this lab and the growth I have achieved as a student under your supervision during these past two years. Thank you for your constant guidance, patience, motivation, and enthusiasm throughout the trials and tribulations, and eventual triumphs of my projects.

Thank you to my advisor, Dr. Chun Peng for your time, insight, questions, and discussions on my projects, which helped me improve my experimental design, think critically about my data, and develop a clear direction for my projects.

A special thanks to Anna Bojagora for training and teaching me everything I know in the lab, as well as David Miller for his constant advice and suggestions regarding my experiments.

Thank you to my lab mates, Krstina Banyameen, Helen Liu, Aneesah Malik, Song Huang, and Nicolas Bragagnolo for your constant support, motivation, and laughs throughout the years.

To my dear mother, father, and grandmother, whom I would like to dedicate this achievement to. Without your resilience, support, values, and teachings, I would not be where I am today.

I would also like to thank Heniretta Lacks, a 31-year-old mother of five who passed due to cervical cancer in 1951. Lacks unknowingly and without consent donated her cells to Johns Hopkins Hospital during treatment for cervical cancer, which has led to many key discoveries and breakthroughs in the field of medicinal science. Thank you as well to the other anonymous individuals who donated their cells for research purposes. Without your generosity, myself and other scientists all over the world would not be able to conduct their research.

Last but not least, I would like to thank the Natural Sciences and Engineering Research Council of Canada for funding and supporting this research.

TABLE OF CONTENTS

LIST OF TABLES

LIST OF FIGURES

LIST OF ABBREVIATIONS

293T	Human Embryonic Kidney Cell Line Stably Expressing the SV40 Large T Antigen
A Ala	Alanine
AR	Androgen Receptor
ATF2	Activating Transcription Factor 2
BACK	BTB and C-terminal Kelch
BMI1	B Cell-Specific Moloney Murine Leukemia Virus Integration Site 1
BRD	Bromodomain
BTB	Bric-à-Brac, Tramtrack and Broad Complex
BubR1	Budding Uninhibited by Benzimidazole-Related 1
C Cys	Cysteine
CAT	Central Catalytic Core Domain
CCNE1	Cyclin E1
Cdc20	Cell Division Cycle Protein 20 Homolog
CDK	Cyclin Dependent Kinase
CHFR	Checkpoint with Forkhead and RING Finger Domain
CO-IP	Co-Immunoprecipitation
CTD	Carboxy-Terminal Domain
Cul	Cullin
Cul3	Cullin 3
D Asp	Aspartic Acid
DAXX	Death Domain-Associated Protein
DDIT3	DNA Damage Inducible Transcript 3
DDX24	DEAD-Box Helicase 24
DNMT1	DNA Methyltransferase 1
DUB	Deubiquitinating Enzyme
E Glu	Glutamic Acid
E1	Ubiquitin Activating Enzyme
E2	Ubiquitin Conjugating Enzyme
E3	Ubiquitin Protein Ligase
EBNA1	Epstein-Barr Nuclear Antigen 1
ER	Estrogen Receptor
ERG	ETS Transcription Factor ERG
EV	Empty Vector
EZH2	Enhancer of Zeste Homolog 2
F Phe	Phenylalanine
FBS	Fetal Bovine Serum
FOXO4	Forkhead Box O4
G Gly	Glycine
GAPDH	Glyceraldehyde-3-Phosphate Dehydrogenase
GST	Glutathione S- Transferase
H His	Histidine
HAUSP	Herpesvirus-Associated Ubiquitin-Specific Protease
HCT116	Human Colorectal Carcinoma Cell Line
HCT116 USP7 $^{-/-}$	USP7 Knockout Human Colorectal Carcinoma Cell Line
HDM2	Human Double Minute 2
HECT	Homologous to the E6-AP Carboxyl Terminus
HeLa	Immortal Human Henrietta Lacks (Cervical Adenocarcinoma) Cell Line
HRD1	HMG-CoA Reductase Degradation Protein 1
HSV-1	Herpes Simplex Virus Type 1
I Ile	Isoleucine

ICP0	Infected Cell Polypeptide 0
INF2	Inverted Formin 2
IPTG	Isopropyl B-D-1 Thiogalactopyranoside
JAMM	JAB1/MPN/Mov34 Metalloenzyme
K Lys	Lysine
KSHV	Kaposi's Sarcoma Associated Herpesvirus
LB	Luria Broth
LSD1	Lysine-Specific Demethylase 1
MATH	Meprin and TRAF Homology
MCM-BP	Mini-Chromosome Maintenance Complex-Binding Protein
MDM2	Murine Double Minute 2
MDM4	Murine Double Minute 4
MDMX	Murine Double Minute X
MJD	Machado Joseph Diseases
MRD	Mismatch Repair Detection
MT	Mutant
NAD	Nicotinamide Adenine Dinucleotide
NAM	Nicotinamide
Nrf1	Nuclear Factor E2-Related Factor 1
NTD	N-Terminal Domain
OTU	Ovarian Tumor
P/S	Penicillin-Streptomycin
p53	Tumor Suppressor Protein 53
PAGE	Polyacrylamide Gel
PDX1	Pancreatic Duodenal Homeobox-1
PHF8	PHD Finger Protein 8
POZ	Pox Virus and Zinc Finger
PR	Progesterone Receptor
PRC1	Polycomb Repressive Complex 1
PTEN	Phosphatase and Tensin Homolog
RBR	RING-Between-RING
RING	Really Interesting New Gene
RNF169	Ring Finger Protein 169
SBC	SPOP Binding Consensus
SDS	Sodium Dodecyl Sulfate
Sir2	Silent Information Regulator 2
siRNA	Small interfering RNA
SIRT1	Sirtuin 1
SIRT2	Sirtuin 2
SIRT3	Sirtuin 3
SIRT4	Sirtuin 4
SIRT5	Sirtuin 5
SIRT6	Sirtuin 6
SIRT7	Sirtuin 7
SPOP	Speckle Type POZ Protein
TB	Terrific Broth
TRAF	Tumor Necrosis Factor Receptor
TRIM24	Tripartite Motif Containing 24
U2OS	Human Osteosarcoma Cell Line
Ub	Ubiquitin
UbE2E1	Ubiquitin-Conjugating Enzyme E2 E1)
Ubl	Ubiquitin-Like
UCHs	Ubiquitin Carboxyl-Terminal Hydrolases

UHRF1	Ubiquitin-Like with PHD and RING Finger Domains 1
UPS	Ubiquitin Proteasome System
UPS	Ubiquitin-Specific Protease
USP7	Ubiquitin-Specific Protease 7
V Val	Valine
vIRF1	Viral Interferon Regulatory Factor 1 Protein
W Trp	Tryptophan
WCLs	Whole Cell Lysates
WT	Wildtype
ZBTB3	Zinc Finger And BTB Domain Containing 3
ZUP	Zinc Finger UB-Specific Proteases

COVID-19 RESEARCH IMPACT STATEMENT

The World Health Organization declared the COVID-19 outbreak a pandemic on March 11, 2020. Shortly following, the Government of Ontario declared a state of emergency in response to COVID-19 on March 17, 2020. In compliance with the new public health and safety guidelines to prevent the risk and spread of COVID-19, York University switched to remote learning, as well as shutdown access to all buildings and research facilities on campus which remained in effect until the beginning of July 2020. As a result of the closure of research facilities from March 2020 to June 2020, I was unable to conduct experiments for my M.Sc. research project which requires mammalian and bacterial cell culturing, and specialized laboratory equipment. Upon returning to campus for research proposes, additional workplace safety measures and restrictions were established and enforced such as but not limited to: reduced lab capacity (2 students per lab bench), rotational shifts of members in the same lab, and restricted access to shared spaces and research equipment (cell culture room). As a result of the highly restricted access following reopening of campus to implement social distancing measures, and the ongoing COVID-19 pandemic, I experienced significant delays in research activities and progress during the two-year period of my graduate studies.

CHAPTER 1: INTRODUCTION

1.1 Overview of the Ubiquitin-Proteasome Pathway

Protein homeostasis— the controlled balance of protein synthesis, folding, assembly, modifications, conformational states, localization, and degradation— is essential for normal cellular function, development, and ultimately, organism viability (Kevei & Hoppe, 2014). Maintaining the structural, quantitative, and functional integrity of the proteome is a constant challenge and requires effective cellular systems to monitor protein homeostasis (Cheng et al., 2018). The ubiquitin-proteasome degradation pathway is one example of a highly conserved cellular system employed to regulate protein turnover — through the ubiquitination of proteins, and subsequent, recognition and degradation by the 26S proteasome **(Figure 1-1)** (Hochstrasser, 1996). The ubiquitin-proteasome degradation pathway functions in protein quality control by removing defective, aggregated, and misfolded proteins that arise within the cell as a result of errors in protein synthesis, upon exposure to environmental and metabolic stressors, as well as over the lifespan of an organism due to aging (Kevei & Hoppe, 2014). The ubiquitin-proteasome degradation pathway also regulates the temporal and spatial cellular persistence of regulatory proteins critical for controlling cellular activities such as gene transcription, signal transduction, and cell cycle progression (Zheng et al., 2009; Micel et al., 2013). Dysregulation of any component of the ubiquitin-proteasome degradation pathway regulating the clearance of damaged, unnecessary, and/or regulatory proteins result in proteome imbalances, and has been implicated in many diseases including cancer pathogenesis (An et al., 2014).

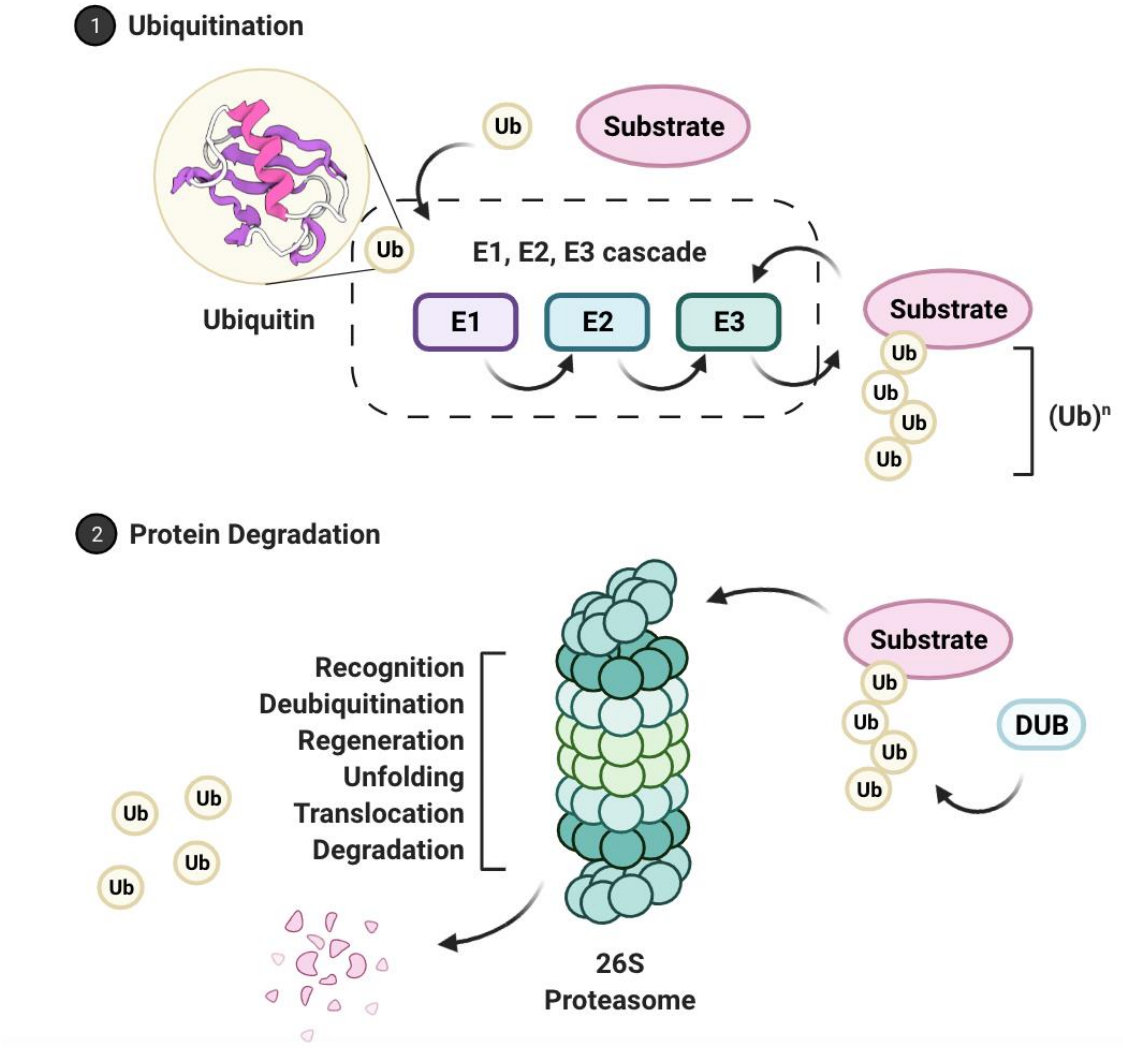

Figure 1-1. Overview of the ubiquitin-proteasome degradation pathway. The ubiquitin-proteasome degradation pathway involves two distinct and consecutive steps: **(1)** the covalent attachment of ubiquitin molecules to proteins catalyzed by three distinct enzymes, a ubiquitin activating enzyme (E1), a ubiquitin conjugating enzyme (E2), and a ubiquitin protein ligase (E3) **(2)** recognition and degradation of the proteins by the 26S proteasome along with the regeneration and release of free ubiquitin mediated by deubiquitinating enzymes (DUBs). Modified from (Leestemaker & Ovaa, 2017) with BioRender.com.

1.2 Ubiquitination

Ubiquitin often referred to as the "molecular kiss of death" is a 76 amino acid residue protein highly conserved in eukaryotes, that is unsurprisingly ubiquitous in regard to its abundance as well as its regulatory control within the cell (Pickart, 2001). The covalent attachment of a ubiquitin tag to a protein substrate is a process termed ubiquitination and involves the formation of an isopeptide bond between the C-terminal glycine 76 residue of ubiquitin to the ε-amino group of a lysine residue of the protein substrate (Pickart, 2001). Although best known for its proteolytic function, that is targeting proteins for degradation by the 26S proteasome, lysosome, or autophagosome, ubiquitination regulates various non-proteolytic cellular processes as well, such as but not limited to: regulating protein interactions, activity, and subcellular localization (Clague & Urbé, 2010; Komander & Rape, 2012). The regulatory impact of ubiquitin and consequently, the fate of the substrate varies depending on the form of ubiquitination. Monoubiquitination refers to the attachment of a single ubiquitin molecule to a single lysine residue of the substrate and multi-monoubiquitination refers to the attachment of several individual ubiquitin molecules to multiple lysine residues of the substrate (Hochstrasser, 1996). Generally, these forms of ubiquitination regulate localization, interaction, activity, DNA repair, and endocytosis (Hochstrasser, 1996; Sun & Chen, 2004). Polyubiquitination refers to the formation of a branched or linear polyubiquitin chain on a single lysine residue of the substrate by the sequential addition of ubiquitin molecules (Komander & Rape, 2012). The formation of a polyubiquitin chain results from the isopeptide linkage of the C-terminal glycine 76 residue of ubiquitin to one of the seven lysine residues: K6, K11, K27, K29, K33, K48 and K63, or the N-terminal methionine in the preceding ubiquitin molecule (Pickart, 2001). The presence of a polyubiquitin chain composed of at least five ubiquitin molecules with K48 linkages, tags the substrate for recognition and subsequent degradation by the 26S proteasome (Sun & Chen, 2004).

Addition of ubiquitin to a substrate involves a three-step mechanism catalyzed by three distinct enzymes: E1, a ubiquitin activating enzyme, E2, a ubiquitin conjugating enzyme, and E3, a ubiquitin protein ligase **(Figure 1-2)** (Pickart, 2001). First, in an ATP-dependent reaction, ubiquitin is activated at its C-terminal glycine 76 residue by forming a thioester bond to the cysteine residue in the active site of E1 (Pickart, 2001). Ubiquitin is then transferred from E1 and attached to E2, similarly at a cysteine residue within its active site, forming a thioester bond (Pickart, 2001). E3 then catalyzes the transfers the ubiquitin either directly or indirectly from E2

to the substrate at its lysine residue or to another ubiquitin molecule previously linked to the substrate (Berndsen & Wolberger, 2014).

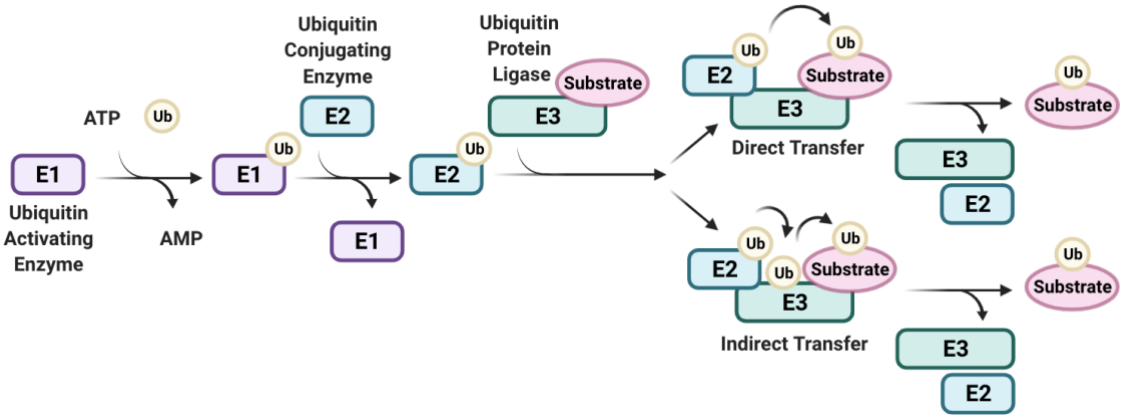

Figure 1-2. Overview of the process of ubiquitination. The covalent attachment of ubiquitin molecules to protein is catalyzed by three distinct enzymes: E1, a ubiquitin activating enzyme, E2, a ubiquitin conjugating enzyme, and E3, a ubiquitin protein ligase. Ubiquitin is first activated in an ATP dependent reaction and attached to E1. Ubiquitin is then transferred from E1 to E2 to E3. E3 then catalyzes the direct or indirect transfer of ubiquitin to the substrate. Modified from (Witting et al., 2017) with BioRender.com.

The human genome encodes for two E1 ubiquitin activating enzymes (UBA1 and UBA6), 38 E2 ubiquitin conjugating enzymes, and approximately 600–1000 E3 ubiquitin protein ligases (Ye & Rape, 2009). Currently, E3 ubiquitin protein ligases can be classified into three main classes based upon the presence of specific domains and the mechanism of ubiquitin transfer: the Really Interesting New Gene (RING) class, the Homologous to the E6-AP Carboxyl Terminus (HECT) class, and the RING-between-RING (RBR) class (Buetow et al., 2016). The HECT and RBR class of E3 ubiquitin protein ligases mediate the indirect transfer of ubiquitin to the substrate through the formation of an E3-ubiquitin thioester intermediate (Berndsen & Wolberger, 2014). The RING class are the most abundant type of E3 ubiquitin protein ligases that do not form a catalytic intermediate with ubiquitin but facilitate direct ubiquitin transfer by bringing the E2 ubiquitin conjugating enzyme and the substrate in close proximity (Buetow et al., 2016; Berndsen & Wolberger, 2014).

The Cullin-RING E3 ubiquitin protein ligases are the largest subset of the RING class of E3 ubiquitin protein ligases **(Figure 1-3)** (Nguyen et al., 2017). The Cullin-RING E3 ubiquitin protein ligases are a multi-subunit protein complex consisting of the central molecular scaffold cullin protein that serves as a docking site for other proteins to bind (Nguyen et al., 2017). At the N-termini of cullin, there is a substrate-specific adaptor protein responsible for recruiting and

binding substrates intended to be tagged with ubiquitin (Nguyen et al., 2017). At the C-termini of cullin, there is a catalytic RING-box (Rbx) protein responsible for recruiting E2 ubiquitin conjugating enzymes with bound ubiquitin (Nguyen et al., 2017). The human genome encodes for seven cullin proteins, (Cul1, Cul2, Cul3, Cul4a, Cul4b, Cul5 or Cul7), two RING-box proteins (Rbx1 and Rbx2), and a diverse array of substrate adaptors (Nguyen et al., 2017).

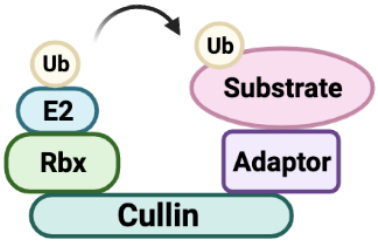

Figure 1-3. Schematic of the Cullin-RING E3 ubiquitin protein ligase. The Cullin-RING E3 ubiquitin protein ligases are a largest subset of the RING class of E3 ubiquitin protein ligases. The Cullin-RING E3 ubiquitin protein ligases are a multi-subunit protein complex consisting of a central cullin protein, an adaptor protein, and a RING-box protein, which collectively function to directly transfer ubiquitin to the bound substrate. Modified from (Nguyen et al., 2017) with BioRender.com.

1.3 Deubiquitination

It is important to note that the process of ubiquitination is reversible (Micel et al., 2013). The process of cleaving ubiquitin from substrates by deubiquitinating enzymes (DUBs) is called deubiquitination (Micel et al., 2013). Deubiquitination involves the hydrolysis of the isopeptide bond between ubiquitin molecules or the isopeptide bond between ubiquitin and the substrate (Nininahazwe et al., 2021). DUBs are critical components of the ubiquitin-proteasome degradation pathway that regulate the removal of ubiquitin from substrates after initiation of degradation by the 26S proteasome, promoting the regeneration and release of free ubiquitin (Ristic et al., 2014). In contrast, DUBs can also function to remove ubiquitin prior to initiation and commitment to degradation by the 26S proteasome (Micel et al., 2013). This reversion of the proteolytic ubiquitin signal rescues substrates from degradation promoting their stability within the cell (Micel et al., 2013). Additional functions of the DUBs besides ubiquitin recycling and reversion of the ubiquitin signal, proteolytic or non-proteolytic, include processing of ubiquitin precursors to produce active, monomeric, and free ubiquitin molecules, as well as, proofreading and editing ubiquitin chains promoting an alternative ubiquitin signal **(Figure 1-4)** (Micel et al., 2013; Ristic et al., 2014; Pozhidaeva & Bezsonova, 2019).

The human genome encodes more than 100 DUBs which can be divided into seven families based upon sequence and structural similarity (Valles et al., 2020; Nininahazwe et al., 2021). The ubiquitin specific proteases (USPs) are the largest family of DUBs comprised of 56 members and are classified as cysteine proteases defined by their highly conserved catalytic triad comprised of a cysteine residue, a histidine residue, and an aspartic acid residue within their active site (Nininahazwe et al., 2021). Additional DUBs classified as cysteine proteases include the ubiquitin carboxyl-terminal hydrolases (UCHs), Machado Joseph Diseases (MJD) proteases, ovarian tumor (OTU) proteases, zinc finger UB-specific proteases (ZUP), and monocyte chemotactic protein-induced proteins (MCPIP) (Nininahazwe et al., 2021). Metalloproteases are another class of DUBs defined by their dependence on zinc and consists of the JAB1/MPN/Mov34 metalloenzyme (JAMM) (Nininahazwe et al., 2021).

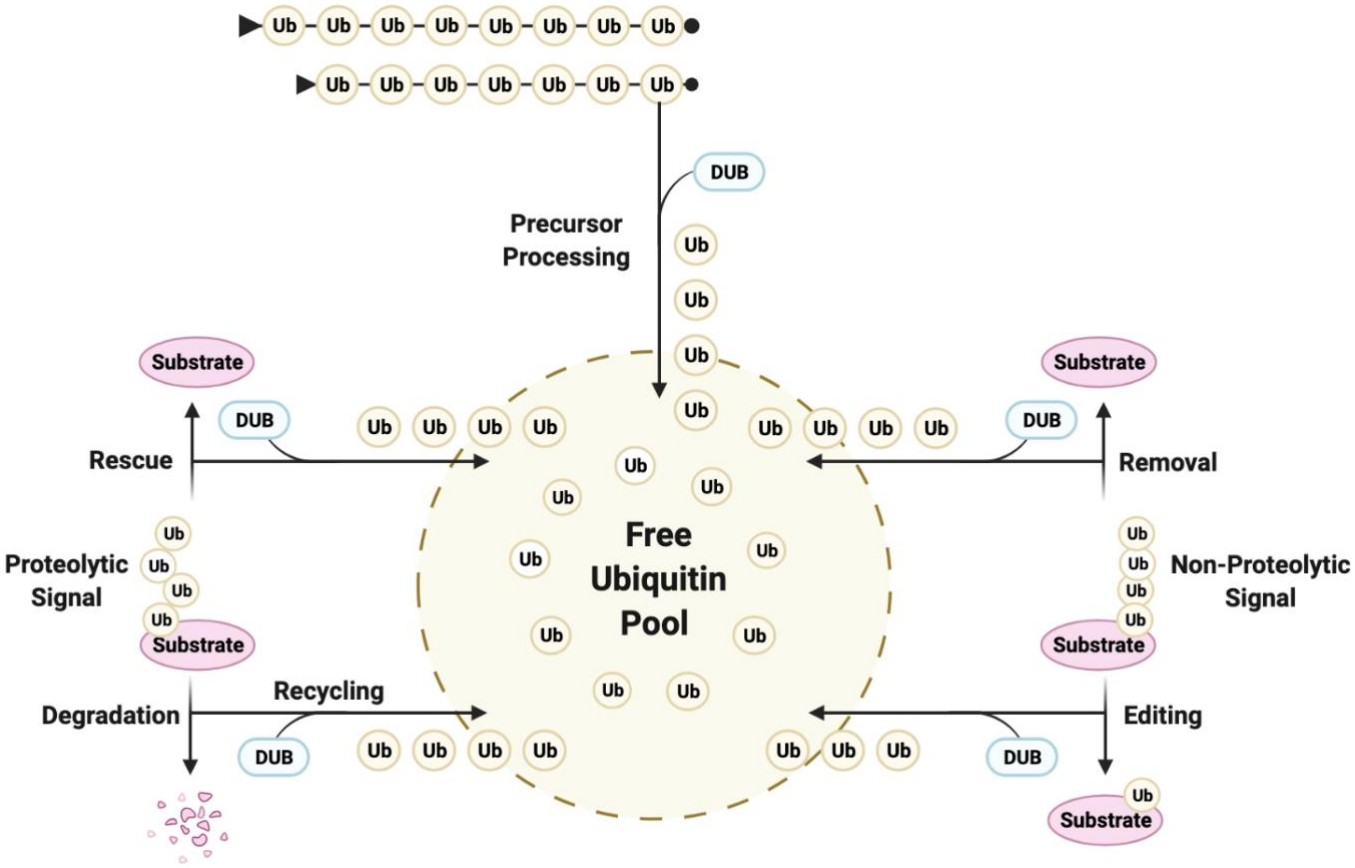

Figure 1-4. Overview of diverse functions of DUBs. DUBs function to process ubiquitin precursors, reverse both proteolytic and non-proteolytic signals, and proofread and edit ubiquitin chains. Modified from (Komander et al., 2009) with BioRender.com.

1.4 Degradation via the 26S Proteasome

The addition of a polyubiquitin chain with K48 linkages tags substates for recognition and degradation by the 26S proteasome (Sun & Chen, 2004). The 26S proteasome is a 2.5 MDa multi-subunit complex located in the nucleus and cytosol (Schrader et al., 2009). The 26S proteasome is composed of a catalytic hollow barrel-shaped 20S core component and two 19S regulatory particles, which associate with the ends of the 20S core (Schrader et al., 2009). The 19S regulatory particles consist of two substructures, a lid and a base comprised of multiple subunits that contain ubiquitin binding sites, ATPase active sites, and deubiquitinating activity (Mani & Gelmann, 2005; Schrader et al., 2009). The 19S lid is involved in substrate recognition and preparation, whereas the 19S base is involved in ATP-dependent unfolding and gate opening, as well as translocation of the substrate to the 20S core component (Murata et al., 2009; Mani & Gelmann, 2005). The 20S core component is composed of four stacked heptameric rings (Lecker et al., 2006). The two outer α- rings of the stack consist of seven α subunits each, which function to form a narrow gate regulating access of substrates into the proteolytic interior cavity (Lecker et al., 2006; Murata et al., 2009). The two inner β rings of the stack which form the proteolytic interior cavity similarly consist of seven β subunits, however only three of the subunits of each β ring contain proteolytic active sites positioned towards the interior of the cavity (Lecker et al., 2006).

Recognition of proteins with K48-linked polyubiquitin chains is mediated by subunits of the 19S lid containing ubiquitin-binding domains (Schrader et al., 2009). Upon binding and commitment to degradation, deubiquitinating enzymes, either those that are subunits or reversibly associate with the 19S cap, cleave the ubiquitin tag (Schrader et al., 2009). Some deubiquitinating enzymes act by cleaving the entire polyubiquitin chain off of proteins, whereas others act by sequentially trimming the polyubiquitin chain from the distal end (Schrader et al., 2009). Deubiquitination is essential as the polyubiquitin chain has been suggested to hinder unfolding and translocation of the polypeptide into the proteolytic core and allows free ubiquitin to be regenerated and recycled (Schrader et al., 2009). After recognition and deubiquitination, proteins are unfolded by the action of the 19S subunits containing ATPase activity (Lecker et al., 2006). Unfolding and linearization of proteins is required for translocation through the narrow-gated channel of the 20S outer ring into proteolytic interior core cavity (Lecker et al., 2006). After entry into the 20S core, the polypeptide is cleaved by the six proteolytic active sites resulting in the formation of small peptides, which are released from the 26S proteasome and subsequently

degraded into amino acids by cytosolic endopeptidases and exopeptidases to synthesize new proteins or to yield energy (Lecker et al., 2006).

1.5 Speckle-Type POZ Protein (SPOP)

1.5.1 SPOP Function and Regulatory Impact

Speckle-type POZ protein (SPOP) discovered in 1997 and named after its discrete speckled pattern in the nuclei and homology to the POZ domain, is a substrate adaptor protein associated with the Cullin 3-RING E3 ubiquitin ligase complex (Nagai et al., 1997; van Geersdaele et al., 2013). The primary function of SPOP within the Cullin 3-RING E3 ubiquitin ligase complex is to recruit and bind substrates destined to be tagged with ubiquitin and promote their degradation by the 26S proteasome **(Figure 1-5)** (Mani, 2014).

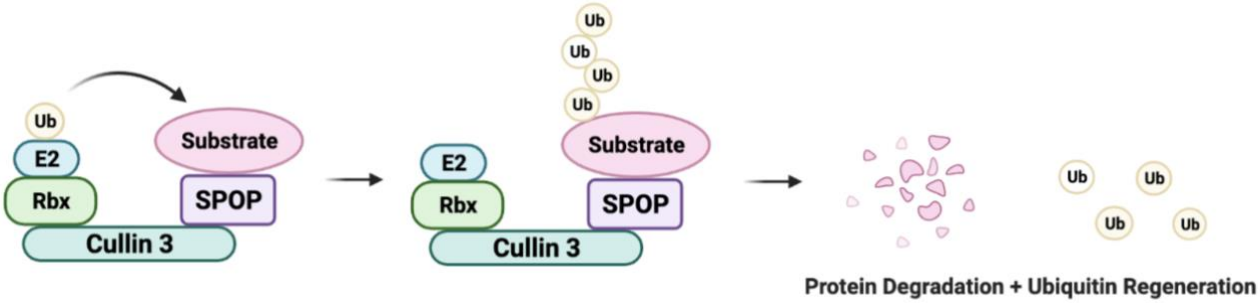

Figure 1-5. SPOP is associated with the Cullin 3-RING E3 ubiquitin ligase complex. SPOP is substrate adaptor protein associated with the Cullin 3-RING E3 ubiquitin ligase complex, that mediates the ubiquitination and degradation of its target substrates via the 26S proteasome. Schematic created with BioRender.com.

Within this complex, SPOP regulates the cellular persistence of several substrates such as the death domain-associated protein (DAXX) involved in apoptosis, the pancreatic duodenal homeobox-1 (PDX1) involved in the development of the pancreas, and the androgen receptor (AR) involved in hormone-dependent signaling **(Table 1-1)** (Mani, 2014; Kwon et al., 2006; Liu et al., 2004; An et al., 2014). Additional cellular processes and functions regulated by SPOP by targeting its substrates for ubiquitination and proteasomal degradation include cellular senescence, transcription, cell cycle progression, DNA damage response, and epigenetic regulation (Mani, 2014). It is important to note in some cases, SPOP delegates non-proteolytic regulatory functions on select substrates by promoting the attachment of other forms of ubiquitination (Mani, 2014). For instance, ubiquitination of the histone variant, MacroH2A1.2 by the SPOP-Cullin 3-RING E3 ubiquitin ligase complex results in its deposition onto the X chromosome leading to stable inactivation (Takahashi et al., 2002; Hernandez-Munoz et al., 2005). Similarly, B cell-specific Moloney murine leukemia virus integration site 1 (BMI1), a component of the Polycomb Repressive Complex 1 (PRC1) is an additional substrate of SPOP, where ubiquitination of BMI1

serves a regulatory function related to recruitment to the X chromosome and remodelling rather than degradation by the 26S proteasome (Hernandez-Munoz et al., 2005).

Table 1-1. List of SPOP substrates. [a] SB = SPOP Binding. [b] SB motif of PDX1 has two mismatch deviations. Retrieved from (Cuneo & Mittag, 2019).

Substrate	SB motifs[a]	Substrate function
Androgen receptor	5	Nuclear receptor related
estrogen receptor	2	Nuclear receptor related
Progesterone receptor	5	Nuclear receptor related
TRIM24: tripartite motif-containing 24	4	Nuclear receptor related
SRC3	12	Nuclear receptor related
BRD2/3/4: bromo domain-containing proteins	2/7/8	Epigenetic/chromatin remodelling
BMI1: B lymphoma Mo-MLV insertion region 1 homolog	3	Epigenetic/chromatin remodelling
Histone variant MacroH2A	2	Epigenetic/chromatin remodelling
SETD2: histone-lysine *N*-methyltransferase	25	Epigenetic/chromatin remodelling
GLYR1: glyoxylate reductase 1 homolog	1	Epigenetic/chromatin remodelling
SCAF1: SR-related CTD-associated factor 1	13	Nucleic acid transactions
WIZ: widely interspaced zinc finger motifs	2	Nucleic acid transactions
DEK: DEK proto oncogene	1	Nucleic acid transactions
BRMS1: breast cancer metastasis-suppressor	1	Transcription
PDX1: pancreatic and duodenal homeobox	1[b]	Transcription
NANOG: homeobox transcription factor	6	Transcription
CAPRIN1: cell cycle-associated protein 1	6	Cell cycle
CDC20: cell division cycle protein 20 homolog	2	Cell cycle
Cyclin E1	2	Cell cycle
cMYC: Myc proto-oncogene protein	6	Cell cycle
DAXX	7	Cell cycle
ERG: ETS transcription factor	3	Cell cycle (transcription)
Gli2/Gli3: glioma-associated oncogene family zinc finger	8/9	Transcription
DUSP6/7: dual-specificity phosphatase	2/2	Phosphatase/cell signalling
PTEN	2	Phosphatase/tumour suppressor
INF2: inverted formin, FH2 and WH2 domain containing	5	Cytoskeleton

1.5.2 SPOP Structure

SPOP is a 374 amino acid residue protein with a molecular mass of 42 kDa located primarily in the nucleus (Zhuang et al., 2009). It is comprised of four distinct domains: an N-terminal meprin and TRAF-C homology (MATH) domain consisting of amino acid residues 28-166, an internal bric-à-brac, tramtrack and broad complex (BTB) domain also known as POZ domain, consisting of amino acid residues 177–296, a C-terminal Kelch (BACK) domain consisting of amino acid residues 296-359, and a C-terminal nuclear localization domain consisting of amino acid residues 359–374 **(Figure 1-6A)** (Zhuang et al., 2009; Errington et al., 2012; van Geersdaele et al., 2013; Cuneo & Mittag, 2019).

The MATH domain of SPOP mediates substrate recognition and binding and has been identified as the site containing majority of cancer associated SPOP mutations **(Figure 1-6B)** (Zhuang et al., 2009; Barbieri et al., 2012). The MATH domain consists of a sandwich of two antiparallel β-sheets that form a central shallow groove that is the recognition and binding site of substrates possessing SPOP binding consensus (SBC) motifs (Zhuang et al., 2009). The SBC motif is a five-residue linear motif with the consensus sequence: ϕ-π-S/T-S/T-S/T, where ϕ = nonpolar, π = polar, , S = serine, T = threonine) (Zhuang et al., 2009). The interaction between the MATH domain of SPOP, more specifically, the amino acid residues Tyr^{87}, Phe^{102}, Tyr^{123}, Trp^{131}, and Phe^{133} and the SBC motifs of substrates consist of hydrophobic and polar interactions (Zhuang et al., 2009). Albeit the SBC motif is a fundamental component for substrate recognition and binding to the MATH domain of SPOP, the interface between SPOP and its substrates have previously shown to extend beyond the core SBC motif (Ostertag et al. 2019).

The BTB domain of SPOP mediates Cullin 3 interaction and is involved in SPOP dimerization **(Figure 1-6C)** (Zhuang et al., 2009). The BTB domain contains an α3-β4 loop that possesses a core ϕ-x-E motif (ϕ = hydrophobic residue, often methionine or leucine, x = non-conserved residue, and E = glutamic acid) (Errington et al., 2012). The ϕ-x-E motif corresponds to the residues Met^{233}, Glu^{234}, and Glu^{235}, where residue Met^{233} has been identified to be a critical residue mediating Cullin 3 and SPOP interactions (Errington et al., 2012). In addition to facilitating Cullin 3 interaction, the BTB domain, more specifically, the hydrophobic interface involving residues Leu^{186}, Leu^{190}, L^{193}, and Ile^{217}, enables dimerization of SPOP (Zhuang et al., 2009). The resulting SPOP dimer engages two Cullin 3 molecules forming a 2:2 complex that possesses two substrate-binding sites from SPOP and two catalytic cores from the Cullin 3-RING-box 1 complex

(Zhuang et al., 2009; Mani, 2014). Mutations of the hydrophobic contacts that promote dimerization of SPOP do not alter Cullin 3 interactions but significantly reduce ubiquitination activity (Zhuang et al., 2009).

The BACK domain of SPOP extends the Cullin 3 binding surface enhancing interaction between Cullin 3 and SPOP **(Figure 1-6D)** (Zhuang et al., 2009; Errington et al., 2012). The BACK domain is contiguous with the BTB domain and contains a paired α-helix motif termed the 3-box (Zhuang et al., 2009; Errington et al., 2012). The 3-box is analogous to the F-box and SOCS box present in other adaptor proteins bound to cullin such as Skp1-Cullin 1 and EloC-Cullin 5, respectively, that functions to extend the interaction surface (Zhuang et al., 2009). The BACK domain also promotes dynamic high-order oligomerization of SPOP (Errington et al., 2012). The BACK domain of SPOP resembles the N-terminal portion of the BACK domain of Kelch-type adaptors also associated with Cullin 3 (van Geersdaele et al., 2013). The BACK domain of Kelch-type adaptors consists of 3–4 repeats of a paired α-helix motif followed by the Kelch repeat substrate binding domain (Errington et al., 2012). In SPOP, the 3-box corresponds to the first paired α-helix repeat within the BACK domain of Kelch-type Cullin 3 adaptors, however, as previously mentioned in SPOP, the substrate binding MATH domain is N-terminal to the BTB domain (Errington et al., 2012). Albeit, the BACK domain of Kelch-type adaptors has not been shown to promote high order oligomerization, the atypical truncated BACK domain of SPOP directs the formation of high order oligomerization (van Geersdaele et al., 2013; Errington et al., 2012).

Collectively, SPOP possesses two types of oligomerization domains: the BTB domain and BACK domain, that function together to form multimeric (>25mers), high molecular mass (>500 kDa) SPOP oligomers that dynamically associate and dissociate in a concentration dependent manner **(Figure 1-6E and Figure 1-6F)** (Errington et al., 2012; van Geersdaele et al., 2013; Marzahn et al., 2016). Moreover, each BTB domain in a SPOP oligomer can recruit a Cullin 3-RING-box 1 complex, generating a SPOP-Cullin 3-RING-box 1 oligomer that augments the rate and processivity of substrate ubiquitination compared to SPOP-Cullin 3-RING-box 1 dimers **(Figure 1-6G)** (Errington et al., 2012). Oligomerization results in increased ubiquitination efficiency of the SPOP-Cullin 3-RING E3 ubiquitin ligase complex through the presentation of multiple binding sites and catalytic centers for substrates, as well as preassembly of optimal conformation of components within the complex (Errington et al., 2012).

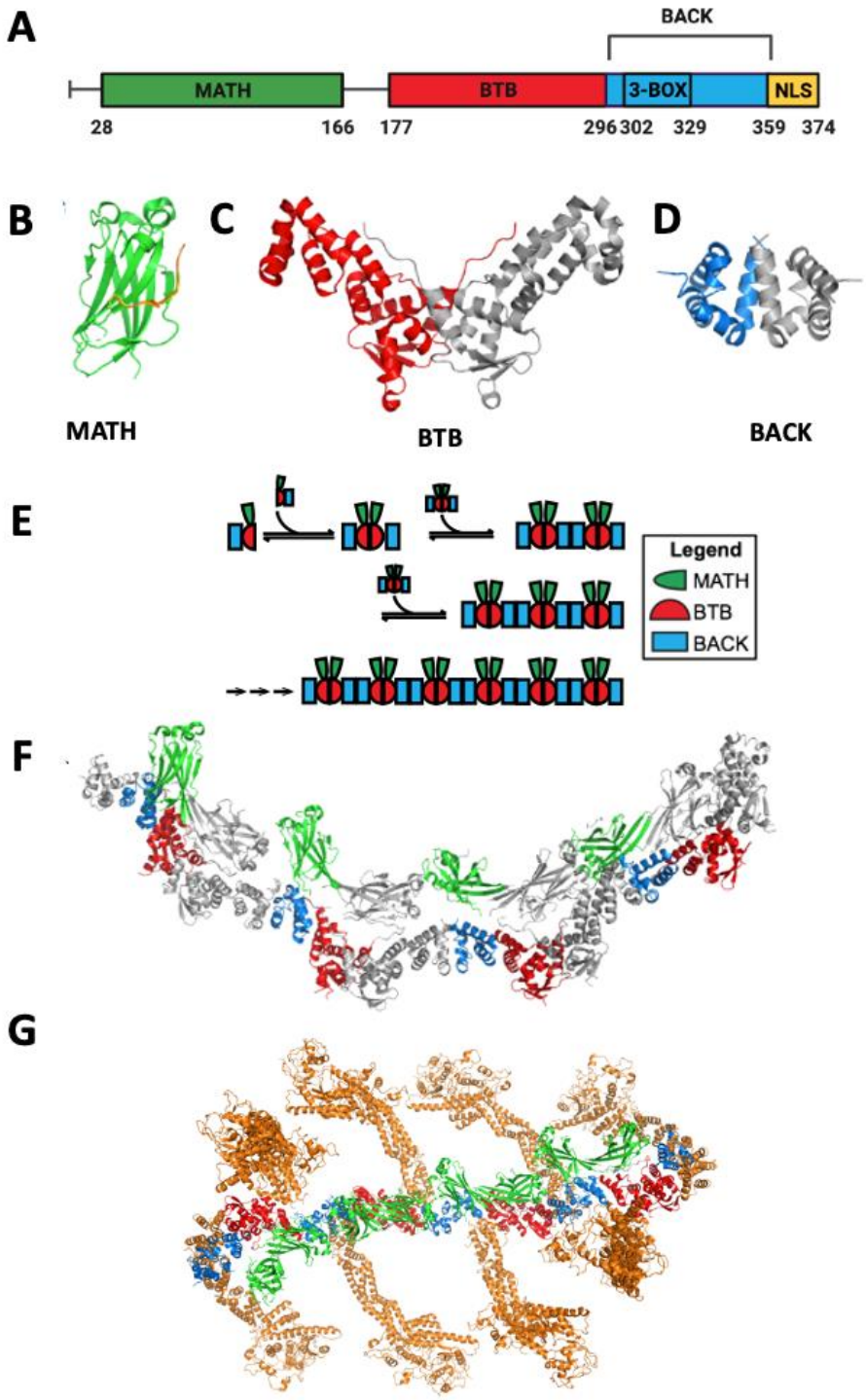

Figure 1-6. SPOP domain, structure, and organization. (a) Schematic of the domains of SPOP. **(b)** Green ribbon representation of the crystal structure of the SPOP MATH domain with a substrate peptide shown in yellow. **(c)** Ribbon representation of the crystal structure of the SPOP BTB domain dimer, with one monomer shown in red and the other grey. **(d)** Ribbon representation of the crystal structure of the SPOP BACK domain dimer, with one monomer shown in blue and the other in grey. **(e)** A schematic diagram depicting the high-order oligomerization of SPOP. **(f)** Model of the SPOP oligomer. **(g)** Model of the SPOP and Cullin 3 oligomer, where the cullin component is shown in orange. Modified from (Marzahn et al., 2016; Cuneo & Mittag, 2019; Zhuang et al., 2009; Errington et al., 2012; van Geersdaele et al., 2013).

1.5.3 SPOP and its Role in Cancer

In recent years, the role of SPOP in cancer development and progression, has gained significant attention and investigation (Clark & Burleson, 2020). The majority of studies examining the role of SPOP in cancer development has been in the context of prostate cancer (Clark & Burleson, 2020). SPOP was first identified as a statistically significant mutated gene in a study detecting somatic mutations in 58 human primary prostate tumour samples using mismatch repair detection (MRD) technology (Kan et al., 2010). Genome-wide sequencing studies have further revealed that SPOP is the most frequently mutated gene in 10% of primary prostate cancers (Barbieri et al., 2012). Mutations in SPOP associated with prostate cancer have been identified within the substrate binding MATH domain as recurrent missense mutations in specific amino acid residues; the residue phenylalanine 133 being the most frequently mutated **(Figure 1-7)** (Cuneo & Mittag, 2019; Mani, 2014). Mutations in the MATH domain of SPOP disrupt substrate recognition and binding, and consequently, allows substrates to escape ubiquitination and their fate of degradation (Batra & Lai, 2014). As mentioned previously, maintaining protein homeostasis is essential for normal cellular function, development, and viability (Kevei & Hoppe, 2014). Dysregulation of the ubiquitin-proteasome degradation pathway as a result of loss of function mutations of SPOP, leads to increased cellular persistence of its substrates implicated in essential cellular processes, and ultimately promotes the progression of prostate cancer (Cuneo & Mittag, 2019).

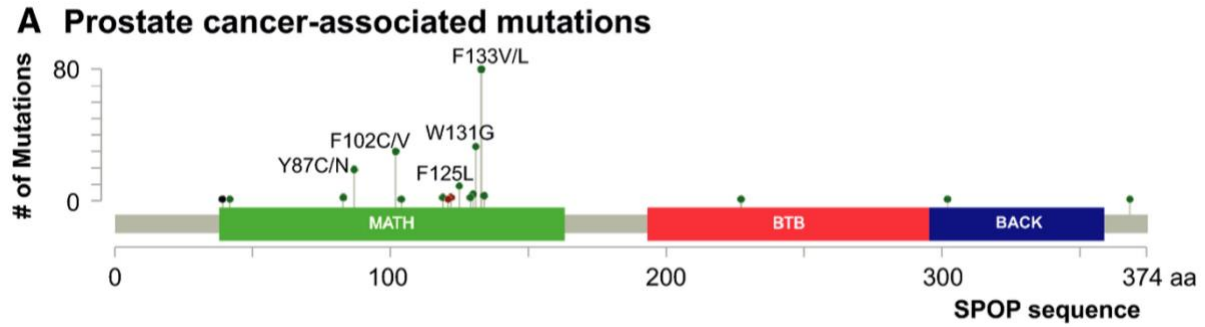

Figure 1-7. Schematic of the prostate-cancer associated mutations in SPOP. Prostate cancer-associated missense mutations are localized primarily in the SPOP MATH substrate binding domain. Retrieved from (Cuneo & Mittag, 2019).

A well characterized example in which SPOP mutations contribute to prostate cancer development is by affecting androgen receptor (AR) stability and activity (Batra & Lai, 2014). The AR is a member of the nuclear receptor superfamily and is essential for normal prostate cell

growth and development, as well as for the initiation and progression of prostate cancer (Li et al., 2014). Prostate cancer associated mutations in the MATH domain of SPOP, allow the AR to escape SPOP-mediated 26S proteasome degradation and thus, AR activity and downstream signalling is maintained (An et al., 2014). SRC-3, a transcriptional co-activator for hormone-activated androgen receptor, is a member of the p160 SRC family and similar to the AR, is a substrate of SPOP (Mani, 2014). Mutations in SPOP prevent ubiquitination and degradation of SRC-3 resulting in its accumulation within the cell (Geng et al., 2013). Stabilization of SRC-3 increases the transcriptional activity and signalling of AR, consequently promoting prostate cancer development (Geng et al., 2013). In addition to promoting the stability of the AR and SRC-3, prostate cancer-associated SPOP mutants promote the stability of other oncogenic substrates due to decreased ubiquitination and proteasomal degradation such as but not limited to: DEK proto-oncogene (DEK), tripartate motif containing 24 (TRIM24) and the bromodomain-containing 2/3/4 proteins (BRD2/3/4), cell division cycle protein 20 homolog (Cdc20), ETS Transcription Factor ERG (ERG), and Cyclin E1 (CCNE1) (Theurillat et al., 2014; Groner et al., 2016; Zhang et al., 2017; Wu et al., 2017; Gan et al., 2015; Ju et al., 2019).

SPOP has also been linked to other cancers such as endometrial, kidney, thyroid, colorectal, breast, lung, and ovarian cancers (Clark & Burleson, 2020; Wang et al., 2020). However, the type of mutation in the SPOP gene and the prevalence of the mutation varies depending on the cancer subtype **(Table 1-2)**. It is important to highlight that the biological function of SPOP as a tumour suppressor or an oncogene varies depending on the cancer subtype, the differential expression and availability of SPOP substrates, as well as expression levels of SPOP (Mani, 2014; Clark & Burleson, 2020; Wang et al., 2020). In the context of prostate cancer, SPOP is a mutated tumor suppressor gene, however in the context of kidney cancer, SPOP has a tumor promoting role (Mani, 2014; Wang et al., 2020).

Table 1-2. List of SPOP alterations in different cancer subtypes. Retrieved from (Cuneo & Mittag, 2019).

Organ	Type(s) of Alteration(s)
Prostate	Missense Mutations, Loss of Expression
Endometrium	Missense Mutations, Loss of Expression
Breast	Loss of Expression
Brain	Loss of Expression
Colorectal	Loss of Expression
Gastric	Loss of Expression
Kidney	Overexpression, Cytoplasmic Localization
Liver	Missense Mutations
Ovary	Amplification, Deletion
Thyroid	Missense Mutations
Lung	Loss of Expression

Recurrent missense mutations in SPOP have been identified in approximately 5% of endometrial cancer patients (Cuneo & Mittag, 2019). However, unlike in prostate cancer, the recurrent missense mutations are located outside of the central substrate binding cleft of the MATH domain (Cuneo & Mittag, 2019). Studies have shown these mutations in SPOP associated with endometrial cancer act as loss of function mutations, decreasing ubiquitination of substrates such as estrogen receptor (ER) but also surprisingly act as gain of function mutations, enhancing ubiquitination of other substrates such as SRC-3 (Cuneo & Mittag, 2019). The molecular mechanism of differential function of SPOP towards substrates remains unknown (Cuneo & Mittag, 2019). Overexpression of SPOP and mislocalization of SPOP to the cytoplasm instead of the nucleus are associated with kidney cancer (Cuneo & Mittag, 2019; Wei et al., 2018). This results in SPOP-mediated ubiquitination of non-target SPOP substrates containing SBC motifs such as dual-specificity phosphatases (DUSPs) promoting tumorigenesis (Wei et al., 2018; Cuneo & Mittag, 2019). Loss of expression or down regulation of SPOP has been implicated in breast cancer initiation, proliferation, and progression, as a result of increased cellular persistence of progesterone receptors (PRs) promoting dysregulated PR signaling upon increased progestogen binding (Gao et al., 2015; Wei et al., 2018).

1.6 Ubiquitin-Specific Protease 7 (USP7)

1.6.1 USP7 Function and Regulatory Impact

Ubiquitin-specific protease 7 (USP7), also known as Herpesvirus associated ubiquitin-specific protease (HAUSP) is one of most extensively studied deubiquitinating enzymes found to interact with a diverse array of viral proteins, as well as cellular proteins regulating their stability, and accordingly has been implicated in several biological processes such as viral replication and infection, epigenetic regulation, DNA repair, transcription, tumour suppression, DNA damage response, and immunity **(Table 1-3)** (Pozhidaeva & Bezsonova, 2019; Bojagora & Saridakis, 2020; Al-Eidan et al., 2020). USP7 was initially discovered and characterized in the 1990s, as a binding partner of the herpes simplex virus type 1 (HSV-1) regulatory protein, infected cell polypeptide 0 (ICP0), previously known as Vmw110 (Everett et al., 1997). Following its discovery, additional viral binding partners of USP7 have been identified including the viral interferon regulatory factor 1 protein (vIRF1) of Kaposi's sarcoma associated herpesvirus (KSHV) and Epstein-Barr nuclear antigen 1 (EBNA1) of Epstein-Barr virus (EBV) (Chavoshi et al., 2016; Holowaty et al., 2003). The first cellular substrate identified to be deubiquitinated and stabilized by USP7 was the tumor suppressor protein p53 (Li et al., 2002). Since then, the list of USP7 cellular substrates continues to grow and includes transcription factors such as forkhead box O4 (FOXO4) and nuclear factor E2-related factor 1 (Nrf1), E3 ubiquitin protein ligases such as checkpoint with forkhead and RING finger domain (CHFR) and mouse double minute 2 homolog (MDM2), as well as epigenetic regulators such as lysine-specific demethylase 1 (LSD1) and DNA methyltransferase 1 (DNMT1) (van der Horst et al., 2006; Han et al., 2021; Oh et al., 2007; Li et al., 2004; Yi et al., 2016; Cheng et al., 2015) It is important to note that although USP7 is well known for regulating the stability of its cellular substrates by removing the proteolytic ubiquitin signal corresponding to degradation mediated by the 26S proteasome, it also regulates the activity and localization of cellular substrates by removing non-proteolytic ubiquitin signals **(Figure 1-8)** (Bojagora & Saridakis, 2020; Pozhidaeva & Bezsonova, 2019).

Table 1-3. List of USP7 substrates/binding partners. Retrieved from (Pozhidaeva & Bezsonova, 2019).

Substrate name	Substrate name
Transcription factors	*Epigenetic control of gene expression*
p53	RING1B
HDM2	Bmi1
Rb	Histone H2B
FOX(O)3	DNMT1
FOX(O)4	UHRF1
PTEN	RNF168
β-catenin	MLL5
PPARγ	Tip60
N-Myc	UbE2E1
DNA replication/Cell cycle control	PHF8
CHFR	*Telomere proteins*
Bub3	TPP1
SUMO	*Immune response*
DNA damage response/DNA repair	NFκB
DAXX	TRAF6
Polymerase η	IKKγ
HLTF	TRIM27
Rad18	*Viral proteins*
Clapsin	EBNA1 from EBV
Chk1	ICP0 from HSV-1
UVSSA	vIRF1 from KSHV
Mule/ARF-BP1	vIRF4 from KSHV

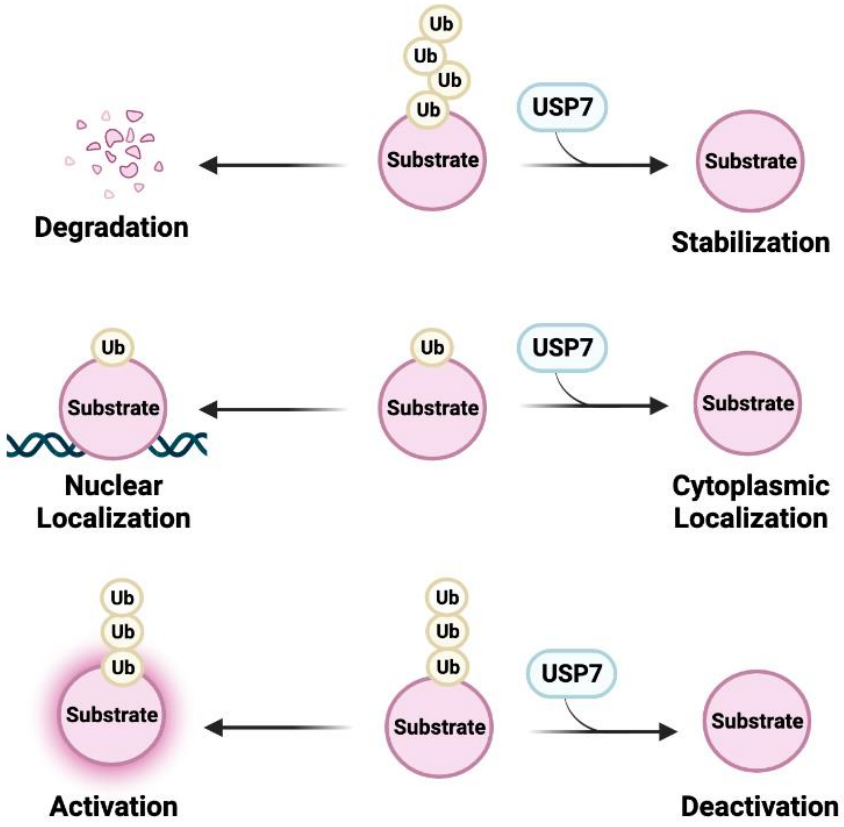

Figure 1-8. Overview of USP7 regulatory roles. USP7 regulates the stability, activity, and localization of its substrates by removing the ubiquitin signal**.** Schematic created with BioRender.com.

1.6.2 USP7 Structure

USP7 is a 1102 amino acid residue protein with a molecular mass of 135 kDa located primary in the nucleus (Pozhidaeva & Bezsonova, 2019; Nininahazwe et al., 2021). USP7 is composed of three distinct domains: the N-terminal tumor necrosis factor receptor–associated factor (TRAF)-like domain consisting of amino acid residues 63-205, followed by the central catalytic core domain (CAT) consisting of amino acid residues 208-560, and the carboxy-terminal domain (CTD) consisting of amino acid residues 562–1102, which is comprised of five tandem ubiquitin-like (Ubl 1-5) subdomains **(Figure 1-9A and Figure 1-9B)** (Pozhidaeva & Bezsonova, 2019; Nininahazwe et al., 2021).

The N-terminus of USP7, required for localization to the nucleus, is comprised of an unstructured region of approximately 50 amino acid residues containing a polyglutamine stretch, followed by the TRAF-like domain (Valles et al., 2020). The N-terminal TRAF-like domain represents one of the two interaction sites of USP7 **(Figure 1-9C)** (Valles et al., 2020). The N-terminal TRAF-like domain consists of an eight-stranded, anti-parallel β-sandwich fold, which mediates recognition and binding of various substrates/binding partners such as but not limited to p53, Epstein-Barr nuclear antigen 1 (EBNA1), murine double minute 2 (MDM2), ubiquitin-conjugating enzyme E2 E1 (UbE2E1), DEAD-box helicase 24 (DDX24), and mini-chromosome maintenance complex-binding protein (MCM-BP) (Saridakis et al., 2005; Sheng et al., 2006; Sarkari et al., 2013; Georges et al., 2018; Jagannathan et al., 2014). Substrates of USP7 that interact with the TRAF-like domain possess a common P/A/ExxS motif (where P = proline, A = alanine, E = glutamic acid, x = any amino acid, and S = serine) (Saridakis et al., 2005; Sheng et al., 2006). This P/A/ExxS motif is recognized by USP7 through the ^{164}DWGF^{167} motif (where D = aspartic acid, W = tryptophan, G = glycine, and F = phenylalanine) located in β-strand 7 which lines the shallow grove on the surface of the TRAF-like domain (Saridakis et al., 2005; Sheng et al., 2006; Sarkari et al., 2013). The Asp^{164} and Trp^{165} residues within the ^{164}DWGF^{167} motif are essential for mediating the interaction between USP7 and its substrates/binding partners; mutations of these residues have been shown to abolish interactions (Sarkari et al., 2013).

The central CAT domain of USP7 is responsible for binding ubiquitin and harbours the active site where hydrolysis of the isopeptide bond between ubiquitin and the substrate occurs (Nininahazwe et al., 2021). The CAT domain of USP7 adopt a right hand-like architecture formed by three subdomains referred to as “fingers, thumb, and palm” (Hu et al., 2002). The finger

subdomain is where ubiquitin binding occurs. The hydrophobic cleft between the thumb and palm subdomains is where the catalytic triad of USP7 consisting of residues Cys^{223}, $His^{464,}$ and Asp^{481} is located (Hu et al., 2002). The Cys^{223} residue of the triad performs the nucleophilic attack of the isopeptide bond between ubiquitin and the substrate, upon deprotonation by His^{464} residue which functions as a proton acceptor. The Asp^{481} residue within this triad functions to restrict rotation and stabilize the sidechain of the His^{464} residue (Pozhidaeva & Bezsonova, 2019; Nininahazwe et al., 2021). Studies have shown that the active site within the catalytic domain of USP7 exists in an inactive conformation, where the residues of the catalytic triad are misaligned and non-reactive (Kim et al., 2016; Faesen et al., 2011). Upon binding of ubiquitin, the CAT domain undergoes an active conformational change that results in the alignment of the catalytic triad enabling its deubiquitination activity (Faesen et al., 2011). The conformational change of the CAT domain upon ubiquitin binding involves the interaction of a small loop near the active site of USP7 also referred to as the "switching loop" consisting of residues 285-291 with the CTD of USP7 (Faesen et al., 2011).

The CTD of USP7 functions as an additional interaction site and enhances the catalytic activity of USP7 (Pozhidaeva & Bezsonova, 2019; Valles et al., 2020). The C-terminal domain of USP7 consists of an α-helix connecting the CAT domain to its five Ubl subdomains (Ubl1-5), which exhibit the common β-grasp ubiquitin fold structure, despite having low sequence similarity to ubiquitin and to each other (Kim et al., 2016; Valles et al., 2020) The Ubl1-5 subdomains are organized into a 2:1:2 configuration, where Ubl1 closely associates with Ubl2 (Ubl12), Ubl3 is separated from Ubl2 and Ubl4 by flexible linker regions, and Ubl4 closely associates with Ubl5 (Ubl45) (Nininahazwe et al., 2021). The Ub12 subdomain represents the second interaction site of USP7 (Pfoh et al., 2015) **(Figure 1-9D)**. More specifically the ^{758}DELMDGD^{764} motif (where D = aspartic acid, E = glutamic acid, L = leucine, M = methionine, and G = glycine) located in a loop ahead of β-strand 4 interacts with substrates/binding partners possessing a highly conserved KxxxK motif (where K = lysine and x = any amino acid) (Pfoh et al., 2015). The lysine residues in the KxxxK motif directly interact with the Asp^{762} and Asp^{764} residues in the ^{758}DELMDGD^{764} motif; mutations of the lysine or aspartic acid residues have shown to decrease binding, revealing that these residues are essential for mediating interaction between USP7 and its substrates/binding partners (Pfoh et al., 2015). Substrates/binding partners shown to interact with the CTD of USP7 include ICP0, enhancer of zeste homolog 2 (EZH2), ring finger protein 169 (RNF169), ubiquitin-

like with PHD and RING finger domains 1 (UHRF1), and DNA methyltransferase 1 (DNMT1) (Pfoh et al., 2015; Gagarina et al., 2020; An et al., 2017; Zhang et al., 2015; Cheng et al., 2015). Not only does the CTD of USP7 mediate recognition and interaction of substrates/binding partners, the CTD domain of USP7 also promotes increased catalytic activity of USP7 (Faesen et al., 2011). Previous studies have shown compared to full-length USP7, the isolated CAT domain of USP7 has weak intrinsic deubiquitinating activity (Faesen et al., 2011; Rougé et al., 2016; (Kim et al., 2016). Further investigation revealed in order to achieve efficient deubiquitinating activity, the direct interaction of the CAT domain with the CTD domain, specifically the Ubl45 subdomain is required (Faesen et al., 2011).

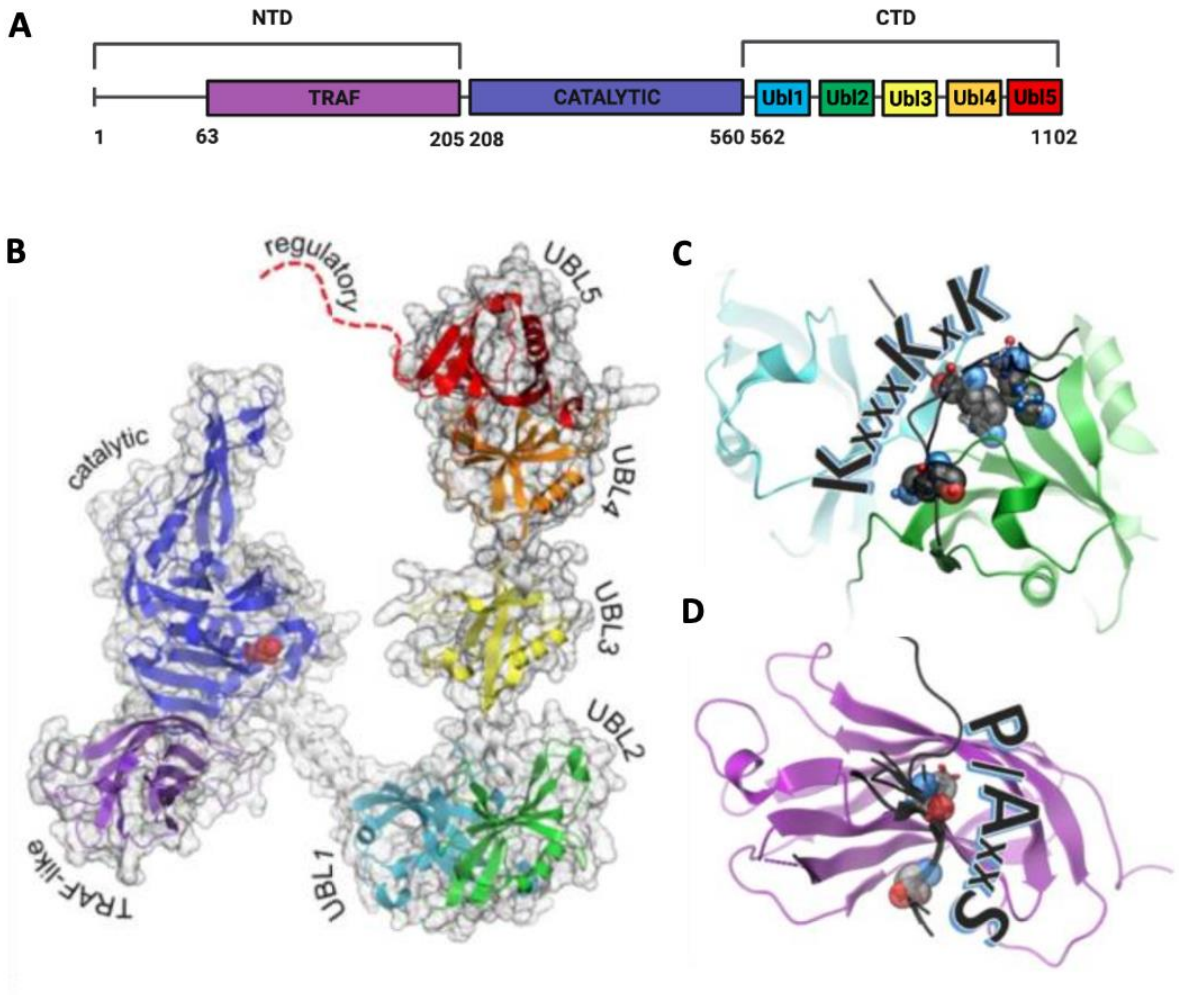

Figure 1-9. USP7 domain, structure, and organization (a) Schematic of the domains of USP7. **(b)** A model of full-length USP7, where the N-terminal TRAF-like domain is shown in purple, the CAT domain is shown in dark blue/purple, and the C-terminal domain containing five ubiquitin-like subdomains, where Ubl1 is shown in light blue, Ubl2 is shown in green, Ubl3 is shown is yellow, Ubl4 is shown in orange, and Ubl5 is shown in red. **(c)** A model of the Ubl2 subdomain shown in green interacting with a substrate peptide shown in black containing the USP7 binding motif: KxxxKxK. Please note the Ubl2 subdomain can also bind substrates containing the USP7 binding motif: KxxxK. **(d)** A model of the TRAF-like domain shown in purple interacting with a substrate peptide shown in black containing the USP7 binding motif: P/AxxS. Please note the TRAF-like domain can also bind substrates containing the USP7 binding motif: P/A/ExxS. Modified from (Pozhidaeva & Bezsonova, 2019)

1.6.3 USP7 and its Role in Cancer

As mentioned previously, USP7 regulates the stability, activity, and localization of various substrates involved in essential cellular processes such as cell cycle control, DNA damage response, tumour suppression, and epigenetic regulation (Pozhidaeva & Bezsonova, 2019; Bojagora & Saridakis, 2020; Al-Eidan et al., 2020). Dysregulation of such substrates as a result of overexpression or aberrant activation of USP7 has been implicated in cancer initiation and progression (Nininahazwe et al., 2021). In fact, USP7 has been found to be overexpressed in a wide variety of cancers such as prostate, breast, lung, ovarian, esophageal, and cervical cancer (Nininahazwe et al., 2021; Hu et al., 2018; Qin et al., 2016). A well characterized example in which USP7 contributes to prostate cancer development is by affecting androgen receptor (AR) stability and activity (Chen et al., 2015). In prostate cancer cells, USP7 has been reported to interact with and mediate AR deubiquitination in an androgen-dependent manner, promoting its stabilization (Chen et al., 2015). Moreover, USP7 has been identified as a co-regulator of AR, facilitating the binding of androgen-activated AR to the chromatin resulting in expression of genes involved in cell proliferation or differentiation (Chen et al., 2015). An additional well-established substrate of USP7 implicated in prostate cancer is enhancer of zeste homolog 2 (EZH2) (Lee et al., 2020). EZH2 is a component of the polycomb repressor complex 2 (PRC2), which mediates the trimethylation of histone 3 at lysine 27 (H3K27) resulting in the silencing of genes involved in cell fate decision, cell differentiation, cell cycle regulation, and senescence (Chang & Hung, 2012). In prostate cancer cells, USP7 overexpression had been reported to directly correlate with tumor aggressiveness and promote cell migration, invasion, and sphere formation partly as a result of EZH2 stabilization (Song et al., 2008; Lee et al., 2020). Phosphatase and tensin homolog (PTEN) is another example of a USP7 substrate implicated in prostate cancer as well as leukemia (Song et al., 2008; Morotti et al., 2014) PTEN is a tumor suppressor that localizes to the nucleus upon monoubiquitination where it functions to maintain genomic integrity and suppress cell growth (Song et al., 2008; Morotti et al., 2014). However, upon deubiquitination by USP7, PTEN is excluded from the nucleus and shuttled into the cytoplasm where it accumulates and is unable to perform its nuclear function (Song et al., 2008; Morotti et al., 2014). In breast cancer, USP7 has also been shown to deubiquitinate and stabilize histone demethylase PHD finger protein 8 (PHF8), leading to the upregulation of cyclin A2, which subsequently activates cyclin dependent kinase 2 (CDK2) and cyclin dependent kinase 1 (CDK1) resulting in cell growth and proliferation (Wang

et al., 2016). Moreover, in non-small cell lung cancer, USP7 promotes cell proliferation through the deubiquitination and stabilization of Ki-67 protein which is implicated in the progression of mitosis (Zhang et al., 2016)

1.7 Thesis Rationale, Objective, and Approach

Prostate cancer is the most common cancer among Canadian men and is the third leading cause of death ("Prostate cancer statistics: Canadian Cancer Society," 2020). Androgen deprivation therapy, which functions to decrease the circulating levels of androgens, is commonly used to treat prostate cancer, however, yields temporary effectiveness, as patients typically develop and progress to castration-resistant forms of prostate cancer caused by various mechanisms such as overexpression of AR leading to androgen-hypersensitivity or mutations in AR resulting in androgen-independent activation (Wadosky & Koochekpour, 2016). These limitations in AR targeted therapies highlight the significance in developing alternative therapeutic targets in the treatment of prostate cancer. Genome-wide sequencing studies have revealed that SPOP is the most frequently mutated gene in primary prostate cancers (Barbieri et al., 2012). Moreover, USP7 has been reported to be overexpressed in prostate cancer and is directly correlated to tumor aggressiveness. These findings together suggest USP7 and SPOP may be potential and promising therapeutic targets in the treatment of prostate cancer. Hence, the objective of this project is to identify novel substrates of SPOP and USP7, and characterize their mode of binding and regulation to provide further insight on the molecular mechanisms in which SPOP and USP7 contribute to prostate cancer development that may have potential in combination to be targeted therapeutically.

After years of extensive research on USP7, the Saridakis lab has newly discovered sequence and structural similarity between the substrate binding N-terminal TRAF-like domain of USP7 and the substrate binding MATH domain of SPOP **(Figure 1-10 and Figure 1-11)**. In addition, the SPOP binding consensus motif (ϕ-π-S/T-S/T-S/T, where ϕ = nonpolar and π = polar) possessed by substrates of SPOP resembles the USP7 binding consensus motif (P/A/ExxS) possessed by substates of USP7. Individual studies focused on identifying novel substrates of USP7 and individual studies focused on identifying novel substrates of SPOP, also reveal many overlapping substrates **(Figure 1-12)**. Collectively, these findings provide a basis for selecting and identify novel substrates of SPOP and USP7 by examining previously established substrates of USP7 and SPOP, respectively.

USP7 TRAF-like DOMAIN: ^{151}SRRISHLFFHKEN**DWGF**SNFMAWSEVTDPE^{180}
SPOP MATH DOMAIN: ^{117}MESQRAYRFVQGK**DWGF**KKFIRRDFLLDEA^{146}

Figure 1-10. Sequence alignment of the USP7 TRAF-like domain and SPOP MATH domain. Complete sequences of the TRAF-like domain of USP7 consisting of residues 68-195 (Q93009) and MATH domain of SPOP consisting of residues 31-161 (O4379) were retrieved from UniProt.

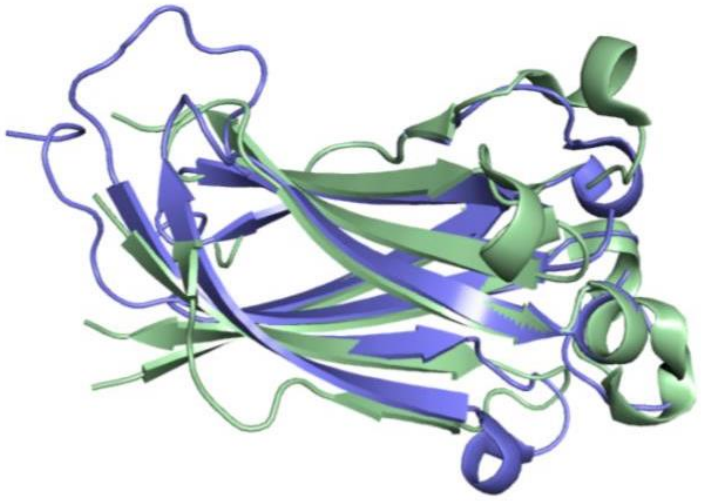

Figure 1-11. Structural alignment of USP7 TRAF-like domain and SPOP MATH domain. Ribbon representation of the structural alignment of USP7 TRAF-like domain shown in blue and SPOP MATH domain shown in green. Retrieved from (Helen Liu, 2019, unpublished).

In order to screen for potential novel substrates of SPOP and USP7, we performed a bioinformatic search using the Eukaryotic Linear Motif (ELM) computational biology resource to detect for SPOP binding consensus motifs (ϕ-π-S/T-S/T-S/T) in established USP7 substrates and USP7 binding consensus motifs (P/A/ExxS) in established SPOP substrates. Here, we investigated whether the SPOP substrate, sirtuin 2 (SIRT2), an NAD^+-dependent deacetylase is a novel substrate of USP7, and whether the USP7 substrate, murine double minute 2 (MDM2), an E3 ubiquitin protein ligase is a novel substrate of SPOP. The relationship between SPOP and MDM2, as well as USP7 and SIRT2, were investigated by employing a combination of biochemical and cell biology techniques as His-tagged based pulldowns, co-immunoprecipitations, siRNA-mediated knockdown, overexpression via transfection, and western blotting. The content of Chapter 2 and Chapter 3 focus on exploring the relationship between SPOP and MDM2, and USP7 and SIRT2, respectively.

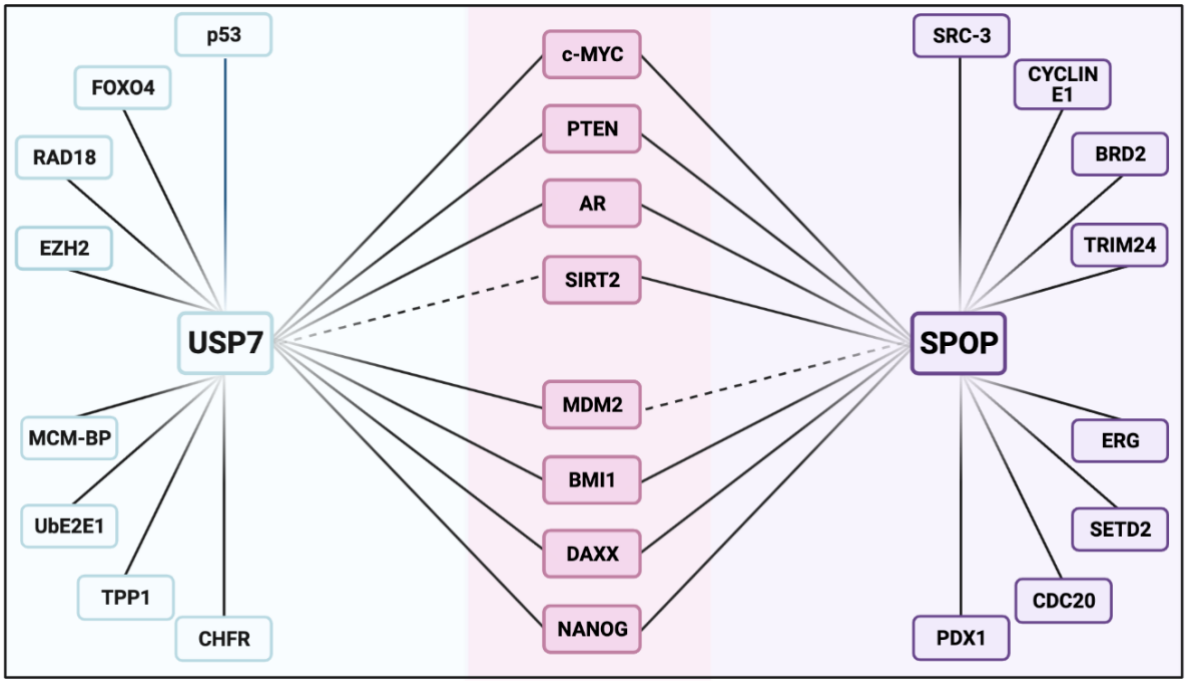

Figure 1-12. Protein interaction map of USP7 and SPOP. Dashed lines represent proteins currently being investigated as potential substrates of SPOP and USP7. Schematic created with BioRender.com.

CHAPTER 2: Investigation of MDM2 as a Novel Substrate of SPOP

2.1 Introduction

2.1.1 MDM2 Function

Murine double minute 2 (MDM2) discovered in 1987, is an oncogenic E3 ubiquitin ligase of the RING class, which recruits and mediates the transfer of ubiquitin from an E2 ubiquitin conjugating enzyme to its target substrate, regulating its stability, activity, and/or localization (Cahilly-Snyder et al., 1987; Marine & Lozano, 2010). MDM2 is best known for its role as the "master regulator" of the tumor suppressor, p53 (Momand et al., 2000). p53 is a transcription factor commonly referred to as the "guardian of the genome" due to its ability to promote DNA repair, senescence, or apoptosis in response to cellular stressors such as DNA damage by activating the expression of its target genes (Shadfan et al., 2012). In the absence of such stressors, the transcriptional activity and intracellular levels of p53 must be regulated to promote normal cell growth and viability (Shadfan et al., 2012). As mentioned previously, MDM2 is a key regulator of p53 (Momand et al., 2000). MDM2 negatively regulates p53 stability, activity, and localization using various mechanisms (Zhao et al., 2014). First, MDM2 can bind to the transactivation domain of p53 inhibiting its transcriptional activity of its target genes (Zhao et al., 2014). MDM2 also can bind to and promote polyubiquitination of p53, corresponding to degradation via the 26S proteasome (Zhao et al., 2014). Lastly, MDM2 can bind to and promote monoubiquitination of p53, corresponding to nuclear export of p53, preventing activation of its target genes (Zhao et al., 2014). Albeit p53 is a well-established substrate of MDM2, additional substrates of MDM2 have been identified. For instance, MDM2 can interact with Numb, implicated in cell fate determination, by promoting its relocalization to the nucleus (Juven-Gershon et al., 1998). MDM2 also binds to the retinoblastoma (Rb) protein inhibiting its activity in promoting cell cycle arrest (Xiao et al., 1995). Moreover, MDM2 can also bind to members of the FOXO (forkhead O) class of transcription factors such as FOXO1 and FOXO3A promoting their ubiquitination and subsequent degradation (Fu et al., 2009).

2.1.2 MDM2 Structure

The human MDM2 gene is located on chromosome 12 (Hou et al., 2019). The full-length mRNA transcript of the MDM2 gene encodes a 491 amino acid residue protein with a molecular weight of 90 kDa (Hou et al., 2019). It is important to note that the pre-MRNA transcript of the MDM2 gene can also undergo alternative splicing producing an isoform with a molecular weight of 75 kDa (Cheng & Cohen, 2006). MDM2 is composed of four distinct domains: the N-terminal p53-binding domain, the central acidic domain and zinc finger domain, and the C-terminal RING domain **(Figure 2-1)** (Zhao et al., 2014). The N-terminal p53-binding domain as its name suggests, interacts with the p53 transactivation domain which functions to downregulate p53 transcription activity (Zhao et al., 2014). The N-terminal p53-binding region can also mediate other protein-protein interactions (Hou et al., 2019). The central region of MDM2 contains a nuclear localization sequence (NLS) and nuclear export sequence (NES) which allows MDM2 to shuttle between the cytoplasm and nucleus, as well as the acidic domain and zinc finger domain (Zhao et al., 2014). The central acidic domain is the site of multiple post-translational modifications such as phosphorylation as well as functions as an additional binding site of p53 (Priest et al., 2010; Kulikov et al., 2006). The central zinc finger domain is the binding site of regulatory proteins such as ribosomal proteins (Lindström et al., 2007). Collectively, the central acidic and zinc finger domains regulate MDM2 function (Kawai et al., 2003; Lindström et al., 2007). The RING domain is responsible for the E3 ubiquitin ligase activity of MDM2, which functions to recruit the E2 ubiquitin conjugating enzyme with bound ubiquitin to promote the ubiquitination of its substrate (Priest et al., 2010). The RING domain also mediates MDM2 homodimerization and/or heterodimerization with the homologous protein murine double minute 4 (MDM4) also known as MDMX (Leslie et al., 2015). Similar to MDM2, MDMX also binds and regulates p53 transcriptional activity, however, lacks intrinsic E3 ubiquitin ligase activity (Leslie et al., 2015; Zhao et al., 2014). MDMX is also involved in stabilizing MDM2 by inhibiting its self-ubiquitination and thus, facilitates ubiquitination of p53 mediated by MDM2 and subsequent degradation by the 26S proteasome (Zhao et al., 2014).

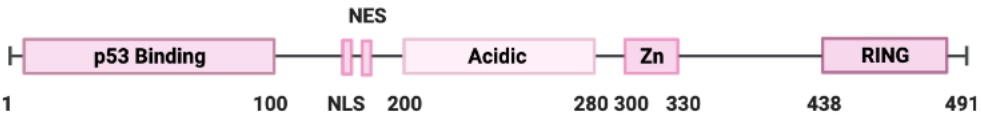

Figure 2-1. Schematic of the domains of MDM2. Modified from (Linke et al., 2008) with BioRender.com.

2.1.3 Project Overview

Here, we investigated whether the USP7 substrate, MDM2, is a novel substrate of SPOP. Initially, His-tagged based pulldowns were performed using purified wildtype and mutated HIS-SPOP MATH domain constructs to determine if SPOP interacts with MDM2 and the specific amino acid residues required for this interaction. Next, to determine whether SPOP regulates the stability of MDM2 within the Cullin 3-RING E3 ubiquitin protein ligase, we examined endogenous levels of MDM2 upon overexpression of SPOP via transfection, as well as siRNA-mediated knockdown of SPOP followed by western blot analysis. Treatment with proteasome and lysosome inhibitors were used to investigate whether SPOP targets MDM2 for degradation via the 26S proteasome or the lysosome.

2.2 Material and Methods

2.2.1 Cell Lines

The human embryonic kidney cell line stably expressing the SV40 large T antigen (293T or HEK293T) was kindly provided as a gift by Dr. Lori Frappier (University of Toronto) and was cultured in DMEM media (Wisent Inc.) supplemented with 10% fetal bovine serum (FBS, Gibco) and 1% Penicillin-Streptomycin (P/S, Wisent Inc.) at 37°C and 5% CO_2. The human osteosarcoma (U2OS) cell line was kindly provided as a gift by Dr. Samuel Benchimol (York University) and was cultured in McCoy's media (Wisent Inc.) supplemented with 10% FBS and 1% P/S at 37°C and 5% CO_2. The immortal human Henrietta Lacks (HeLa) cell line was kindly provided as a gift by Dr. Samuel Benchimol (York University) and was cultured in DMEM media supplemented with 10% FBS and 1% P/S at 37°C and 5% CO_2.

2.2.2 Plasmids

Plasmids used for transfections were isolated and purified using the Plasmid Maxi Plus Kit (Qiagen) following the manufacturer's protocol. Before use, plasmids were verified by sequencing by the Centre for Applied Genomics (TCAG) operated by The Hospital for Sick Children (SickKids, Toronto). The plasmids used for mammalian transfection include: pcDNA3.1/FLAG and pcDNA3.1/FLAG-SPOP. pcDNA3.1/FLAG-SPOP was kindly provided as a gift from Dr. Gil Privé (University of Toronto).

2.2.3 DNA Transfection

18-24 hours prior to transfection, cells were seeded into 10 cm plates to reach a confluency of 70-80% at the time of transfection. Media containing 10% FBS and 1% P/S was changed 30 minutes prior to transfection. Cells were transiently transfected with plasmids using Polyjet™ In Vitro DNA transfection reagent (SignaGen Laboratories). Unless otherwise stated, 5 µg of plasmid DNA was transfected with 15 uL of Polyjet™. To reduce cytotoxicity, the media containing the PolyJet™/DNA complex was removed 5 hours after transfection and replaced with fresh media containing 10% FBS and 1% P/S. Cells were then harvested 24 hours post-transfection.

2.2.4 siRNA Transfection

18-24 hours prior to transfection, cells were seeded into 10 cm plates, to reach a confluency of 70% at the time of transfection. Media containing 10% FBS and 1% P/S was changed 30 minutes prior to transfection. Cells were transiently transfected with siRNA purchased from GenePharma Co., Ltd. (Shanghai, China) using Lipofectamine 3000 (Thermo, USA) **(Table 2-1)**. The siRNA mediated knockdown of endogenous SPOP was performed using 50 mM of siSPOP #1 and siSPOP #2. A scrambled siRNA was used as a negative control. To reduce cytotoxicity, the media containing the Lipofectamine 3000/siRNA complex was removed 5 hours after transfection and replaced with fresh media containing 10% FBS and 1% P/S. Cells were then harvested 72 hours post-initial transfection.

Table 2-1. List of double stranded siRNA sequences used. siRNA molecules were purchased from GenePharma Co., Ltd. (Shanghai GenePharma).

siRNA target	**Sequence 5'-3'**
Human SPOP #1	GGAGAACGCUGCAGAAAUUTT AAUUUCUGCAGCGUUCUCCTT
Human SPOP #2	GCAAACGCCUGAAGCAAUCTT GAUUGCUUCAGGCGUUUGCTT
Scrambled Negative Control	GUAGGACGACGUAUGAACATT UGUUCAUACGUCGUCCUACTT

2.2.5 Harvest, Lysis, and Sample Preparation

Cells were incubated with 0.25% trypsin-EDTA (Gibco) for 5 minutes at 37°C and 5% CO_2 followed by the addition of McCoys or DMEM media supplemented with 10% FBS, and 1% P/S to inhibit and neutralize further trypsinization. Detached cells were harvested by centrifugation at 1000 x g for 5 minutes at room temperature. The cellular pellet was washed twice with ice-cold PBS to remove residual media and was either stored at -80°C or immediately lysed with 1% NP-40 Buffer [50 mM Tris-HCl, pH 8, 150 mM NaCl, 1% (v/v) NP-40, 1 mM benzamidine, 1 mM PMSF, 1 x cOmplete protease inhibitor cocktail (Roche)] or RIPA buffer [50 mM Tris-HCl, pH 8, 150 mM NaCl, 1% (v/v) NP-40, 0.5% sodium deoxycholate, 0.1% SDS, 1 mM benzamidine, 1 mM PMSF, 1 x cOmplete protease inhibitor cocktail (Roche)] by mechanical rotation for 45 minutes at 4°C or by sonication at 10% amplitude for 0.5 seconds ON and 10 seconds OFF, a total of three times on ice (Sonic Dismembrator Model 500, Fisher Scientific). Cellular debris was pelleted by centrifugation at 17,000 x g for 15 minutes at 4°C and the supernatant was collected.

Protein concentration was determined using the BCA reagent following the manufacturer's instructions (Thermo Scientific Pierce BCA Protein Assay Kit, 23225). Samples containing equal amounts of protein were prepared by boiling the lysate with 1 x SDS loading dye [5% β-mercaptoethanol, 10% SDS, 30% glycerol, 250 mM Tris-HCl, pH 6.8, 0.02% Bromophenol blue] for 5 minutes. Samples were stored at -20°C for later use or immediately resolved on a 12% SDS-polyacrylamide gel.

2.2.6 Immunoblotting

Samples containing equal amounts of proteins were separated by electrophoresis set to 160V for 1.5 hours using a 12% SDS-polyacrylamide gels. Resolved proteins were transferred to a 0.45 μm Immobilon-P PVDF membrane (Millipore) activated with methanol and equilibrated with 1 x Western Transfer buffer [25 mM Tris, pH 8.3, 192 mM Glycine, 20% methanol]. Traditional wet transfers were performed at 4°C and on ice, set to 80V for 1.5 to 2 hours. The membrane was then blocked in 5% non-fat dry milk in 1 x PBS-T [1 x PBS, 0.1% Tween-20] for 1 hour at room temperature. After blocking, the membrane was cut into strips according to the visible protein marker and incubated with the corresponding diluted primary antibody overnight at 4°C with gentle rocking. The following day, the membranes were washed with 1 x PBS-T in 5-minute intervals a total of 3 times, followed by incubation with diluted secondary rabbit or mouse antibody conjugated with horseradish peroxidase for 1 hour at room temperature. The membranes were then washed a total of three times with 1 x PBS-T in 15-minute intervals and incubated with Amersham ECL Prime Western Blotting Detection Reagent (GE Healthcare) for 2-3 minutes. Excess ECL reagent was removed, and the signals were detected using MicroChemi (DNR BioImaging System).

2.2.7 Antibodies

The following primary antibodies were used for immunoblotting: anti-GAPDH (0411) mouse monoclonal (Santa Cruz Biotechnology Inc, 47724), anti-His (H-3) mouse monoclonal (Santa Cruz Biotechnology Inc, 8036), anti-BMI1 (D42B3) rabbit monoclonal (Cell Signaling Technology, 5856), anti-MDM2 (D1V2Z) rabbit monoclonal (Cell Signaling Technology, 86934), anti-DAXX (25C12) rabbit monoclonal (Cell Signaling Technology, 4533), anti-p53 mouse monoclonal (Santa Cruz Biotechnology Inc, 126), anti-SPOP rabbit polyclonal (Proteintech,

16750-1-AP), and anti-FLAG (clone M2) mouse monoclonal (Sigma-Aldrich, F1804) **(Table 2.2)**. The following secondary antibodies were used for immunoblotting: anti-mouse IgG HRP-conjugated goat polyclonal (ThermoFisher Scientific, 31430) and anti-rabbit IgG HRP-linked (Cell Signalling Technology, 7074) **(Table 2.2)**.

Table 2-2. List of primary and secondary antibodies.

Target	Company	Catalogue Number	Species	Dilution	Application
BMI1	Cell Signaling Technology	5856	Rabbit	1:1000 in 5% w/v BSA in 1 x PBS-T	Immunoblotting
DAXX	Cell Signaling Technology	86934	Rabbit	1:2000 in 5% w/v BSA in 1 x PBS-T	Immunoblotting
FLAG	Sigma-Aldrich	F1804	Mouse	1:2000 in 5% non-fat dry milk in 1 x PBS-T	Immunoblotting
GAPDH	Santa Cruz Biotechnology Inc	sc-47724	Mouse	1:10,000 in 5% non-fat dry milk in 1 x PBS-T	Immunoblotting
His	Santa Cruz Biotechnology Inc	sc-8036	Mouse	1:1000 in 5% non-fat dry milk in 1 x PBS-T	Immunoblotting
MDM2	Cell Signaling Technology	86934	Rabbit	1:2000 in 5% w/v BSA in 1 x PBS-T	Immunoblotting
SPOP	Proteintech	16750-1-AP	Rabbit	1:2000 in 5% non-fat dry milk in 1 x PBS-T	Immunoblotting
anti-mouse IgG HRP-conjugated	ThermoFisher Scientific	31430	Goat	0.1:2000 in 2% non-fat dry milk in 1 x PBS-T	Immunoblotting
anti-rabbit IgG HRP-linked	Cell Signalling Technology	7074	Goat	1:2000 in 5% non-fat dry milk in 1 x PBS-T	Immunoblotting

2.2.8 FLAG-SPOP Dose Dependent Overexpression

293T cells were seeded into 10 cm plates and were transiently transfected with pcDNA3.1/FLAG-SPOP in a dose dependent manner (5 μg, 7.5 μg, and 10 μg). Cells were harvested 24 hours post-transfection and were lysed in 1% NP-40 Buffer [50 mM Tris-HCl, pH 8, 150 mM NaCl, 1% (v/v) NP-40, 1 mM benzamidine, 1 mM PMSF, 1 x cOmplete protease inhibitor cocktail (Roche)] under mechanical agitation for 45 minutes at 4°C. 50 ug of samples were

prepared with 1 x SDS loading dye and resolved using a 12% SDS-polyacrylamide gel followed by immunoblotting with the indicated antibodies.

2.2.9 MG132 Treatment

U2OS, HeLa, and 293T cells were treated with 10 μM MG132 for 8 hours to inhibit degradation mediated by the 26S proteasome. DMSO was used as a negative control. U2OS cells transiently transfected with pcDNA3.1/FLAG or pcDNA3.1/FLAG-SPOP for 24 hours were treated with 20 μM MG132 for 4 hours. DMSO was used as a negative control. U2OS cells transiently transfected with pcDNA3.1/FLAG or pcDNA3.1/FLAG-SPOP for 24 hours were treated with 20 μM MG132 for 10 hours or 20 μM chloroquine (CQ) for 9 hours. DMSO was used as a negative control.

2.2.10 Protein Expression and Purification

All 6xHis tagged SPOP MATH constructs were expressed in BL21 mgk *Escherichia coli* (E.coli) in Luria Broth (LB) media (Bioshop) with 100 μg/ml ampicillin (Bioshop) and 50 μg/ml kanamycin (Bioshop) **(Table 2-3)**. The cultures were grown at 37°C at 200 rpm until the OD_{600nm} of 0.8 was reached, followed by induction with 0.4 mM of Isopropyl β-D-1 thiogalactopyranoside (IPTG, Bioshop) overnight at 16°C at 200 rpm. The cells were pelleted by centrifugation at 6,000 x g at room temperature for 20 minutes with a JLA 16.250 Beckman rotor (Beckman Coulter Avanti J-E centrifuge). The pellets were resuspended in ice-cold binding/lysis buffer [50 mM Tris, pH 7.5, 500 mM NaCl, 5 mM Imidazole, and 5% Glycerol] with protease inhibitors [1 mM benzamidine, 1 mM PMSF, 1 x cOmplete protease inhibitor cocktail (Roche)]. The resuspended pellets were sonicated on ice at 30% amplitude for a total of 4 minutes (15 seconds ON, 30 seconds OFF) (Branson Digital Sonifier D450). The supernatants were collected by centrifugation at 30,000 x g at 4°C for 30 minutes with a JA-25.50 Beckman rotor (Beckman Coulter Avanti J-E centrifuge). The supernatants were then incubated with 1 mL of Ni^{2+}-NTA-agarose beads (Qiagen) for 1 hour at 4°C on the rotator. After incubation, the beads were washed a total of six times with ice-cold wash buffer [50 mM Tris, pH 7.5, 500 NaCl, 20 mM Imidazole, and 5% Glycerol] and stored at -80°C until needed.

All 6xHis tagged USP7 NTD constructs were expressed in BL21 mgk E.coli, induced with IPTG, pelleted, and stored at -80°C by a previous student in the Saridakis lab **(Table 2-3)**. These constructs were purified following the same method described previously.

Table 2-3. **Plasmid constructs used for bacterial expression and purification.**

Protein	Vector	Tag	Residues	Mutation
6xHis-SPOP MATH^{DWGF}	pET15b	His	28-166	WT
6xHis-SPOP MATH^{DWGV}	pET15b	His	28-166	F133V
6xHis-SPOP MATH^{DDGF}	pET15b	His	28-166	W131D
6xHis-SPOP MATH^{DAGA}	pET15b	His	28-166	W131A/F133A
6xHis-USP7 NTD^{DWGF}	pET15b	His	62-205	WT
6xHis-USP7 NTD^{AAGF}	pET15b	His	62-205	D164A/W165A

2.2.11 His Pull-Down Assay

293T cells were lysed in ice-cold 1% NP-40 buffer [50 mM Tris-HCl, pH 8, 150 mM NaCl, 1% (v/v) NP-40] containing protease inhibitors [1 mM benzamidine, 1 mM PMSF, 1 x cOmplete protease inhibitor cocktail (Roche)] on a rotary shaker at 4°C for 45 minutes. The cell lysate was centrifuged at 17,000 x g for 15 minutes at 4°C to pellet cellular debris. Protein concentration of the clarified lysate was measured using the BCA assay following the manufacturer's instructions (Thermo Scientific Pierce BCA Protein Assay Kit, 23225).

To reduce non-specific binding, the clarified lysate was incubated with 50 uL of empty Ni^{2+}-NTA Agarose beads under constant rotation at 4°C for 1 hour. 6xHis tagged SPOP MATH and USP7 NTD constructs bound to Ni^{2+}-NTA agarose beads were pre-blocked with 5% BSA in 1 x PBS for 1 hour rotating at 4°C. 1000 ug of the pre-cleared lysate was incubated with 20 uL of pre-blocked Ni^{2+}-NTA-agarose beads with bound 6xHis tagged SPOP MATH and USP7 NTD constructs in a total volume of 500 uL. After incubation at 4°C for 2 hours, the beads were washed six times with 1 mL of high salt wash buffer [50 mM Tris-HCl, pH 7.4, 500mM NaCl, 0.1% (v/v) NP-40] in 5-minute intervals on a rotating device at 4°C. Samples were prepared by boiling the 6xHis tagged SPOP MATH and USP7 NTD constructs bound to Ni^{2+}-NTA agarose beads with 1 x SDS loading dye for 5 minutes. Samples were resolved on 12% SDS-polyacrylamide gels followed by immunoblotting with the indicated antibodies.

2.3 Results

2.3.1 Analysis of MDM2 as a potential substrate of SPOP

In order to screen for potential novel substrates of SPOP, we performed a bioinformatic search using the Eukaryotic Linear Motif (ELM) computational biology resource to detect for SPOP binding consensus motifs (ϕ-π-S/T-S/T-S/T, where ϕ = nonpolar and π = polar) in established USP7 substrates. Analysis of the full-length protein sequence of MDM2 revealed the presence of two putative SPOP binding consensus motifs: ^{156}PSTSS^{160} and ^{397}PSTSS^{401}. Alignment of the putative SPOP binding sites of MDM2 with the SPOP binding consensus motifs of established SPOP substrates suggests that SPOP may interact with MDM2 through its MATH domain **(Figure 2-2)**. Moreover, the two putative SPOP binding consensus motifs of MDM2 are identical to the putative SPOP binding consensus motif of BMI1 (^{266}PSTSS^{270}) a known SPOP substrate, albeit the exact binding site of BMI1 mediating its interaction with SPOP remains unconfirmed (Hernandez-Munoz et al., 2005). These findings together prompted us to investigate whether MDM2 is a novel substrate of USP7.

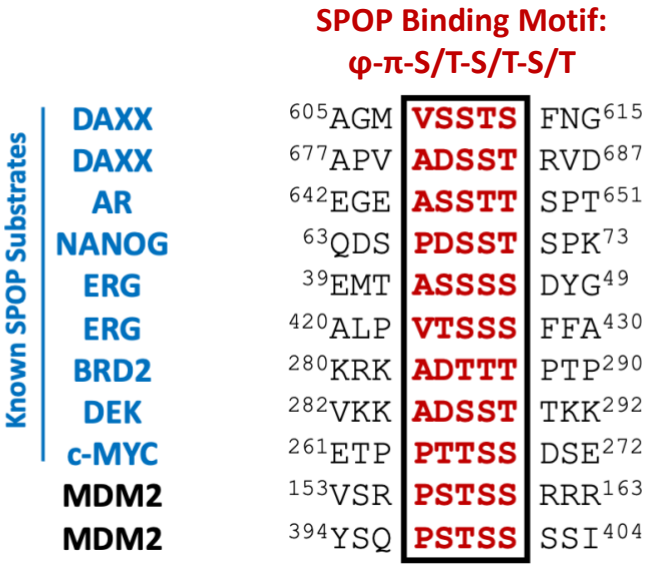

Figure 2-2. Putative SPOP binding sites of MDM2. Sequence alignment and comparison of the putative SPOP binding sites in MDM2 with the SPOP binding consensus motif defined in known SPOP substrates.

2.3.2 SPOP interacts with MDM2, through the "DWGF" motif in its N-terminal MATH domain

The N-terminal MATH domain of SPOP is responsible for substrate recognition and binding (Mani, 2014). Previous studies have shown that mutations in SPOP associated with prostate cancer are localized within the MATH domain, preventing substrate binding, and thus ubiquitination mediated degradation (Cuneo & Mittag, 2019; Batra & Lai, 2014). To determine if SPOP can interact with MDM2 through its N-terminal MATH domain and the specific amino acid residues required for this interaction, we employed a series of His-tagged based pulldowns using the following purified constructs: wildtype HIS-SPOP $MATH^{DWGF}$, double mutant HIS-SPOP $MATH^{DAGA}$ in which residue Trp^{131} and Phe^{133} were changed to alanine residues, and prostate cancer associated mutants, HIS-SPOP $MATH^{DWGV}$ in which residue Phe^{133} was changed to a valine residue, and HIS-SPOP $MATH^{DDGF}$, in which residue Trp^{131} was changed to an aspartic acid residue **(Figure 2-3B)**. Since MDM2 has been previously established as a USP7 substrate, and the substrate binding N-terminal TRAF-like domain of USP7 exhibits sequence and structural similarity with the substrate binding MATH domain of SPOP, we also employed His-tagged based pulldowns using purified wildtype HIS-USP7 NTD^{DWGF} and double mutant HIS-USP7 NTD^{AAGF} as a positive control **(Figure 2-3C)**. The indicated purified His-tagged constructs bound to Ni-NTA agarose beads were incubated with lysate derived from 293T cells. As expected and previously shown, MDM2 interacts with wildtype HIS-USP7 NTD^{DWGF}, whereas this interaction is abolished with double mutant HIS-USP7 NTD^{AAGF}, in which residue Asp^{164} and Trp^{165} were changed to alanine residues. Notably and similar to the pulldowns with HIS-USP7 NTD, MDM2 interacts with wildtype HIS-SPOP $MATH^{DWGF}$, whereas this interaction is abolished with the double mutant HIS-SPOP $MATH^{DAGA}$ and prostate cancer associated mutant, HIS-SPOP $MATH^{DDGF}$. Surprisingly, MDM2 was found to slightly interact with the prostate cancer associated mutant HIS-SPOP $MATH^{DWGV}$, however, this interaction is not as strong in comparison to the wildtype. DAXX and BMI1 are established substrates of both USP7 and SPOP substrate and consequently were used additional controls. As expected and similar to MDM2, DAXX and BMI1 bind to wildtype HIS-SPOP $MATH^{DWGF}$ and HIS-USP7 NTD^{DWGF}, and this interaction is not observed with double mutants HIS-SPOP $MATH^{DAGA}$ and HIS-USP7 NTD^{AAGF}, or the prostate cancer associated mutant, HIS-SPOP $MATH^{DDGF}$. DAXX and BMI1 were also found to slightly interact with the prostate cancer associated mutant, His-SPOP $MATH^{DWGV}$.

Overall, the results of this His-tagged based pulldowns indicate that the ^{130}DWGF^{133} motif within the N-terminal MATH domain of SPOP is essential for the interaction with MDM2 **(Figure 2-3A)**.

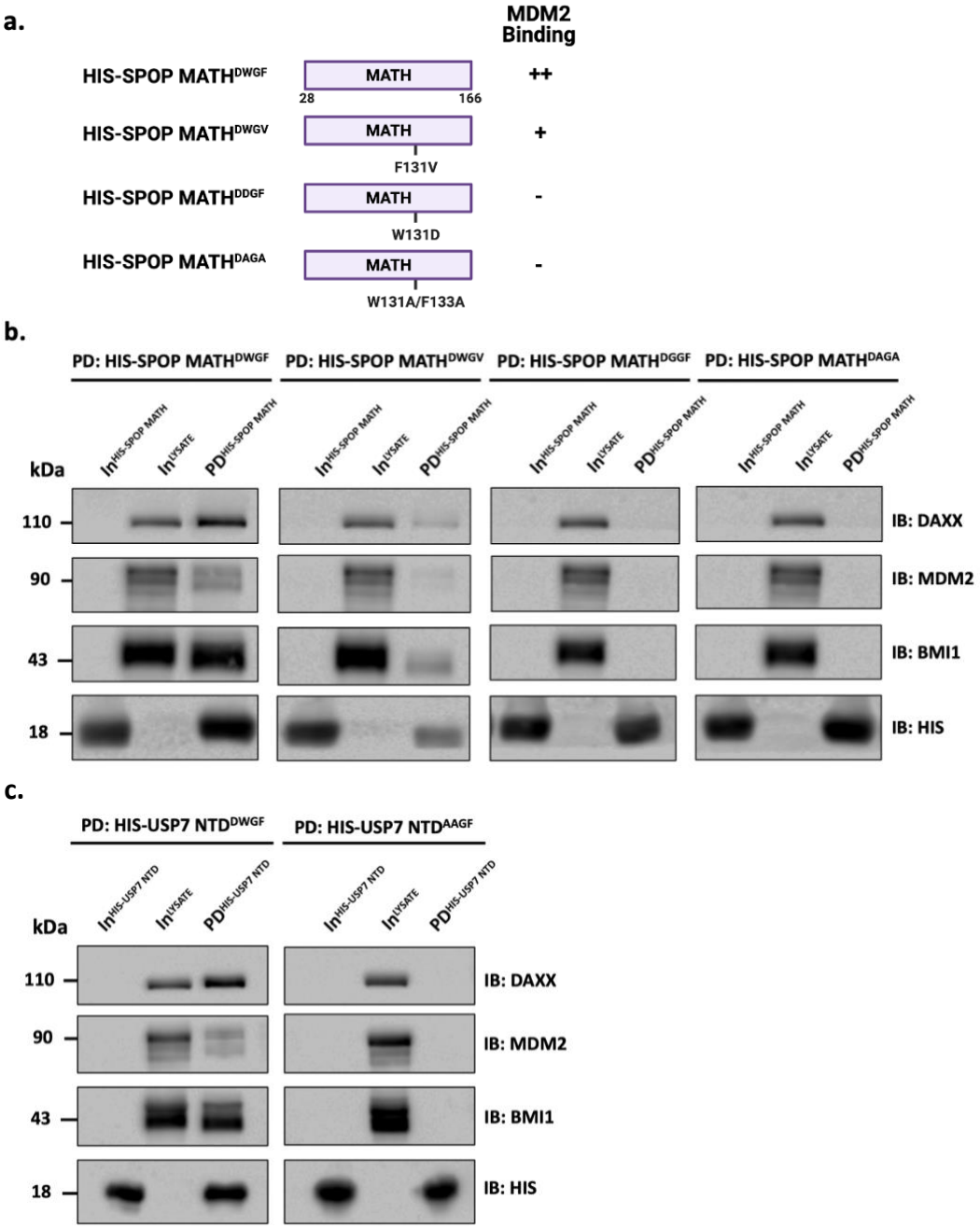

Figure 2-3. SPOP interacts with MDM2 via the "DWGF" motif in its N-terminal MATH domain.
(a) Schematic representation of HIS-SPOP MATH constructs. Binding capacity of MDM2 to HIS-SPOP MATH constructs is indicated with the symbol (+/-). **(b)** His-tagged based pulldowns using purified wildtype HIS-SPOP MATH^{DWGF}, double mutant HIS-SPOP MATH^{DAGA}, prostate cancer associated mutants HIS-SPOP MATH^{DWGV} and HIS-SPOP MATH^{DGGF} bound to Ni^{2+}-NTA-agarose beads incubated with 1000 µg of whole cell lysate derived from 293T cells. **(c)** His-tagged based pulldowns using purified wildtype HIS-USP7 NTD^{DWGF} and double mutant HIS-USP7 NTD^{AAGF} bound to Ni^{2+}-NTA-agarose beads incubated with 1000 µg of whole cell lysate derived from 293T cells. In = Input, PD = Pulldown. For each pulldown, lane 1 (input) represents the purified HIS-USP7/SPOP construct, lane 2 (input) represents 50 µg of whole cell lysate derived from 293T cells, and lane 3 represents the result of the His-tagged based pulldown after extensive washing.

2.3.2 SPOP negatively regulates the stability of endogenous MDM2

To determine whether SPOP regulates the stability of endogenous MDM2, FLAG-SPOP was transfected into 293T cells in a dose dependent manner. DAXX, previously identified as an SPOP substrate targeted for degradation by the 26S proteasome, was used as a positive control (Kwon et al., 2006). BMI1 also identified as an SPOP substrate was used as a control as well, however unlike DAXX, ubiquitination of BMI1 mediated by SPOP-Cullin 3-RING E3 ubiquitin ligase complex serves a regulatory function related to recruitment to the X chromosome rather than degradation by the 26S proteasome (Hernandez-Munoz et al., 2005). As shown in **(Figure 2-4A)**, upon overexpression of FLAG SPOP, the endogenous levels of MDM2 decrease in a dose dependent manner similar to DAXX and unlike BMI1, where no changes in stability were observed. Moreover, siRNA-mediated knockdown of endogenous SPOP in U2OS cells slightly increased the endogenous levels of MDM2 similar to DAXX, where BMI1 levels remain once again unchanged **(Figure 2-4B)**. Together, the results suggest that SPOP negatively regulates the stability of MDM2.

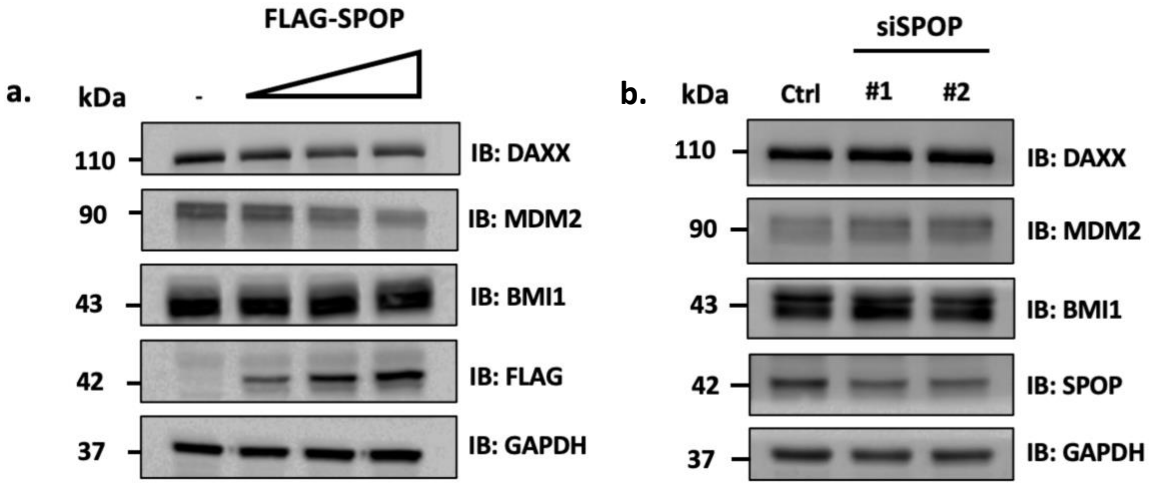

Figure 2-4. SPOP regulates the stability of endogenous MDM2. (a) Western blot of WCLs of 293T cells transfected with the indicated plasmid in a dose dependent manner (5, 7.5, and 10 μg) for 24 hours. **(b)** Western blot of WCLs of U2OS cells transfected with 50 nM of control or siRNAs against SPOP for 72 hours.

2.3.3 SPOP regulates MDM2 stability in a proteasome-dependent manner

We next investigated whether SPOP regulates the stability of MDM2 in a proteasome-dependent manner by first verifying that the ubiquitin-proteasome system is involved in MDM2 stability. As seen in **(Figure 2-5A)**, treatment with the proteasome inhibitor, MG132, increased MDM2 levels compared to the DMSO control in 293T, U2OS, and HeLa cells. Moreover, as seen in **(Figure 2-5B)**, overexpression of FLAG-SPOP followed by treatment with MG132 slightly rescued SPOP-mediated degradation of MDM2 in U2OS cells. Considering that another major pathway regulating protein degradation is mediated by the lysosome, we wanted to determine if SPOP targets MDM2 for lysosomal degradation. In contrast to the proteasomal inhibitor MG132, the lysosome inhibitor, chloroquine, had no effect on SPOP-mediated degradation of MDM2 **(Figure 2-5C)**. Overall, these results indicated that SPOP negatively regulates the stability of MDM2 potentially via the ubiquitin-proteasome degradation pathway instead of the lysosomal-degradation pathway.

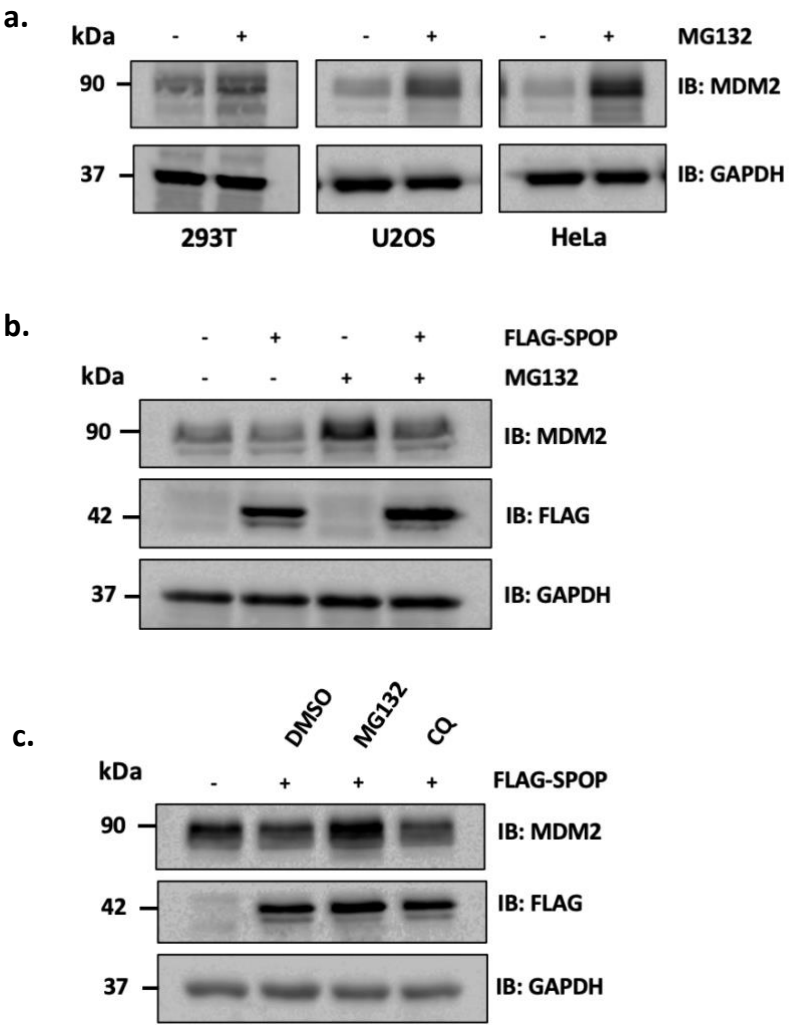

Figure 2-5. SPOP regulates MDM2 stability in a proteasome-dependent manner. (a) Western blot of WCLs of 293T, U2OS, and HeLa cells treated with 10 μM MG132 for 8 hours. **(b)** Western blot of WCLs of U2OS cells transfected with the indicated plasmids for 24 hours, followed by treatment with 20μM MG132 or DMSO for 4 hours. **(c)** Western blot of WCLs of U2OS cells transfected with the indicated plasmids for 24 hours, followed by treatment with 20 μM MG132 for 10 hours, 20 μM chloroquine (CQ) for 9 hours, or DMSO for 10 hours.

2.4 Discussion

The objective of this project was to identify a novel substrate of SPOP and characterize its mode of binding and regulation to provide further insight on the molecular mechanisms in which SPOP contributes to prostate cancer development. Here, we demonstrated that SPOP interacts specifically with MDM2 through the ^{130}DWGF^{133} motif within its N-terminal MATH domain in vitro. We further showed that SPOP negatively regulates the stability of MDM2 in vivo via the ubiquitin-proteasome degradation pathway. Together, these results suggest that MDM2 may be a novel substrate of SPOP.

2.4.1 SPOP interacts with MDM2, through the "DWGF" motif in its N-terminal MATH domain

Analysis of the full-length protein sequence of MDM2 revealed the presence of two putative SPOP binding consensus motifs: ^{156}PSTSS^{160} and ^{397}PSTSS^{401} suggesting that SPOP may interact with MDM2. Previous studies have shown that the N-terminal MATH domain of SPOP is responsible for substrate recognition and binding (Mani, 2014). Moreover, mutations in SPOP associated with prostate cancer are localized within the MATH domain, preventing substrate binding (Cuneo & Mittag, 2019; Batra & Lai, 2014). To determine if SPOP can interact with MDM2 through its N-terminal MATH domain, we employed a series of His-tagged based pulldowns using the following purified constructs bound to Ni-NTA agarose beads: wildtype HIS-SPOP MATH^{DWGF}, double mutant HIS-SPOP MATH^{DAGA}, and prostate cancer association mutants, HIS-SPOP MATH^{DWGV} and HIS-SPOP MATH^{DDGF}. After incubation with lysate derived from 293T cells and extensive washing, the results of the His-tagged based pulldowns show that endogenous MDM2 interacts with wildtype HIS-SPOP MATH^{DWGF}, whereas this interaction is abolished with the double mutant HIS-SPOP MATH^{DAGA} and prostate cancer associated mutant HIS-SPOP MATH^{DDGF}. Surprisingly, MDM2 was found to slightly interact with the prostate cancer associated mutant HIS-SPOP MATH^{DWGV}, however, this interaction is not as strong in comparison to the wildtype HIS-SPOP MATH^{DWGF}. This weak interaction may be a result of the hydrophobic nature of the amino acid residue phenylalanine being retained by the hydrophobic amino acid residue, valine, suggesting that the prostate cancer associated SPOP mutant, F113V, may be capable of binding and promoting the polyubiquitination and degradation of its substrates to a lesser extent compared to wildtype SPOP. However, in contrast to this, previous studies have

demonstrated that the prostate cancer associated SPOP mutant, F113V, is defective in binding, polyubiquitinating, and degrading various substrates in vivo such as the activating transcription factor 2 (ATF2), inverted formin 2 (INF2), AR, and Geminin (Ma et al., 2018; Jin et al., 2017; Geng et al., 2014; An et al., 2014; Ma et al., 2021). Consequently, this suggest that albeit HIS-SPOP MATH^{DWGV} slightly interacts with endogenous MDM2, as well as other established SPOP substrates, DAXX and BMI1, in vitro, this interaction may not occur in vivo. To verify this, co-immunoprecipitation and in vivo ubiquitination assays should be performed to determine if this SPOP mutant, F113V, interacts with endogenous MDM2 and promotes it polyubiquitination. Moreover, MDM2 levels should be examined upon overexpression of this prostate cancer associated SPOP mutant to determine if it destabilizes MDM2 in comparison to wildtype SPOP.

Overall, the results of this His-tagged based pulldowns indicate that the ^{130}DWGF^{133} motif within the N-terminal MATH domain of SPOP is essential for the recognition of and interaction with MDM2 in vitro. In order to determine if this interaction between SPOP and MDM2 occurs in vivo, endogenous co-immunoprecipitations in a normal benign prostate cell lines such as RWPE-1 and the malignant prostate cancer cell lines such as LNCaP, DU145, and PC3 need to be performed.

2.4.2 SPOP negatively regulates the stability of endogenous MDM2 in a proteasome-dependent manner

To determine whether SPOP regulates the stability of endogenous MDM2, FLAG-SPOP was transfected into 293T cells in a dose dependent manner. Upon overexpression of FLAG SPOP, the endogenous levels of MDM2 decreased in a dose dependent manner. Conversely, siRNA-mediated knockdown of endogenous SPOP in U2OS cells slightly increased the endogenous levels of MDM2. Together, these results suggest that SPOP negatively regulates the stability of MDM2. As mentioned previously, mutations in SPOP associated with prostate cancer have been identified within the MATH domain disrupting substrate binding and attachment of the proteolytic polyubiquitination signal, ultimately leading to increased cellular persistence of SPOP substrates (Mani, 2014). Consequently, we suspect that overexpression of prostate cancer associated mutants of SPOP such as F133V, W131G, and W131D will stabilize MDM2 levels in comparison to wildtype SPOP. However, in order to verify this, further experiments need to be performed.

MDM2 negatively regulates the activity, localization, and stability of the tumor suppressor, p53 (Zhao et al., 2014). p53 is a transcription factor that activates the expression of its target genes implicated in DNA repair, cell-cycle arrest, senescence, or apoptosis in response to cellular stressors such as DNA damage (Shadfan et al., 2012). Overexpression of MDM2 resulting in the inhibition of tumor suppressive activity of p53 has been reported in a wide variety of cancers (Nininahazwe et al., 2021). Inactivation of p53 favours the development of cancer due to the accumulation of unrepaired DNA damage and uncontrolled cell proliferation (Chène, 2003). Consequently, inhibiting the MDM2-p53 interaction to reactive p53 has emerged as a promising cancer therapy (Chène, 2003). Upon discovering that overexpression of wildtype SPOP negatively regulates the stability of MDM2, it would be interesting to further investigate the downstream functions of MDM2 on p53. It is suspected that since MDM2 polyubiquitinates p53 targeting it for degradation by the 26S proteasome, destabilization of MDM2 upon overexpression of wildtype SPOP, should stabilize p53 levels. In contrast, overexpression of prostate cancer associated mutants of SPOP, should stabilize MDM2, and thus destabilize p53 levels. If so, this may reveal a novel molecular mechanism in which SPOP promotes prostate cancer progression and development through the regulation of the MDM2 and its downstream function on p53. However, in order to verify this, further experiments need to be performed.

We next investigated whether SPOP regulates the stability of MDM2 in a proteasome-dependent manner. We found that overexpression of FLAG-SPOP followed by treatment with MG132 slightly rescued SPOP-mediated degradation of MDM2 in U2OS cells. It is important to note that treatment with MG132 did not completely rescue or block SPOP-mediated degradation of MDM2 as expected. This effect may be a result of insufficient treatment time with MG132. In contrast to the proteasome inhibitor, the lysosome inhibitor, chloroquine, had no effect on SPOP-mediated degradation of MDM2. Overall, these results indicate that SPOP negatively regulates the stability of MDM2 via the ubiquitin-proteasome degradation pathway instead of the lysosomal-degradation pathway. This finding is consistent with previous studies investigating whether SPOP regulates the stability of other substrates in a proteasome-dependent manner such as but limited to zinc finger and BTB domain containing 3 (ZBTB3), DNA damage inducible transcript 3 (DDIT3) Cyclin E1, and ATF2 (Jin et al., 2019; Zhang et al., 2014; Ju et al., 201l; Ma et al., 2018). More specifically, treatment with proteasome inhibitors MG132 and bortezomib blocked degradation of ZBTB3, ATF2, and DDIT3 mediated by SPOP whereas the lysosome inhibitor, chloroquine had

no effect (Jin et al., 2019; Ma et al., 2018; Zhang et al., 2014). Moreover, treatment with proteasome inhibitor MG132 blocked SPOP-mediated degradation of Cyclin E1, whereas treatment with the lysosomal inhibitors NH_4Cl or chloroquine had no effect (Ju et al., 201l).

The SPOP-Cullin 3-RING E3 ubiquitin ligase complex promotes the degradation of its substrates by the 26S proteasome through the addition of polyubiquitination chains with K48 linkages (Mani, 2014). Consequently, similar to other substrates of SPOP, we suspect that the SPOP-Cullin 3-RING E3 ubiquitin ligase complex polyubiquitinates MDM2. To determine whether degradation of MDM2 is the result of polyubiquitination mediated by SPOP-Cullin 3-RING E3 ubiquitin ligase complex, in vivo ubiquitination assays need to be performed by transfecting HA-Ub, HA-Ub and FLAG-MDM2, and HA-Ub, FLAG-MDM2, and MYC-SPOP, followed by immunoprecipitation of FLAG-MDM2. It is expected that overexpression of SPOP will increase the polyubiquitination of overexpressed MDM2 compared to the additional transfection controls.

CHAPTER 3: Investigation of SIRT2 as a Novel Substrate of USP7

3.1 Introduction

3.1.1 The Sirtuin Family

Sirtuins (SIRTs) are an evolutionarily conserved family of nicotinamide adenine dinucleotide $(NAD)^+$- dependent deacetylases, founded by the silent information regulator 2 (Sir2) in budding yeast, *Saccharomyces cerevisiae* (Kupis et al., 2016). Sirtuins target histone and non-histone substrates such as transcription factors, cell signalling molecules, DNA repair proteins, tumor suppressors, and structural proteins for deacetylation, and consequently regulate a range of biological processes, such as cell cycle progression, differentiation, genomic stability, gene expression, metabolism, and aging (Olmos et al., 2011). Sirtuins function to transfer the acetyl group from the lysine residue of a substrate to the NAD^+ cofactor, resulting in nicotinamide (NAM), 2′-*O*-acetyl-ADP-ribose, and a deacetylated substrate **(Figure 3-1)**. (Fiorino et al., 2014). In mammals, seven sirtuin homologs (SIRT1-SIRT7) have been identified, which share a conserved central NAD^+ binding catalytic core domain but possess distinct N-terminal and C-terminal domains of varying lengths that are targets of posttranslational modifications regulating substrate binding and sirtuin activity (Kupis et al., 2016; Flick & Lüscher, 2012). The seven mammalian sirtuins are ubiquitously expressed, however differ with respect to subcellular locations, isoforms, enzymatic activities, well as substrate targets (Flick & Lüscher, 2012; Kupis et al., 2016;). More specifically, SIRT1 is primarily located in the nucleus but can also shuttle to the cytoplasm, SIRT6 is located in the nucleus whereas SIRT7 is located in the nucleolus, SIRT3, SIRT4, and SIRT5 localize to the mitochondria, and SIRT2 is primarily located in the cytoplasm but can also localize to the nucleus in a cell-cycle dependent manner (Kupis et al., 2016). SIRT1, SIRT2, and SIRT3 exhibit strong deacetylase activity in contrast to SIRT4, SIRT5, SIRT6, and SIRT7 which exhibit weak deacetylase activity (Hirschey, 2011). Moreover, the SIRT5, SIRT3, and SIRT2 genes encode for 4, 2, and 3 isoforms respectively (Du et al., 2018; Bao et al., 2010; Maxwell et al., 2011). Of all the mammalian sirtuins, SIRT1 is the best characterized, whereas SIRT2 is one of the least studied (Kupis et al., 2016; North et al., 2014).

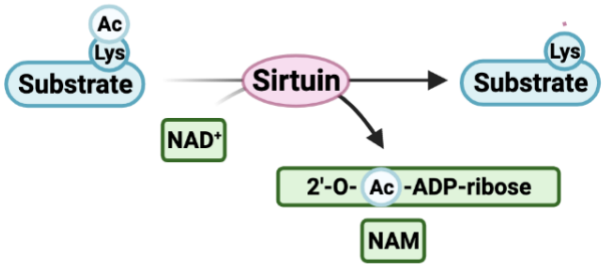

Figure 3-1. Sirtuins are NAD$^+$- dependent deacetylase. Sirtuins catalyze the transfer the acetyl group from the lysine residue of a substrate to the nicotinamide adenine dinucleotide $(NAD)^+$ resulting in nicotinamide (NAM), 2′-*O*-acetyl-ADP-ribose, and a deacetylated substrate. Modified from (Fiorino et al., 2014) with BioRender.com.

3.1.2 SIRT2 Structure and Regulatory Impact

The human SIRT2 gene is located on chromosome 19 (Zhang et al., 2017). The SIRT2 gene produces three distinct isoforms as a result of alternative splicing and/or alternative translational start sites: full-length isoform 1 containing all 16 exons and two translational start sites, isoform 2 where the exon 2 is spliced out resulting in pre-mature termination, and isoform 3 where exons 2, 3, and 4 are spliced out resulting in one translational start site (North & Verdin, 2007; Maxwell et al., 2011; Zhang et al., 2017). Isoforms 1 and 2 undergo phosphorylation at two sites: serine residues 368 and 372, and serine residues 331 and 335, respectively, which function to regulate mitotic progression and deacetylase activity (North & Verdin, 2007; Nahhas et al., 2007). Of the three isoforms, isoform 3 is the least characterized (Maxwell et al., 2011). As mentioned previously, SIRT2 is primarily a cytoplasmic protein, but can also shuttle to the nucleus, and as a result can target and deacetylate both cytoplasmic and nuclear proteins implicated in various processes ranging from cell cycle regulation, cancer progression, longevity, adipocyte differentiation, and lipid and glucose metabolism (de Oliveira et al., 2012). The first identified cytoplasmic substrate of SIRT2 was α-tubulin (North et al., 2003). It is suspected that deacetylation of α-tubulin at the lysine 40 residue by SIRT2 regulates microtubule dynamics and stability, however, the function of this modification currently remains unknown (North et al., 2003). Another cytoplasmic substrate of SIRT2 is the mitotic spindle assembly checkpoint protein kinase BubR1, previously implicated in aging in mice (North et al., 2014). SIRT2 deacetylates BubR1 at the lysine 668 residue which promote BubR1 stability, by inhibiting ubiquitination corresponding to degradation by the 26S proteasome (North et al., 2014). Interestingly, overexpression of SIRT2 in mice hypomorphic for BubR1 increases lifespan (North

et al., 2014). This finding links SIRT2 to longevity and aging as previously described in budding yeast, *Saccharomyces cerevisiae*, nematode, *Caenorhabditis elegans*, and fruit flies, *Drosophila melanogaster* with respect to the Sir2, sir2.1, and dsir2 homologs (Kaeberlein et al., 1999; Tissenbaum & Guarente, 2001; Rogina & Helfand, 2004). A notable nuclear substrate of SIRT2 is histone H4 (Vaquero et al., 2006). More specifically, SIRT2 shuttles to the nucleus by an unknown mechanism during the G2/M transition of mitosis (North & Verdin, 2007; Vaquero et al., 2006). In the nucleus, SIRT2 associates with chromatin, where it deacetylates the histone H4 lysine 16 (H4K16) (Vaquero et al., 2006). SIRT2 also regulates the deposition of H4K20me1 by deacetylating the lysine 90 residue of the histone methyltransferase, PR-SET7, promoting its enzymatic activity and localization to the chromatin (Serrano et al., 2013). The function of these histone modifications (H4K20me1 and H4K16) have been shown to regulate chromosomal condensation, genome stability during mitosis, as well as cell cycle progression (Serrano et al., 2013; Vaquero et al., 2006).

3.1.3 Project Overview

Here, we investigated whether SIRT2, an established SPOP substrate is a novel substrate of USP7. Initially, overexpressed and endogenous co-immunoprecipitations were performed to verify protein-protein interactions in vivo. In order to identify and map the domain mediating the interaction, His-tagged based pulldowns were performed using purified wildtype and mutated HIS-USP7 constructs. To determine whether USP7 regulates the stability of SIRT2, we examined endogenous levels of SIRT2 upon overexpression of MYC-USP7, and in wildtype and USP7 knockout HCT116 cell lines via western blot analysis.

3.2 Material and Methods

3.2.1 Cell Lines

The human osteosarcoma (U2OS) cell line was kindly provided as a gift by Dr. Samuel Benchimol (York University) and was cultured in McCoy's media (Wisent Inc.) supplemented with 10% fetal bovine serum (FBS, Gibco) and 1% Penicillin-Streptomycin (P/S, Wisent Inc.) at 37°C and 5% CO_2. The wildtype human colorectal carcinoma cell line (HCT116) and USP7 knockout human colorectal carcinoma cell line (HCT116 USP7$^{-/-}$) were kindly provided as a gift by Dr. Bert Vogelstein (John Hopkins) and were cultured in McCoy's media containing 10% FBS and 1% P/S.

3.2.2 Plasmids

Plasmids used for transfections were isolated and purified using the Plasmid Maxi Plus Kit (Qiagen) following the manufacturer's protocol. Before use, plasmids were verified by sequencing by the Centre for Applied Genomics (TCAG) operated by The Hospital for Sick Children (SickKids, Toronto). The plasmids used for mammalian transfection include: pcDNA3, pCAN/Myc-USP7^{WT}, and pcDNA3.1+/FLAG-SIRT2. pcDNA3.1+/FLAG-SIRT2 was kindly provided as a gift from Eric Verdin (Addgene plasmid # 13813; http://n2t.net/addgene:13813; RRID:Addgene_13813).

3.2.3 DNA Transfection

18-24 hours prior to transfection, cells were seeded into 10 cm plates to reach a confluency of 70-80% at the time of transfection. Media containing 10% FBS and 1% P/S was changed 30 minutes prior to transfection. Cells were transiently transfected with plasmids using Polyjet^{TM} In Vitro DNA transfection reagent (SignaGen Laboratories. Unless otherwise stated, 5 μg of plasmid DNA was transfected with 15 uL of Polyjet^{TM} per 10 cm plate. To reduce cytotoxicity, the media containing the PolyJet™/DNA complex was removed 5 hours after transfection and replaced with fresh media. Cells were then harvested 24 hours post-transfection.

3.2.4 Harvest, Lysis, and Sample Preparation

Cells were incubated with 0.25% trypsin-EDTA (Gibco) for 5 minutes at 37°C and 5% CO_2 followed by the addition of McCoys or DMEM media supplemented with 10% FBS, and 1% P/S to inhibit and neutralize further trypsinization. Detached cells were harvested by centrifugation at 1000 x g for 5 minutes at room temperature. The cellular pellet was washed twice with ice-cold PBS to remove residual media and was either stored at -80°C or immediately lysed with 1% NP-40 Buffer [50 mM Tris-HCl, pH 8, 150 mM NaCl, 1% (v/v) NP-40, 1 mM benzamidine, 1 mM PMSF, 1 x cOmplete protease inhibitor cocktail (Roche)] or RIPA buffer [50 mM Tris-HCl, pH 8, 150 mM NaCl, 1% (v/v) NP-40, 0.5% sodium deoxycholate, 0.1% SDS, 1 mM benzamidine, 1 mM PMSF, 1 x cOmplete protease inhibitor cocktail (Roche)] by mechanical rotation for 45 minutes at 4°C or by sonication at 10% amplitude for 0.5 seconds ON and 10 seconds OFF, a total of three times on ice (Sonic Dismembrator Model 500, Fisher Scientific). Cellular debris was pelleted by centrifugation at 17,000 x g for 15 minutes at 4°C and the supernatant was collected. Protein concentration was determined using the BCA reagent following the manufacturer's instructions (Thermo Scientific Pierce BCA Protein Assay Kit, 23225). Samples containing equal amounts of protein were prepared by boiling the lysate with 1 x SDS loading dye [5% β-mercaptoethanol, 10% SDS, 30% glycerol, 250 mM Tris-HCl, pH 6.8, 0.02% Bromophenol blue] for 5 minutes. Samples were stored at -20°C for later use or immediately resolved on a 12% SDS-polyacrylamide gel.

3.2.5 Immunoblotting

Samples containing equal amounts of proteins were separated by electrophoresis set to 160V for 1.5 hours using a 12% SDS-polyacrylamide gels. Resolved proteins were transferred to a 0.45 μm Immobilon-P PVDF membrane (Millipore) activated with methanol and equilibrated with 1 x Western Transfer buffer [25 mM Tris, pH 8.3, 192 mM Glycine, 20% methanol]. Traditional wet transfers were performed at 4°C and on ice, set to 80V for 1.5 to 2 hours. The membrane was then blocked in 5% non-fat dry milk in 1 x PBS-T [1 x PBS, 0.1% Tween-20] for 1 hour at room temperature. After blocking, the membrane was cut into strips according to the visible protein marker and incubated with the corresponding diluted primary antibody overnight at 4°C with gentle rocking. The following day, the membranes were washed with 1 x PBS-T in 5-minute intervals a total of 3 times, followed by incubation with diluted secondary rabbit or mouse

antibody conjugated with horseradish peroxidase for 1 hour at room temperature. The membranes were then washed a total of three times with 1 x PBS-T in 15-minute intervals and incubated with Amersham ECL Prime Western Blotting Detection Reagent (GE Healthcare) for 2-3 minutes. Excess ECL reagent was removed, and the signals were detected using MicroChemi (DNR BioImaging System).

3.2.6 Antibodies

The following primary antibodies were used for immunoblotting: anti-GAPDH (0411) mouse monoclonal (Santa Cruz Biotechnology Inc, 47724), anti-His (H-3) mouse monoclonal (Santa Cruz Biotechnology Inc, 8036), anti-SIRT2 rabbit polyclonal (MilliporeSigma, 09-843), anti-SIRT2 (EPR20411-105) rabbit monoclonal (Abcam, ab211033), anti-USP7 (clone 1G7) mouse monoclonal (MilliporeSigma, 05-1946), anti-FLAG (clone M2) mouse monoclonal (Sigma-Aldrich, F1804), anti-MYC (clone 4A6) mouse monoclonal (MilliporeSigma, 05-724), and anti-BubR1 rabbit polyclonal (Bethyl Laboratories Inc, A300-386A) **(Table 3-1)**. The following secondary antibodies were used for immunoblotting: anti-mouse IgG HRP-conjugated goat polyclonal (ThermoFisher Scientific, 31430), anti-rabbit IgG HRP-linked (Cell Signalling Technology, 7074), and VeriBlot for IP detection HRP-linked (Abcam, ab131366) **(Table 3-1)**. The following primary antibodies were used for immunoprecipitation: anti-SIRT2 rabbit polyclonal (MilliporeSigma, 09-843), normal rabbit IgG (Santa Cruz Biotechnology In, 2027), anti-USP7 (clone 1G7) mouse monoclonal (MilliporeSigma, 05-1946), and normal mouse IgG (Santa Cruz Biotechnology In, 2025) **(Table 3-1)**.

Table 3-1. List of primary and secondary antibodies.

Target	Company	Catalogue Number	Species	Dilution	Application
His	Santa Cruz Biotechnology Inc	sc-8036	Mouse	1:1000 in 5% non-fat dry milk in 1 x PBS-T	Immunoblotting
GAPDH	Santa Cruz Biotechnology Inc	sc-47724	Mouse	1:10,000 in 5% non-fat dry milk in 1 x PBS-T	Immunoblotting
SIRT2	MilliporeSigma	09-843	Rabbit	1:1000 in 2% non-fat dry milk in 1 x PBS-T, 2 or 3 ug per 1 mg of protein	Immunoblotting, Immunoprecipitation
SIRT2	Abcam	ab211033	Rabbit	1:2000 in 5% non-fat dry milk in 1 x PBS-T	Immunoblotting
USP7	MilliporeSigma	05-1946	Mouse	1:2000 in 5% non-fat dry milk in 1 x PBS-T, 2-3 ug per 1 mg of protein	Immunoblotting, Immunoprecipitation
FLAG	Sigma-Aldrich	F1804	Mouse	1:2000 in 5% non-fat dry milk in 1 x PBS-T	Immunoblotting
MYC	MilliporeSigma	05-724	Mouse	1:10,000 in 5% non-fat dry milk in 1 x PBS-T	Immunoblotting
BubR1	Bethyl Laboratories Inc	A300-386A	Rabbit	1:2000 in 5% non-fat dry milk in 1 x PBS-T	Immunoblotting
normal mouse IgG	Santa Cruz Biotechnology Inc	sc-2025	Mouse	2-3 ug per 1 mg of protein	Immunoprecipitation
normal rabbit IgG	Santa Cruz Biotechnology Inc	sc-2027	Rabbit	2-3 ug per 1 mg of protein	Immunoprecipitation
anti-mouse IgG HRP-conjugated	ThermoFisher Scientific	31430	Goat	0.1:2000 in 2% non-fat dry milk in 1 x PBS-T	Immunoblotting
anti-rabbit IgG HRP-linked	Cell Signalling Technology	7074	Goat	1:2000 in 5% non-fat dry milk in 1 x PBS-T	Immunoblotting
VeriBlot for IP detection HRP-linked	Abcam	ab131366	Rabbit	1:10,000 in 5% non-fat dry milk in 1 x PBS-T	Immunoblotting

3.2.7 Endogenous Co-Immunoprecipitation of SIRT2 and USP7

Cells were lysed in 1% NP-40 buffer [50 mM Tris-HCl, pH 8, 150 mM NaCl, 1% (v/v) NP-40, 1 mM benzamidine, 1 mM PMSF, 1 x cOmplete protease inhibitor cocktail (Roche)] under mechanical rotation for 45 minutes at 4°C. The cell lysate was centrifuged at 17,000 x g for 15 minutes at 4°C to pellet cellular debris. Protein concentration of the clarified lysate was measured using the BCA reagent following the manufacturer's instructions (Thermo Scientific Pierce BCA Protein Assay Kit, 23225). The cell lysate was pre-cleared with 1.0 μg of normal rabbit IgG antibody and 20 uL of pre-blocked Protein A/G PLUS-Agarose beads (Santa Cruz Biotechnology Inc, sc-2003). 1000 μg of the pre-cleared lysate was incubated with either 2 μg of primary rabbit polyclonal antibody against SIRT2 or normal rabbit IgG antibody as a negative control, in a total volume of 500 uL, overnight rotating at 4°C. The following day, 50 uL of Protein A/G PLUS-Agarose beads were pre-blocked with 5% BSA in 1 x PBS for 1 hour rotating at 4°C, before use to reduce non-specific binding. 50 uL of pre-blocked Protein A/G PLUS-Agarose beads were added and incubated for 1 hour rotating at 4°C to capture the immunocomplex, followed by centrifugation at 1000 x g for 5 minutes at 4°C. The immunocomplex now bound to Protein A/G PLUS-Agarose beads were washed 3 times with 500 uL of 1 x PBS followed by centrifugation at 1000 x g for 5 minutes at 4°C. Samples were prepared by boiling the Protein A/G PLUS-Agarose beads with 40 uL of 1 x SDS-PAGE loading dye for 5 minutes. The supernatant and beads were separated by centrifugation at 1000 x g for 5 minutes at 4°C and the supernatant was resolved on a 10% SDS-polyacrylamide gel, followed by immunoblotting with the indicated antibodies.

3.2.8 Overexpressed Co-Immunoprecipitation of FLAG-SIRT2 and MYC-USP7

U2OS cells in 10 cm plates were co-transfected with 2.5 μg of FLAG-SIRT2 and 2.5 μg of MYC-USP7 and harvested 24 hours post-transfection. Reciprocal co-immunoprecipitations of exogenously expressed MYC-USP7 and FLAG-SIRT2 were performed as previously described above using 2 μg of primary rabbit polyclonal antibody against SIRT2 or normal rabbit IgG antibody as a negative control, and 2 μg of primary mouse monoclonal antibody against USP7 or normal mouse IgG used as a negative control.

3.2.9 FLAG-SIRT2 and USP7 Co-Immunoprecipitation

U2OS cells in 10 cm plates were co-transfected with 2.5 μg of FLAG SIRT2 and harvested 24 hours post-transfection. Co-immunoprecipitation of exogenously expressed FLAG-SIRT2 was performed as previously described above using 2 μg of primary rabbit polyclonal antibody against SIRT2 or normal rabbit IgG antibody as a negative control.

3.2.10 Protein Expression and Purification

6xHis tagged SPOP MATH constructs were expressed in BL21 mgk *Escherichia coli* (E.coli) in Luria Broth (LB) media (Bioshop) with 100 μg/ml ampicillin (Bioshop) and 50 μg/ml kanamycin (Bioshop) **(Table 3-2)**. The cultures were grown at 37°C at 200 rpm until the OD_{600nm} of 0.8 was reached, followed by induction with 0.4 mM of Isopropyl β-D-1 thiogalactopyranoside (IPTG, Bioshop) overnight at 16°C at 200 rpm. The cells were pelleted by centrifugation at 6,000 x g at room temperature for 20 minutes with a JLA 16.250 Beckman rotor (Beckman Coulter Avanti J-E centrifuge). The pellets were resuspended in ice-cold binding/lysis buffer [50 mM Tris, pH 7.5, 500 mM NaCl, 5 mM Imidazole, and 5% Glycerol] with protease inhibitors [1 mM benzamidine, 1 mM PMSF, 1 x cOmplete protease inhibitor cocktail (Roche)]. The resuspended pellets were sonicated on ice at 30% amplitude for a total of 4 minutes (15 seconds ON, 30 seconds OFF) (Branson Digital Sonifier D450). The supernatants were collected by centrifugation at 30,000 x g at 4°C for 30 minutes with a JA-25.50 Beckman rotor (Beckman Coulter Avanti J-E centrifuge). The supernatants were then incubated with 1 mL of Ni^{2+}-NTA-agarose beads (Qiagen) for 1 hour at 4°C on the rotator. After incubation, the beads were washed a total of six times with ice-cold wash buffer [50 mM Tris, pH 7.5, 500 NaCl, 20 mM Imidazole, and 5% Glycerol] and stored at -80°C until needed.

All 6xHis tagged USP7 NTD and CTD constructs were expressed in BL21 mgk E.coli, induced with IPTG, pelleted, and stored at -80°C by a previous student in the Saridakis lab **(Table 3-2)**. Full-length His-USP7 construct was expressed in *Spodoptera frugiperda* (Sf9) cells using the baculovirus expression system and stored at -80°C by a previous student in the Saridakis lab. These constructs were purified following the same method described previously.

Table 3-2. Plasmid constructs used for bacterial expression and purification.

Protein	Vector	Tag	Residues	Mutation
6xHis-SPOP MATH^{DWGF}	pET15b	His	28-166	WT
6xHis-SPOP MATH^{DAGA}	pET15b	His	28-166	W131A/F133A
6xHis-USP7 NTD^{DWGF}	pET15b	His	62-205	WT
6xHis-USP7 NTD^{AAGF}	pET15b	His	62-205	D164A/W165A
6xHis-USP7 CTD	p15TVL	His	535-1102	WT
6xHis-USP7	pFastBac	His	Full-length	WT

3.2.11 His Pull-down Assay

U2OS cells transfected with 5 ug of FLAG-SIRT2 for 24 hours were harvested and lysed in ice-cold 1% NP-40 buffer [50 mM Tris-HCl, pH 8, 150 mM NaCl, 1% (v/v) NP-40] containing protease inhibitors [1 mM benzamidine, 1 mM PMSF, 1 x cOmplete protease inhibitor cocktail (Roche)] on a rotary shaker at 4°C for 45 minutes. The cell lysate was centrifuged at 17,000 x g for 15 minutes at 4°C to pellet cellular debris. Protein concentration of the clarified lysate was measured using the BCA assay following the manufacturer's instructions (Thermo Scientific Pierce BCA Protein Assay Kit, 23225). 500 μg of lysate containing overexpressed FLAG-SIRT2 was incubated with 20 uL of pre-blocked Ni^{2+}-NTA-agarose beads with bound 6xHis tagged USP7 and SPOP constructs in a total volume of 500 uL. After incubation at 4°C for 2 hours, the beads were washed three times with 500 uL of wash buffer [50 mM Tris-HCl, pH 7.4, 250 mM NaCl, 0.05% NP-40] in 1-minute intervals on a rotating device at 4°C. Samples were prepared by boiling the 6xHis tagged USP7 and SPOP constructs bound to Ni^{2+}-NTA agarose beads with 1 x SDS loading dye for 5 minutes. Samples were resolved on 12% SDS-polyacrylamide gels followed by immunoblotting with the indicated antibodies.

3.2.12 MG132 Treatment

HCT116 and HCT116 USP7$^{-/-}$ cells were treated with 40 μM MG132 for 1 hour to inhibit degradation mediated by the 26S proteasome. DMSO was used as a negative control.

3.3 Results

3.3.1 Analysis of SIRT2 as a potential substrate of USP7

In order to screen for potential novel substrates of USP7, we thoroughly reviewed current literature on SPOP and its substrates and performed a bioinformatic search using the Eukaryotic Linear Motif (ELM) computational biology resource to detect for USP7 binding consensus motifs (P/A/ExxS). Analysis of the full-length protein sequence of SIRT2, an established substrate of SPOP, revealed the presence of one putative USP7 binding consensus motif: ^{363}PSTS^{366}. Alignment of the putative USP7 binding site of SIRT2 with the USP7 binding consensus motifs of established USP7 substrates/binding partners suggests that USP7 may interact with SIRT2 through its N-terminal TRAF-like domain **(Figure 3-2)**. Other members of the mammalian sirtuin family, SIRT1 and SIRT7, have also been identified as USP7 substrates, albeit the exact binding sites mediating the interaction are not verified (Song et al., 2019; Jiang et al., 2017). However, sequence analysis of SIRT1 and SIRT7 using ELM reveals the presence of the following corresponding USP7 binding consensus motifs: ^{171}ASSS^{174} and ^{375}PLSS^{378}. These findings together prompted us to investigate whether SIRT2 is a novel substrate of USP7.

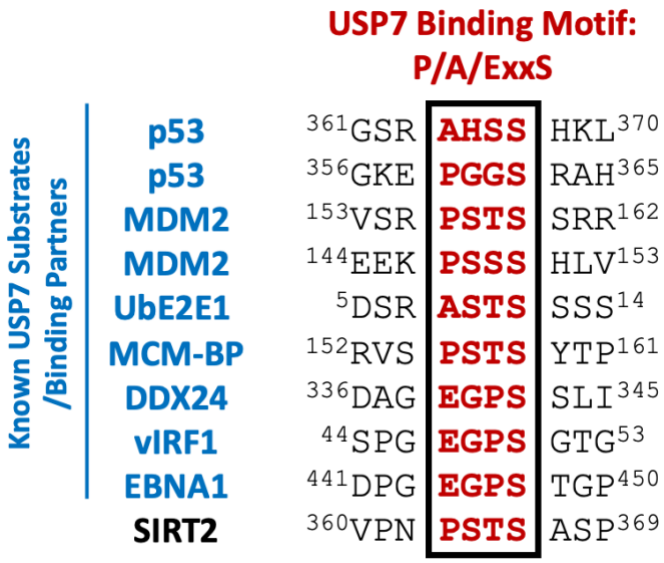

Figure 3-2. Putative USP7 binding site of SIRT2. Sequence alignment and comparison of the putative USP7 binding site in SIRT2 with the USP7 binding consensus motif defined in known USP7 substrates.

3.1.2 USP7 and SIRT2 interact in vivo

To determine if SIRT2 is a novel USP7 substrate, we first examined whether exogenously expressed MYC-USP7 and FLAG-SIRT2 interact in vivo, by performing reciprocal co-immunoprecipitations using anti-SIRT2 rabbit polyclonal and anti-USP7 mouse monoclonal antibodies, where normal rabbit IgG and normal mouse IgG were used as a control, respectively. As shown in **(Figure 3-3A)**, exogenously expressed FLAG-SIRT2 was co-immunoprecipitated by MYC-USP7 and similarly, MYC-USP7 was co-immunoprecipitated by FLAG-SIRT2, suggesting an interaction between the two exogenously expressed proteins in U2OS cells. Next, we investigated if exogenously expressed FLAG-SIRT2 interacts with endogenous USP7 by performing co-immunoprecipitations as described previously. As shown in **(Figure 3-3B)**, endogenous USP7 was co-immunoprecipitated by FLAG-SIRT2. To verify if this interaction occurs endogenously, we once again performed co-immunoprecipitations using anti-SIRT2 rabbit polyclonal antibody and normal rabbit IgG as a control in three different cell lines: U2OS, 293T, and HeLa. As shown in **(Figure 3-3C)**, USP7 was co-immunoprecipitated by SIRT2 in all cell lines suggesting an endogenous interaction between the two proteins. Overall, our data together demonstrates that SIRT2 and USP7 physically interact with each other in vivo.

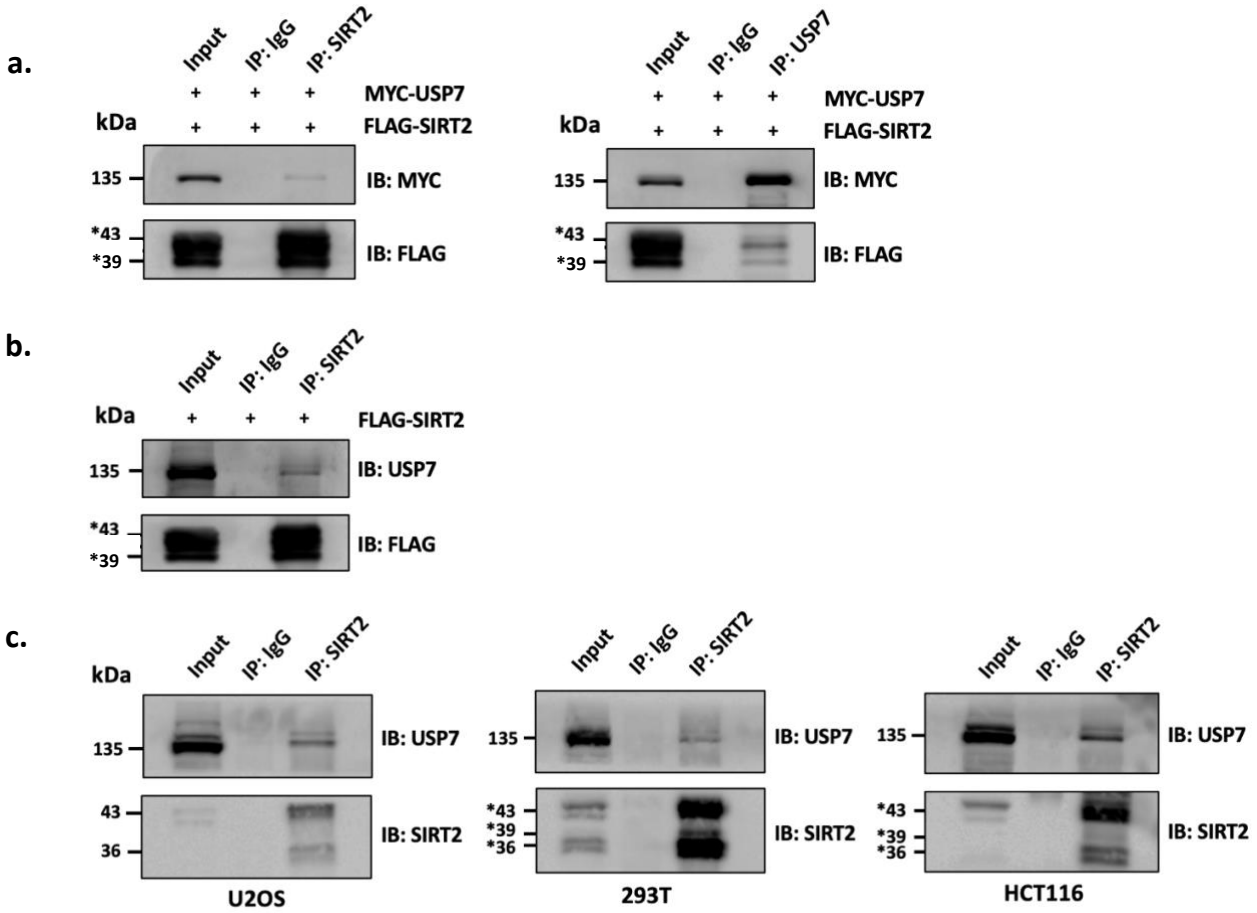

Figure 3-3. USP7 and SIRT2 interact in vivo. (a) Exogenous MYC-USP7 and FLAG-SIRT2 interact in vivo. Western blot of WCLs and co-IP samples of U2OS cells co-transfected with pcDNA3.1+/FLAG-SIRT2 and pCAN/MYC-USP7. **(b)** Exogenous FLAG-SIRT2 interacts with endogenous USP7 in vivo. Western blot of WCLs and co-IP samples of U2OS cells transfected with pcDNA3.1+/FLAG-SIRT2. **(c)** Endogenous USP7 and SIRT2 interact in vivo in different cell lines. Western blot of WCLs and co-IP samples of U2OS, 293T, and HCT116 cells. IP= Immunoprecipitation * Exogenously expressed SIRT2 can be translated from two different start sites. Endogenous SIRT2 exists as multiple isoforms (43 kDa, 39 kDa, and 36 kDa) due to either alternative splicing and/or translational start sites. Two of the SIRT2 isoforms (43 kDa and 36 kDa) migrate as two distinct species due to the post-translational phosphorylation modifications.

3.1.3 USP7 interacts with SIRT2 via the "DWGF" motif within its N-terminal TRAF-like domain

Previous studies have shown that the N-terminal TRAF-like domain containing the ^{164}DWGF^{167} motif and the C-terminal ubiquitin-like (Ubl2) subdomain containing the ^{761}MDGD^{764} motif of USP7 mediates its interaction with substrates and/or binding partners containing the P/A/ExxS motif and the KxxxK motif, respectively (Saridakis et al., 2005; Sarkari et al., 2013; Pfoh et al., 2015). To map which substrate binding domains of USP7 mediates its interaction with SIRT2, we employed a series of His-tagged based pulldowns using the following purified constructs: full length HIS-USP7, wildtype HIS-USP7 NTD^{DWGF}, double mutant HIS-USP7 NTD^{AAGF}, and wildtype HIS-USP7 CTD **(Figure 3-4B)**. Since SIRT2 has been previously established as an SPOP substrate, and the substrate binding MATH domain of SPOP exhibits sequence and structural similarity between the substrate binding N-terminal TRAF-like domain of USP7, we also employed His-tagged based pulldowns using purified wildtype HIS-SPOP MATH^{DWGF} and double mutant HIS-SPOP MATH^{DAGA} as a positive control **(Figure 3-4B)**. The indicated purified His-tagged constructs bound to Ni-NTA agarose beads were incubated with lysate derived from U2OS cells transfected with FLAG-SIRT2. As shown previously in vivo, full length HIS-USP7 containing both substrate binding domains interacts with FLAG-SIRT2 in vitro. As expected, FLAG-SIRT2 interacts with wildtype HIS-SPOP MATH^{DWGF}, whereas this interaction is abolished with double mutant HIS-SPOP MATH^{DAGA}, in which residue Trp^{131} and Phe^{133} were changed to alanine residues. Notably and similar to the pulldowns with HIS-SPOP MATH, FLAG-SIRT2 interacts with wildtype HIS-USP7 NTD^{DWGF}, whereas this interaction is abolished with the double mutant HIS-USP7 NTD^{AAGF} in which residue Asp^{164} and Trp^{165} were changed to alanine residues. DAXX, an established substrate of both USP7 and SPOP substrate, was used an additional control. As expected, endogenous DAXX binds to wildtype HIS-SPOP MATH^{DWGF} and HIS-USP7 NTD^{DWGF}, and does not bind to the double mutant HIS-SPOP MATH^{DAGA} and HIS-USP7 NTD^{AAGF}. Lastly, FLAG-SIRT2 does not appear to interact with HIS-USP7 CTD. Overall, the results of this His-tagged based pulldowns indicate that the ^{164}DWGF^{167} motif within the N-terminal TRAF-like domain of USP7 mediates its interaction with overexpressed FLAG-SIRT2 in vitro **(Figure 3-4A)**.

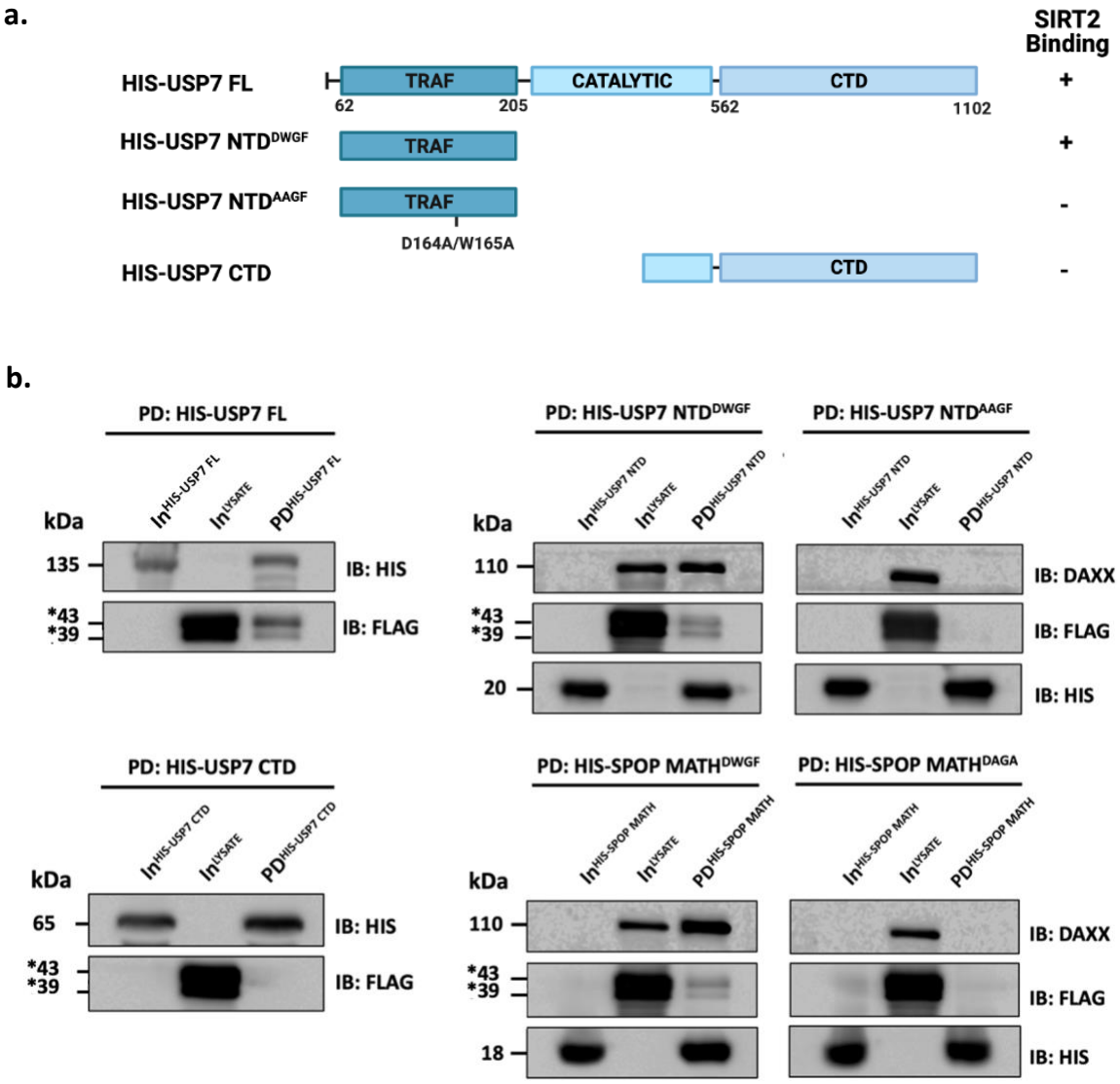

Figure 3-4. USP7 interacts with SIRT2 via the "DWGF" motif within its N-terminal TRAF-like domain. **(a)** Schematic representation of HIS-USP7 constructs. Binding capacity of FLAG-SIRT2 to HIS-USP7 constructs is indicated with the symbol (+/-). **(b)** His-tagged based pulldowns using purified wildtype HIS-USP7 NTD^{DWGF}, double mutant HIS-USP7 NTD^{AAGF}, HIS-USP7 CTD, and full-length HIS-USP7 bound to Ni^{2+}-NTA-agarose beads incubated with 500 µg of whole cell lysate derived from U2OS cells transfected with 5 µg of FLAG-SIRT2. Purified wildtype HIS-SPOP MATH^{DWGF} and HIS-SPOP MATH^{DAGA} bound to Ni^{2+}-NTA-agarose beads were used as positive controls. In = Input, PD = Pulldown. For each pulldown, lane 1 (input) represents the purified HIS-USP7/SPOP construct, lane 2 (input) represents 50 µg the whole cell lysate derived from U2OS cells transfected with 5 µg of FLAG-SIRT2, and lane 3 represents the result of the His-tagged based pulldown after extensive washing. *Exogenously expressed SIRT2 can be translated from two different start sites. Endogenous SIRT2 exists as multiple isoforms (43 kDa, 39 kDa, and 36 kDa) due to either alternative splicing and/or translational start sites. Two of the SIRT2 isoforms (43 kDa and 36 kDa) migrate as two distinct species due to the post-translational phosphorylation modifications.

3.1.4 SIRT2 stability is UPS and USP7 dependent

Next, considering that USP7 plays a fundamental role in the stability of its substrates by cleaving the ubiquitin signal associated with proteasomal degradation, we investigated if USP7 and the ubiquitin proteasome system are involved in SIRT2 stability (Bojagora & Saridakis, 2020). First, we compared the levels of SIRT2 in wildtype human colorectal carcinoma cell line (HCT116) and USP7 knockout (KO) human colorectal carcinoma cell line (HCT116 USP7$^{-/-}$) after treatment with the proteasomal inhibitor MG132 or DMSO as a control **(Figure 3-5A)**. In both wildtype and USP7 KO HCT116 cell lines treatment with MG132 increased the endogenous levels of SIRT2 compared to the DMSO control, suggesting the involvement of the ubiquitin proteasome system in SIRT2 stability. Moreover, SIRT2 levels were slightly lower in the USP7 KO HCT116 cell line compared to the wildtype HCT116 cell line after treatment with DMSO suggesting that USP7 may also play a role in SIRT2 stability. This was further observed when comparing SIRT2 levels in the wildtype and USP7 KO HCT116 cell lines without the additional treatment of MG132 or DMSO as seen in **(Figure 3-5B)**. Additionally, upon overexpression of MYC-USP7 in a dose-dependent manner in U2OS cells, we observed a slight increase in SIRT2 levels **(Figure 3-5C)**. Together, these results indicate that USP7 regulates the stability of SIRT2.

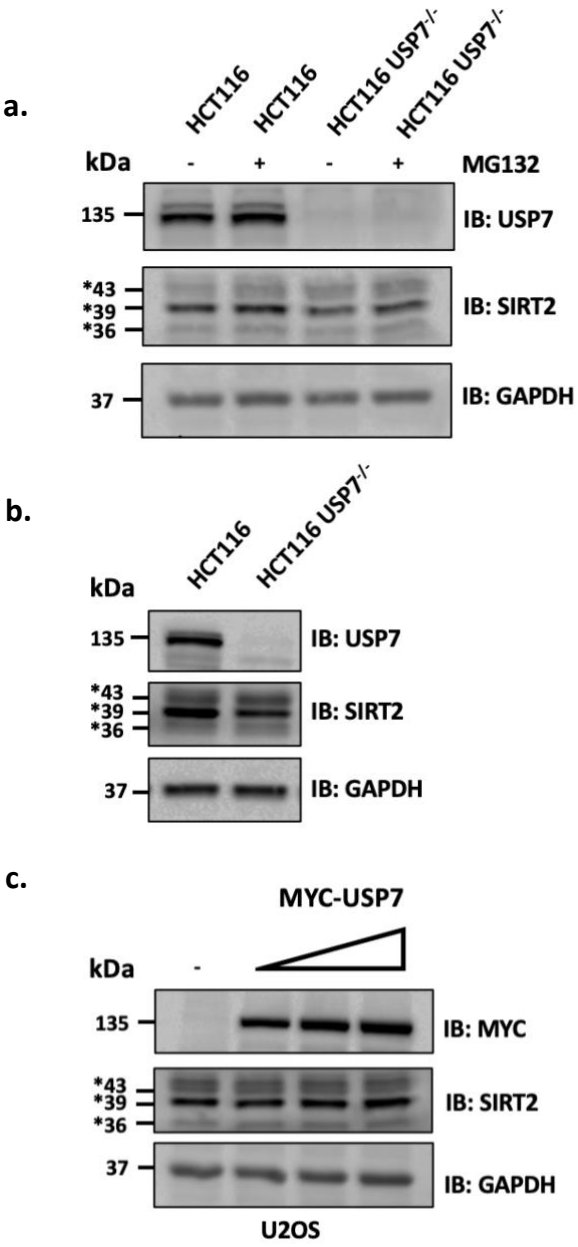

Figure 3-5. SIRT2 stability is UPS and USP7 dependent. (a) Western blot of WCLs of HCT116 and HCT116 USP7$^{-/-}$ cells treated with 40μM MG132 or DMSO for 1 hour. **(b)** Western blot of WCLs of HCT116 and HCT116 USP7$^{-/-}$ cells. **(c)** Western blot of WCLs of U2OS cells transfected with the indicated plasmid in a dose dependent manner (1, 2.5, and 5 μg) for 24 hours. *Endogenous SIRT2 exists as multiple isoforms (43 kDa, 39 kDa, and 36 kDa) due to either alternative splicing and/or translational start sites. Two of the SIRT2 isoforms (43 kDa and 36 kDa) migrate as two distinct species due to the post-translational phosphorylation modifications.

3.1.4 USP7 may regulate SIRT2 function

We next investigated whether or not USP7 regulates the function of SIRT2 by examining the downstream effects on BubR1, a mitotic checkpoint kinase previously established as a SIRT2 substrate, in response to stable USP7 knockout. As seen in **(Figure 3-6)**, SIRT2 levels and notably, BubR1 levels are decreased in the USP7 KO HCT116 cell line in comparison to the wildtype HCT116 cell line suggesting that USP7 may regulate SIRT2 downstream function. This finding is consistent with literature examining the relationship between SIRT2 and BubR1; SIRT2 has been reported to interact and stabilize BubR1 levels by deacetylation of residue K668 (North et al., 2014).

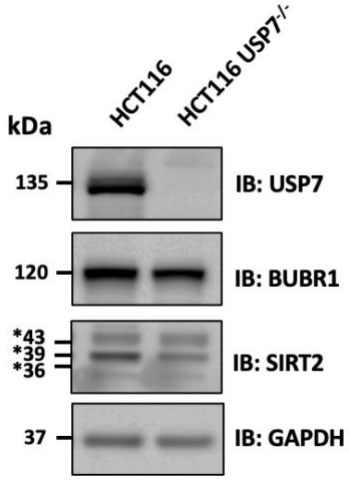

Figure 3-6. USP7 may regulate SIRT2 downstream function. Western blot of WCLs of HCT116 and HCT116 USP7$^{-/-}$ cells. *Endogenous SIRT2 exists as multiple isoforms (43 kDa, 39 kDa, and 36 kDa) due to either alternative splicing and/or translational start sites. Two of the SIRT2 isoforms (43 kDa and 36 kDa) migrate as two distinct species due to the post-translational phosphorylation modifications.

3.4 Discussion

The objective of this project was to identify a novel substrate of USP7 and characterize its mode of binding and regulation. We identified SIRT2, an NAD^+-dependent deacetylase, as a novel substrate of USP7. We showed that USP7 interacts with SIRT2 in vivo as well as in vitro. We further demonstrated that the N-terminal TRAF-like domain of USP7 is critical in mediating its interaction with SIRT2 in vitro. Finally, we established that USP7 regulates SIRT2 stability and downstream function.

3.4.1 USP7 and SIRT2 interact in vivo

To determine if SIRT2 and USP7 physically interact with each other in vivo, we performed a series of co-immunoprecipitations. We showed that exogenously expressed FLAG-SIRT2 was co-immunoprecipitated by MYC-USP7 and similarly, exogenously expressed MYC-USP7 was co-immunoprecipitated by FLAG-SIRT2, suggesting an interaction between the two exogenously expressed proteins. Moreover, endogenous USP7 was co-immunoprecipitated by exogenously expressed FLAG-SIRT2, however endogenous SIRT2 was not co-immunoprecipitated by exogenously expressed MYC-USP7 (data not shown). Additionally, USP7 was co-immunoprecipitated by SIRT2 in U2OS, 293T, and HeLa cell lines, suggesting an endogenous interaction between the two proteins. When performing the reciprocal co-immunoprecipitation, SIRT2 was not co-immunoprecipitated by USP7 (data not shown). The inability to detect the co-immunoprecipitation of endogenous SIRT2 by overexpressed MYC-USP7 and endogenous USP7 may be due to the low endogenous levels of SIRT2. Nonetheless, our data together demonstrates that SIRT2 and USP7 physically interact with each other in vivo.

3.4.2 USP7 interacts with SIRT2 via the "DWGF" motif within its N-terminal TRAF-like domain

Previous studies have shown that the N-terminal TRAF-like domain containing the ^{164}DWGF^{167} motif and C-terminal the ubiquitin-like (Ubl2) subdomain containing the ^{761}MDGD^{764} motif of USP7 mediates its interaction with substrates and/or binding partners containing the P/A/ExxS motif and the KxxxK motif, respectively (Saridakis et al., 2005; Sarkari et al., 2013; Pfoh et al., 2015). Analysis of the full-length protein sequence of SIRT2 using ELM revealed the presence of one putative USP7 binding consensus motif (P/A/ExxS) ^{363}PSTS^{366}, suggesting that

USP7 interacts with SIRT2 through its N-terminal TRAF-like domain rather than its Ubl2 C-terminal subdomain. To verify this, we employed a series of His-tagged based pulldowns using the following purified constructs bound to Ni-NTA agarose beads: full length HIS-USP7, wildtype HIS-USP7 NTD^{DWGF}, double mutant HIS-USP7 NTD^{AAGF}, and HIS-USP7 CTD. After incubation with lysate derived from U2OS cells overexpressing FLAG-SIRT2 and extensive washing, the results of the His-tagged based pulldowns indicate that the N-terminal TRAF-domain of USP7 mediates its interaction with SIRT2. FLAG-SIRT2 was shown to interact with wildtype HIS-USP7 NTD^{DWGF}. This interaction with FLAG-SIRT2 was abolished with the double mutant HIS-USP7 NTD^{AAGF} in which Asp^{164} and Trp^{165} were changed to alanine residues, suggesting that these residues within the N-terminal TRAF-like domain are critical for mediating binding to SIRT2. This finding is consistent with previous studies that similarly investigated which residues within the N-terminal TRAF-like domain of USP7 mediates its interaction with the cellular substrate, UbE2E1, and the viral binding partner, vIRF1 (Sarkari et al., 2013; Chavoshi et al., 2016). In analogous GST-tagged based pulldowns, wildtype GST-USP7 NTD^{DWGF} bound to glutathione (GSH) agarose beads was shown to bind purified HIS-UbE2E1, whereas the double mutant GST-USP7 NTD^{AAGF} was unable to (Sarkari et al., 2013). Similarly, once again employing GST-tagged based pulldowns, GST-vIRF1 bound to glutathione (GSH) agarose beads was shown to bind purified wildtype HIS-USP7 NTD^{DWGF} and unable to bind the purified double mutant HIS-USP7 NTD^{AAGF} (Chavoshi et al., 2016).

Moreover, the results of the His-tagged based pulldowns show that FLAG-SIRT2 does not bind and interact with HIS-USP7 CTD possessing the Ubl2 subdomain. Considering that analysis of the full-length protein sequence of SIRT2 using ELM did not detect a KxxxK motif, we did not find this surprising. Overall, we demonstrated that ^{164}DWGF^{167} motif within the N-terminal TRAF-like domain of USP7 mediates its interaction with overexpressed FLAG-SIRT2 in vitro as previously shown with USP7 and its other substrates such as DDX24, UbE2E1, and MCM-BP (Georges et al., 2018; Sarkari et al., 2013; Jagannathan et al., 2014).

3.4.3 SIRT2 stability is UPS and USP7 dependent

USP7 plays a fundamental role in the stability of its substrates by cleaving the ubiquitin signal associated with proteasomal degradation (Bojagora & Saridakis, 2020). As a result, we investigated if USP7 and the ubiquitin-proteasome pathway are involved in SIRT2 stability. In

both wildtype and USP7 KO HCT116 cell lines treatment with the proteasome inhibitor, MG132, increased the endogenous levels of SIRT2 compared to the DMSO control, indicating that SIRT2 stability is dependent on the ubiquitin-proteasome pathway. This finding is supported by previous reports in which SIRT2 levels were stabilized upon treatment with proteasome inhibitors lactacystin and epoxomicin in the human primary osteogenic sarcoma cell line (Saos2), and upon treatment with MG132 in adenocarcinomic human alveolar basal epithelial (A549) cell line (Dryden et al., 2003; Luo et al., 2017). To date, two E3 ubiquitin ligases, SPOP and HMG-CoA reductase degradation protein 1 (HRD1) have been identified to promote SIRT2 ubiquitination and degradation by the 26S proteasome (Luo et al., 2017; Liu et al., 2020). However, no deubiquitinating enzymes have been identified to regulate SIRT2 stability. Here, we demonstrated that SIRT2 levels are lower in the USP7 KO HCT116 cell line in comparison to the wildtype HCT116 cell line suggesting that USP7 plays a role in SIRT2 stability. Moreover, upon overexpression of USP7 in a dose-dependent manner in U2OS cells, we observed a slight increase in SIRT2 levels. This increase in SIRT2 levels is more evident upon transfection and expression of 5 μg of MYC-USP7 compared to the empty vector control. Taken together, these results indicate that USP7 is novel regulator of SIRT2 stability.

It is important to note that albeit the levels of SIRT2 are lower in USP7 KO HCT116 cell line in comparison to the wildtype HCT116 cell line, stable knockout of USP7 did not result in the complete loss or destabilization of SIRT2. This suggests that the stability of SIRT2 may be influenced by additional regulatory proteins and/or post-translational modifications. As mentioned previously, SIRT1 is the best characterized member of mammalian sirtuin family (Kupis et al., 2016). SIRT1 similar to SIRT2 is a nuclear/cytoplasmic protein that has previously been identified to be regulated by USP7, as well as another member of the UPS family, USP22, which similarly mediates the deubiquitination and stabilization of SIRT1 (Song et al., 2019; Lin et al., 2012). Moreover, another member of the mammalian sirtuin family, SIRT6 localized to the nucleus, has been reported to be regulated by USP10 (Lin et al., 2013). Considering that USP22 and USP10 are expressed in HCT116, these DUBs may promote SIRT2 stability by cleaving the ubiquitin signal despite complete knockdown of USP7. To verify this, further research needs to be conducted to determine if SIRT2 interacts with USP10 and/or USP22 and if USP10 and/or USP22 regulate SIRT2 stability upon siRNA-mediated knockdown of USP22 and USP10. It would be interesting to see if double siRNA-mediated knockdown of USP22 and USP7, or USP10 and USP7

destabilizes SIRT2 levels more than the singular siRNA-mediated knockdown of USP7, USP22, and USP10.

Considering that SIRT2 is polyubiquitinated and targeted for degradation by the 26S proteasome and that USP7 rescues its substrates from degradation by the 26S proteasome through its deubiquitination activity, we suspect that USP7 binds and cleaves K48-conjugated polyubiquitin chains from SIRT2 promoting its stabilization (Liu et al., 2020; Nininahazwe et al., 2021). However, in order to verify this, additional experiments need to be performed such as overexpressing the catalytic inactive USP7 mutant (C223S) to examine if SIRT2 stability is dependent on the enzymatic activity of USP7, as well as in vivo deubiquitination assay by transfecting HA-Ub, HA-Ub and FLAG-SIRT2. and HA-Ub, FLAG-SIRT2, and MYC-USP7, followed by immunoprecipitation of FLAG-SIRT2 to determine if overexpression of USP7 deubiquitinates and reduces the level of polyubiquitination of overexpressed SIRT2 in comparison to the other transfection controls.

3.4.4 USP7 may regulate SIRT2 function

Finally, we investigated whether or not USP7 regulates the function of SIRT2 by examining the downstream effects on its cytoplasmic substrate, BubR1, a mitotic checkpoint kinase which is a critical regulator of aging and longevity in mice (North et al., 2014). In response to the stable knockout of USP7 in the HCT116 cell line, SIRT2 and BubR1 levels were lower compared to the wildtype HCT116 cell line. This finding is consistent with literature examining the relationship between SIRT2 and BubR1. SIRT2 has been reported to interact and stabilize BubR1 levels by deacetylation of residue K668 (North et al., 2014). To verify if the decreased levels of BubR1 is a direct result of the destablization of SIRT2 upon knockdown of USP7, and overall if USP7 directly regulates SIRT2 function, acetylation and deacetylation levels of the K668 residue of BubR1 levels should be further examined.

As mentioned previously SIRT2 is primarily a cytoplasmic protein but also shuttles to the nucleus during the G2/M transition of mitosis where it associates with chromatin, and deacetylates nuclear substates such as histone H4 lysine 16 (H4K16) regulating genome stability and cell cycle progression (North & Verdin, 2007; Vaquero et al., 2006). Consequently, it would be interesting to investigate if USP7 regulates SIRT2 stability and downstream function on H4 during its nuclear localization upon synchronization and arrest at G2/M phase of the cell cycle.

Currently, it remains unknown how SIRT2 is transported to the nucleus as it lacks a nuclear localization signal, however, phosphorylation of SIRT2 has been suggested to potentially play a role (Flick & Lüscher, 2012). Considering that USP7 also regulates the localization of its substrates, it would be interesting to further investigate if USP7 is implicated in SIRT2 nuclear transport by cleaving other forms of ubiquitination conjugated to SIRT2.

3.4.5 USP7, Sirtuins, and Prostate Cancer

As mentioned previously, USP7 has been reported to be overexpressed in prostate cancer and is directly correlated to tumor aggressiveness (Song et al., 2008). Similar to USP7, SIRT1 have been reported to be significantly upregulated in prostate cancer cell lines compared to normal prostate cell lines (Jung-Hynes et al., 2009). Further investigation of the role of SIRT1 in prostate cancer revealed that inhibition of SIRT1 activity by nicotinamide and/or sirtinol, as well as post-transcriptional gene silencing of SIRT1 via shRNA, significantly inhibited the growth and viability of human prostate cancer cells, while having no effect on normal prostate cells (Jung-Hynes et al., 2009). Therefore, inhibition of SIRT1 has been proposed as a potential novel target to prevent and/or treat prostate cancer (Jung-Hynes et al., 2009). Recently, USP7 has been identified to regulate the stability of SIRT1 through its deubiquitination activity, however the relationship between USP7 and SIRT1 in the context of prostate cancer has not been established (Song et al., 2019). Considering that SIRT1 and USP7 have been implicated in prostate cancer in individual studies, it is suspected that the relationship between USP7 and SIRT1 is relevant in prostate cancer cells.

Similar to SIRT1, SIRT2 has been reported to be significantly upregulated in prostate cancer cell lines compared to normal prostate cell lines, however the role in which SIRT2 plays in prostate cancer remains unknown (Jung et al., 2007). Previous studies have shown that knockdown of SIRT2 induces p53 accumulation, promoting apoptosis of cancerous cells (Li et al., 2010). This finding although not in the context of prostate cancer, suggests that overexpression of SIRT2 is involved in cancerous growth and survival. Here, we have identified that similar to SIRT1, USP7 interacts with SIRT2 revealing a potential novel molecular mechanism in which USP7 may potentially contribute to prostate cancer development through the regulation of SIRT2 stability. However, to determine if the relationship between USP7 and SIRT2 is significant in prostate cancer, further investigation is required.

Chapter 4: Conclusions

Dysregulation of the ubiquitin-proteasome degradation pathway result in proteome imbalances and has been implicated in cancer initiation and progression (An et al., 2014). Genome-wide sequencing studies have revealed that SPOP, a substrate adaptor protein associated with the Cullin 3-RING E3 ubiquitin ligase complex is the most frequently mutated gene in primary prostate cancers (Barbieri et al., 2012). Moreover, the deubiquitinating enzyme, USP7, has been reported to be overexpressed in prostate cancer and is directly correlated to tumor aggressiveness (Song et al., 2008). The objective of this project was to identify novel substrates of SPOP and USP7 and characterize their mode of binding and regulation to provide further insight on the molecular mechanisms in which SPOP and USP7 contribute to prostate cancer development. Due to the sequence and structural similarity between the substrate binding N-terminal TRAF-like domain of USP7 and MATH domain of SPOP, previously established substrates of USP7 and SPOP provided a basis for selecting and identifying potential novel substrate of SPOP and USP7, respectively. In order to screen for potential novel substrates of SPOP and USP7, we performed a bioinformatic search using the Eukaryotic Linear Motif (ELM) computational biology resource to detect for SPOP binding consensus motifs (ϕ-π-S/T-S/T-S/T) in established USP7 substrates and USP7 binding consensus motifs (P/A/ExxS) in established SPOP substrates.

Analysis of the full-length protein sequence of MDM2, an E3 ubiquitin protein ligase, revealed the presence of two putative SPOP binding consensus motifs: ^{156}PSTSS^{160} and ^{397}PSTSS^{401} prompting us to investigate whether MDM2 is a novel substrate of SPOP **(Figure 4-1A).** Using a series of His-tagged based pulldowns, we demonstrated that SPOP through the ^{130}DWGF^{133} motif within its MATH domain interacts with MDM2 in vitro. Whereas prostate cancer associated mutations of the SPOP MATH domain completely or partially disrupted this interaction with MDM2. We further demonstrated that SPOP regulates the stability of MDM2 via siRNA-mediated knockdown and overexpression via transfection. Upon treatment with MG132, we determined that SPOP within the Cullin 3-RING E3 ubiquitin ligase complex targets MDM2 for degradation via the 26S proteasome. These findings collectively suggest that MDM2 may potentially be a novel substrate of SPOP, however further experiments need to be performed to verify this such as co-immunoprecipitation assays to determine if MDM2 and SPOP interact in

vivo in prostate cancer cell lines, and in vivo ubiquitination assays to determine if the SPOP-Cullin 3-RING E3 ubiquitin ligase complex mediates the polyubiquitination of MDM2.

In addition, analysis of the full-length protein sequence of the NAD^+-dependent deacetylase, SIRT2, an established substrate of SPOP, revealed the presence of one putative USP7 binding consensus motif: ^{363}PSTS^{366} prompting us to investigate whether SIRT2 is a novel substrate of USP7 **(Figure 4-1B)**. Here, we demonstrated that USP7 interacts with SIRT2 in vivo in various cell lines, as well as in vitro. We further demonstrated using a series of His-tagged based pulldowns, that the ^{164}DWGF^{167} motif within the N-terminal TRAF-like domain of USP7 is critical in mediating its interaction with SIRT2. Finally, we established that USP7 regulates SIRT2 stability upon stable knockout of USP7 in the HCT116 cell line. Together, these results indicate that SIRT2 is a novel substrate of USP7. However, further experiments need to be performed to determine if USP7 regulates SIRT2 stability through its deubiquitination activity. Collectively, our results suggest a potential mechanism in which SPOP and USP7 may contribute to prostate cancer pathogenesis through the regulation of MDM2 and SIRT2, that may have potential in combination to be targeted therapeutically, however further studies need to be conducted to shed light on this.

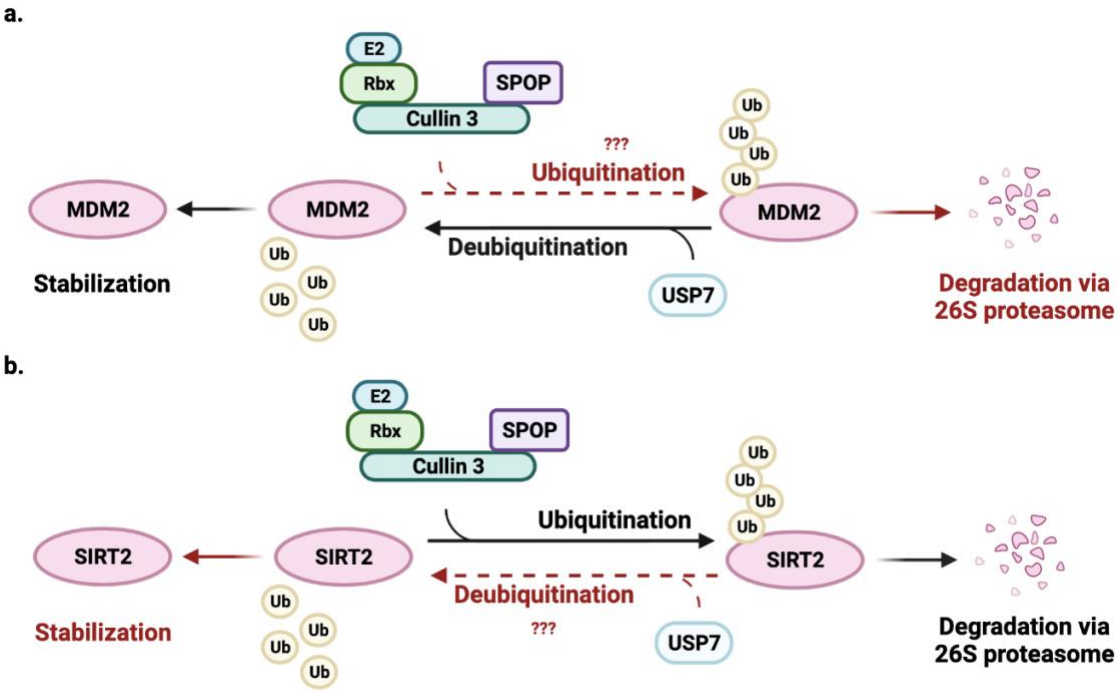

Figure 4-1. Overview of the relationship of USP7 and SPOP with SIRT2 and MDM2. (a) MDM2 is an established USP7 substrate. USP7 has previously been shown to regulate the stability of MDM2 through its deubiquitinating activity. Notably, we demonstrated that SPOP interacts with MDM2 through its substrate binding MATH domain in vitro and negatively regulates the stability of MDM2 in a proteasome dependent manner in vivo. Further experiments are required to determine if SPOP interacts with MDM2 in vivo and if the SPOP-Cullin 3-RING E3 ubiquitin ligase complex polyubiquitinates MDM2. **(b)** SIRT2 is an established SPOP substrate. The SPOP-Cullin 3-RING E3 ubiquitin ligase complex has previously been shown to polyubiquitinate and target SIRT2 for degradation by the 26S proteasome, thus regulating its stability. Notably, we demonstrated that SIRT2 is a novel substate of USP7 and that USP7 regulates the stability of SIRT2 presumably through its deubiquitination activity, however this needs to be confirmed by further experiments. Red arrows represent novel findings by the Saridakis lab. Black arrows represent previous findings by other researchers. Red dashed arrows represent processes that require further investigation and remain unconfirmed. Schematic created with BioRender.com.

References

1. Al-Eidan, A., Wang, Y., Skipp, P., & Ewing, R. M. (2020). The USP7 protein interaction network and its roles in tumorigenesis. *Genes & Diseases*. https://doi.org/10.1016/j.gendis.2020.10.004
2. An, J., Wang, C., Deng, Y., Yu, L., & Huang, H. (2014). Destruction of Full-Length Androgen Receptor by Wild-Type SPOP, but Not Prostate-Cancer-Associated Mutants. *Cell Reports*, *6*(4), 657–669. https://doi.org/10.1016/j.celrep.2014.01.013
3. An, J., Wang, C., Deng, Y., Yu, L., & Huang, H. (2014). Destruction of Full-Length Androgen Receptor by Wild-Type SPOP, but Not Prostate-Cancer-Associated Mutants. *Cell Reports*, *6*(4), 657–669. https://doi.org/10.1016/j.celrep.2014.01.013
4. An, L., Jiang, Y., Ng, H. H. W., Man, E. P. S., Chen, J., Khoo, U.-S., Gong, Q., & Huen, M. S. Y. (2017). Dual-utility NLS drives RNF169-dependent DNA damage responses. *Proceedings of the National Academy of Sciences*, *114*(14), E2872–E2881. https://doi.org/10.1073/pnas.1616602114
5. Bao, J., Lu, Z., Joseph, J. J., Carabenciov, D., Dimond, C. C., Pang, L., Samsel, L., McCoy, J. P., Leclerc, J., Nguyen, P., Gius, D., & Sack, M. N. (2010). Characterization of the murine SIRT3 mitochondrial localization sequence and comparison of mitochondrial enrichment and deacetylase activity of long and short SIRT3 isoforms. *Journal of Cellular Biochemistry*, *110*(1), 238–247. https://doi.org/10.1002/jcb.22531
6. Barbieri, C. E., Baca, S. C., Lawrence, M. S., Demichelis, F., Blattner, M., Theurillat, J.-P., White, T. A., Stojanov, P., Van Allen, E., Stransky, N., Nickerson, E., Chae, S.-S., Boysen, G., Auclair, D., Onofrio, R. C., Park, K., Kitabayashi, N., MacDonald, T. Y., Sheikh, K., & Vuong, T. (2012). Exome sequencing identifies recurrent SPOP, FOXA1 and MED12 mutations in prostate cancer. *Nature Genetics*, *44*(6), 685–689. https://doi.org/10.1038/ng.2279
7. Batra, J., & Lai, J. (2014). Speckle-type POZ protein mutations interrupt tumor suppressor function of speckle-type POZ protein in prostate cancer by affecting androgen receptor degradation. *Asian Journal of Andrology*, *16*(5), 659. https://doi.org/10.4103/1008-682x.133323
8. Berndsen, C. E., & Wolberger, C. (2014). New insights into ubiquitin E3 ligase mechanism. *Nature Structural & Molecular Biology*, *21*(4), 301–307. https://doi.org/10.1038/nsmb.2780
9. Bojagora, A., & Saridakis, V. (2020). USP7 manipulation by viral proteins. *Virus Research*, *286*, 198076. https://doi.org/10.1016/j.virusres.2020.198076
10. Buetow, L., & Huang, D. T. (2016). Structural insights into the catalysis and regulation of E3 ubiquitin ligases. *Nature Reviews Molecular Cell Biology*, *17*(10), 626–642. https://doi.org/10.1038/nrm.2016.91
11. Cahilly-Snyder, L., Yang-Feng, T., Francke, U., & George, D. L. (1987). Molecular analysis and chromosomal mapping of amplified genes isolated from a transformed mouse 3T3 cell line. *Somatic Cell and Molecular Genetics*, *13*(3), 235–244. https://doi.org/10.1007/bf01535205
12. Chang, C.-J. ., & Hung, M.-C. . (2012). The role of EZH2 in tumour progression. *British Journal of Cancer*, *106*(2), 243–247. https://doi.org/10.1038/bjc.2011.551
13. Chavoshi, S., Egorova, O., Lacdao, I. K., Farhadi, S., Sheng, Y., & Saridakis, V. (2016). Identification of Kaposi Sarcoma Herpesvirus (KSHV) vIRF1 Protein as a Novel Interaction Partner of Human Deubiquitinase USP7. *The Journal of Biological Chemistry*, *291*(12), 6281–6291. https://doi.org/10.1074/jbc.M115.710632
14. Chen, S.-T., Okada, M., Nakato, R., Izumi, K., Bando, M., & Shirahige, K. (2015). The Deubiquitinating Enzyme USP7 Regulates Androgen Receptor Activity by Modulating Its Binding to Chromatin. *The Journal of Biological Chemistry*, *290*(35), 21713–21723. https://doi.org/10.1074/jbc.M114.628255
15. Chène, P. (2003). Inhibiting the p53–MDM2 interaction: an important target for cancer therapy. *Nature Reviews Cancer*, *3*(2), 102–109. https://doi.org/10.1038/nrc991
16. Cheng, J., North, B. J., Zhang, T., Dai, X., Tao, K., Guo, J., & Wei, W. (2018). The emerging roles of protein homeostasis-governing pathways in Alzheimer's disease. *Aging Cell*, *17*(5), e12801. https://doi.org/10.1111/acel.12801

17. Cheng, J., Yang, H., Fang, J., Ma, L., Gong, R., Wang, P., Li, Z., & Xu, Y. (2015). Molecular mechanism for USP7-mediated DNMT1 stabilization by acetylation. *Nature Communications*, *6*(1). https://doi.org/10.1038/ncomms8023
18. Cheng, T.-H., & Cohen, S. N. (2006). Human MDM2 Isoforms Translated Differentially on Constitutive versus p53-Regulated Transcripts Have Distinct Functions in the p53/MDM2 and TSG101/MDM2 Feedback Control Loops. *Molecular and Cellular Biology*, *27*(1), 111–119. https://doi.org/10.1128/mcb.00235-06
19. Clague, M. J., & Urbé, S. (2010). Ubiquitin: Same Molecule, Different Degradation Pathways. *Cell*, *143*(5), 682–685. https://doi.org/10.1016/j.cell.2010.11.012
20. Clark, A., & Burleson, M. (2020). SPOP and cancer: a systematic review. *American Journal of Cancer Research*, *10*(3), 704–726. https://www.ncbi.nlm.nih.gov/pmc/articles/PMC7136909/
21. Cuneo, M. J., & Mittag, T. (2019). The ubiquitin ligase adaptor SPOP in cancer. *The FEBS Journal*, *286*(20), 3946–3958. https://doi.org/10.1111/febs.15056
22. de Oliveira, R. M., Sarkander, J., Kazantsev, A. G., & Outeiro, T. F. (2012). SIRT2 as a Therapeutic Target for Age-Related Disorders. *Frontiers in Pharmacology*, *3*(82). https://doi.org/10.3389/fphar.2012.00082
23. Dryden, S. C., Nahhas, F. A., Nowak, J. E., Goustin, A.-S., & Tainsky, M. A. (2003). Role for Human SIRT2 NAD-Dependent Deacetylase Activity in Control of Mitotic Exit in the Cell Cycle. *Molecular and Cellular Biology*, *23*(9), 3173–3185. https://doi.org/10.1128/mcb.23.9.3173-3185.2003
24. Du, Y., Hu, H., Hua, C., Du, K., & Wei, T. (2018). Tissue distribution, subcellular localization, and enzymatic activity analysis of human SIRT5 isoforms. *Biochemical and Biophysical Research Communications*, *503*(2), 763–769. https://doi.org/10.1016/j.bbrc.2018.06.073
25. Errington, W. J., Khan, M. Q., Bueler, S. A., Rubinstein, J. L., Chakrabartty, A., & Privé, G. G. (2012). Adaptor Protein Self-Assembly Drives the Control of a Cullin-RING Ubiquitin Ligase. *Structure*, *20*(7), 1141–1153. https://doi.org/10.1016/j.str.2012.04.009
26. Everett, R. D., Meredith, M., Orr, A., Cross, A., Kathoria, M., & Parkinson, J. (1997). A novel ubiquitin-specific protease is dynamically associated with the PML nuclear domain and binds to a herpesvirus regulatory protein. *The EMBO Journal*, *16*(7), 1519–1530. https://doi.org/10.1093/emboj/16.7.1519
27. Faesen, A. C., Dirac, A. M. G., Shanmugham, A., Ovaa, H., Perrakis, A., & Sixma, T. K. (2011). Mechanism of USP7/HAUSP Activation by Its C-Terminal Ubiquitin-like Domain and Allosteric Regulation by GMP-Synthetase. *Molecular Cell*, *44*(1), 147–159. https://doi.org/10.1016/j.molcel.2011.06.034
28. Fiorino, E., Giudici, M., Ferrari, A., Mitro, N., Caruso, D., De Fabiani, E., & Crestani, M. (2014). The sirtuin class of histone deacetylases: Regulation and roles in lipid metabolism. *IUBMB Life*, *66*(2), 89–99. https://doi.org/10.1002/iub.1246
29. Flick, F., & Lüscher, B. (2012). Regulation of Sirtuin Function by Posttranslational Modifications. *Frontiers in Pharmacology*, *3*(29). https://doi.org/10.3389/fphar.2012.00029
30. Fu, W., Ma, Q., Chen, L., Li, P., Zhang, M., Ramamoorthy, S., Nawaz, Z., Shimojima, T., Wang, H., Yang, Y., Shen, Z., Zhang, Y., Zhang, X., Nicosia, S. V., Zhang, Y., Pledger, J. W., Chen, J., & Bai, W. (2009). MDM2 Acts Downstream of p53 as an E3 Ligase to Promote FOXO Ubiquitination and Degradation. *The Journal of Biological Chemistry*, *284*(21), 13987–14000. https://doi.org/10.1074/jbc.M901758200
31. Gagarina, V., Bojagora, A., Lacdao, I. K., Luthra, N., Pfoh, R., Mohseni, S., Chaharlangi, D., Tan, N., & Saridakis, V. (2020). Structural Basis of the Interaction Between Ubiquitin Specific Protease 7 and Enhancer of Zeste Homolog 2. *Journal of Molecular Biology*, *432*(4), 897–912. https://doi.org/10.1016/j.jmb.2019.12.026
32. Gan, W., Dai, X., Lunardi, A., Li, Z., Inuzuka, H., Liu, P., Varmeh, S., Zhang, J., Cheng, L., Sun, Y., Asara, John M., Beck, Andrew H., Huang, J., Pandolfi, P., & Wei, W. (2015). SPOP Promotes Ubiquitination and Degradation of the ERG Oncoprotein to Suppress Prostate Cancer Progression. *Molecular Cell*, *59*(6), 917–930. https://doi.org/10.1016/j.molcel.2015.07.026

33. Gao, K., Jin, X., Tang, Y., Ma, J., Peng, J., Yu, L., Zhang, P., & Wang, C. (2015). Tumor suppressor SPOP mediates the proteasomal degradation of progesterone receptors (PRs) in breast cancer cells. *American Journal of Cancer Research*, *5*(10), 3210–3220. https://pubmed.ncbi.nlm.nih.gov/26693071/
34. Geng, C., He, B., Xu, L., Barbieri, C. E., Eedunuri, V. K., Chew, S. A., Zimmermann, M., Bond, R., Shou, J., Li, C., Blattner, M., Lonard, D. M., Demichelis, F., Coarfa, C., Rubin, M. A., Zhou, P., O'Malley, B. W., & Mitsiades, N. (2013). Prostate cancer-associated mutations in speckle-type POZ protein (SPOP) regulate steroid receptor coactivator 3 protein turnover. *Proceedings of the National Academy of Sciences*, *110*(17), 6997–7002. https://doi.org/10.1073/pnas.1304502110
35. Geng, C., Rajapakshe, K., Shah, S. S., Shou, J., Eedunuri, V. K., Foley, C., Fiskus, W., Rajendran, M., Chew, S. A., Zimmermann, M., Bond, R., He, B., Coarfa, C., & Mitsiades, N. (2014). Androgen receptor is the key transcriptional mediator of the tumor suppressor SPOP in prostate cancer. *Cancer Research*, *74*(19), 5631–5643. https://doi.org/10.1158/0008-5472.CAN-14-0476
36. Georges, A., Marcon, E., Greenblatt, J., & Frappier, L. (2018). Identification and Characterization of USP7 Targets in Cancer Cells. *Scientific Reports*, *8*(1). https://doi.org/10.1038/s41598-018-34197-x
37. Groner, A. C., Cato, L., de Tribolet-Hardy, J., Bernasocchi, T., Janouskova, H., Melchers, D., Houtman, R., Cato, A. C. B., Tschopp, P., Gu, L., Corsinotti, A., Zhong, Q., Fankhauser, C., Fritz, C., Poyet, C., Wagner, U., Guo, T., Aebersold, R., Garraway, L. A., & Wild, P. J. (2016). TRIM24 is an oncogenic transcriptional activator in prostate cancer. *Cancer Cell*, *29*(6), 846–858. https://doi.org/10.1016/j.ccell.2016.04.012
38. Han, J. J. W., Ho, D. V., Kim, H. M., Lee, J. Y., Jeon, Y. S., & Chan, J. Y. (2021). The deubiquitinating enzyme USP7 regulates the transcription factor Nrf1 by modulating its stability in response to toxic metal exposure. *Journal of Biological Chemistry*, *296*. https://doi.org/10.1016/j.jbc.2021.100732
39. Hernandez-Munoz, I., Lund, A. H., van der Stoop, P., Boutsma, E., Muijrers, I., Verhoeven, E., Nusinow, D. A., Panning, B., Marahrens, Y., & van Lohuizen, M. (2005). Stable X chromosome inactivation involves the PRC1 Polycomb complex and requires histone MACROH2A1 and the CULLIN3/SPOP ubiquitin E3 ligase. *Proceedings of the National Academy of Sciences*, *102*(21), 7635–7640. https://doi.org/10.1073/pnas.0408918102
40. Hirschey, Matthew D. (2011). Old Enzymes, New Tricks: Sirtuins Are NAD+-Dependent De-acylases. *Cell Metabolism*, *14*(6), 718–719. https://doi.org/10.1016/j.cmet.2011.10.006
41. Hochstrasser, M. (1996). UBIQUITIN-DEPENDENT PROTEIN DEGRADATION. *Annual Review of Genetics*, *30*(1), 405–439. https://doi.org/10.1146/annurev.genet.30.1.405
42. Holowaty, M. N., Zeghouf, M., Wu, H., Tellam, J., Athanasopoulos, V., Greenblatt, J., & Frappier, L. (2003). Protein Profiling with Epstein-Barr Nuclear Antigen-1 Reveals an Interaction with the Herpesvirus-associated Ubiquitin-specific Protease HAUSP/USP7. *Journal of Biological Chemistry*, *278*(32), 29987–29994. https://doi.org/10.1074/jbc.m303977200
43. Hou, H., Sun, D., & Zhang, X. (2019). The role of MDM2 amplification and overexpression in therapeutic resistance of malignant tumors. *Cancer Cell International*, *19*(1). https://doi.org/10.1186/s12935-019-0937-4
44. Hu, M., Li, P., Li, M., Li, W., Yao, T., Wu, J.-W., Gu, W., Cohen, R. E., & Shi, Y. (2002). Crystal Structure of a UBP-Family Deubiquitinating Enzyme in Isolation and in Complex with Ubiquitin Aldehyde. *Cell*, *111*(7), 1041–1054. https://doi.org/10.1016/S0092-8674(02)01199-6
45. Hu, T., Zhang, J., Sha, B., Li, M., Wang, L., Zhang, Y., Liu, X., Dong, Z., Liu, Z., Li, P., & Chen, P. (2018). Targeting the overexpressed USP7 inhibits esophageal squamous cell carcinoma cell growth by inducing NOXA-mediated apoptosis. *Molecular Carcinogenesis*, *58*(1), 42–54. https://doi.org/10.1002/mc.22905
46. Jagannathan, M., Nguyen, T., Gallo, D., Luthra, N., Brown, G. W., Saridakis, V., & Frappier, L. (2014). A Role for USP7 in DNA Replication. *Molecular and Cellular Biology*, *34*(1), 132–145. https://doi.org/10.1128/MCB.00639-13
47. Jiang, L., Xiong, J., Zhan, J., Yuan, F., Tang, M., Zhang, C., Cao, Z., Chen, Y., Lu, X., Li, Y., Wang, H., Wang, L., Wang, J., Zhu, W.-G., & Wang, H. (2017). Ubiquitin-specific peptidase 7 (USP7)-mediated deubiquitination of the histone deacetylase SIRT7 regulates gluconeogenesis. *The Journal of Biological Chemistry*, *292*(32), 13296–13311. https://doi.org/10.1074/jbc.M117.780130

48. Jin, X., Wang, J., Gao, K., Zhang, P., Yao, L., Tang, Y., Tang, L., Ma, J., Xiao, J., Zhang, E., Zhu, J., Zhang, B., Zhao, S.-M., Li, Y., Ren, S., Huang, H., Yu, L., & Wang, C. (2017). Dysregulation of INF2-mediated mitochondrial fission in SPOP-mutated prostate cancer. *PLoS Genetics*, *13*(4), e1006748. https://doi.org/10.1371/journal.pgen.1006748
49. Jin, X., Wang, J., Li, Q., Zhuang, H., Yang, J., Lin, Z., Lin, T., Lv, Z., Shen, L., Yan, C., Zheng, J., Zhu, J., Gong, Z., Wang, C., & Gao, K. (2019). SPOP targets oncogenic protein ZBTB3 for destruction to suppress endometrial cancer. *American Journal of Cancer Research*, *9*(12), 2797–2812. https://www.ncbi.nlm.nih.gov/pmc/articles/PMC6943363/
50. Ju, L.-G., Zhu, Y., Long, Q.-Y., Li, X.-J., Lin, X., Tang, S.-B., Yin, L., Xiao, Y., Wang, X.-H., Li, L., Zhang, L., & Wu, M. (2019). SPOP suppresses prostate cancer through regulation of CYCLIN E1 stability. *Cell Death & Differentiation*, *26*(6), 1156–1168. https://doi.org/10.1038/s41418-018-0198-0
51. Jung-Hynes, B., Nihal, M., Zhong, W., & Ahmad, N. (2009). Role of Sirtuin Histone Deacetylase SIRT1 in Prostate Cancer. *The Journal of Biological Chemistry*, *284*(6), 3823–3832. https://doi.org/10.1074/jbc.M807869200
52. Jung, B., Zhong, W., & Ahmad, N. (2007). Sirtuin histone deacetylases SIRT1 and SIRT2 as novel targets for the management of prostate cancer. *Cancer Research*, *67*(9 Supplement), 643–643. https://cancerres.aacrjournals.org/content/67/9_Supplement/643
53. Juven-Gershon, T., Shifman, O., Unger, T., Elkeles, A., Haupt, Y., & Oren, M. (1998). The Mdm2 Oncoprotein Interacts with the Cell Fate Regulator Numb. *Molecular and Cellular Biology*, *18*(7), 3974–3982. https://www.ncbi.nlm.nih.gov/pmc/articles/PMC108982/
54. Kaeberlein, M., McVey, M., & Guarente, L. (1999). The SIR2/3/4 complex and SIR2 alone promote longevity in Saccharomyces cerevisiae by two different mechanisms. *Genes & Development*, *13*(19), 2570–2580. https://doi.org/10.1101/gad.13.19.2570
55. Kan, Z., Jaiswal, B. S., Stinson, J., Janakiraman, V., Bhatt, D., Stern, H. M., … Seshagiri, S. (2010). Diverse somatic mutation patterns and pathway alterations in human cancers. *Nature*, *466*(7308), 869–873. https://doi.org/10.1038/nature09208
56. Kawai, H., Wiederschain, D., & Yuan, Z.-M. . (2003). Critical Contribution of the MDM2 Acidic Domain to p53 Ubiquitination. *Molecular and Cellular Biology*, *23*(14), 4939–4947. https://doi.org/10.1128/mcb.23.14.4939-4947.2003
57. Kevei, É., & Hoppe, T. (2014). Ubiquitin sets the timer: impacts on aging and longevity. *Nature Structural & Molecular Biology*, *21*(4), 290–292. https://doi.org/10.1038/nsmb.2806
58. Kim, R. Q., van Dijk, W. J., & Sixma, T. K. (2016). Structure of USP7 catalytic domain and three Ubl-domains reveals a connector α-helix with regulatory role. *Journal of Structural Biology*, *195*(1), 11–18. https://doi.org/10.1016/j.jsb.2016.05.005
59. Komander, D., & Rape, M. (2012). The Ubiquitin Code. *Annual Review of Biochemistry*, *81*(1), 203–229. https://doi.org/10.1146/annurev-biochem-060310-170328
60. Komander, D., Clague, M. J., & Urbé, S. (2009). Breaking the chains: structure and function of the deubiquitinases. *Nature Reviews Molecular Cell Biology*, *10*(8), 550–563. https://doi.org/10.1038/nrm2731
61. Kulikov, R., Winter, M., & Blattner, C. (2006). Binding of p53 to the Central Domain of Mdm2 Is Regulated by Phosphorylation *. *Journal of Biological Chemistry*, *281*(39), 28575–28583. https://doi.org/10.1074/jbc.M513311200
62. Kupis, W., Pałyga, J., Tomal, E., & Niewiadomska, E. (2016). The role of sirtuins in cellular homeostasis. *Journal of Physiology and Biochemistry*, *72*(3), 371–380. https://doi.org/10.1007/s13105-016-0492-6
63. Kwon, J. E., La, M., Oh, K. H., Oh, Y. M., Kim, G. R., Seol, J. H., Baek, S. H., Chiba, T., Tanaka, K., Bang, O. S., Joe, C. O., & Chung, C. H. (2006). BTB Domain-containing Speckle-type POZ Protein (SPOP) Serves as an Adaptor of Daxx for Ubiquitination by Cul3-based Ubiquitin Ligase. *Journal of Biological Chemistry*, *281*(18), 12664–12672. https://doi.org/10.1074/jbc.m600204200
64. Lecker, S. H., Goldberg, A. L., & Mitch, W. E. (2006). Protein Degradation by the Ubiquitin–Proteasome Pathway in Normal and Disease States. *Journal of the American Society of Nephrology*, *17*(7), 1807–1819. https://doi.org/10.1681/asn.2006010083

65. Lecker, S. H., Goldberg, A. L., & Mitch, W. E. (2006). Protein Degradation by the Ubiquitin–Proteasome Pathway in Normal and Disease States. *Journal of the American Society of Nephrology*, *17*(7), 1807–1819. https://doi.org/10.1681/asn.2006010083
66. Lee, J. E., Park, C. M., & Kim, J. H. (2020). USP7 deubiquitinates and stabilizes EZH2 in prostate cancer cells. *Genetics and Molecular Biology*, *43*(2). https://doi.org/10.1590/1678-4685-GMB-2019-0338
67. Leestemaker, Y., & Ovaa, H. (2017). Tools to investigate the ubiquitin proteasome system. *Drug Discovery Today: Technologies*, *26*, 25–31. https://doi.org/10.1016/j.ddtec.2017.11.006
68. Leslie, P. L., Ke, H., & Zhang, Y. (2015). The MDM2 RING Domain and Central Acidic Domain Play Distinct Roles in MDM2 Protein Homodimerization and MDM2-MDMX Protein Heterodimerization. *Journal of Biological Chemistry*, *290*(20), 12941–12950. https://doi.org/10.1074/jbc.m115.644435
69. Li, B., Lu, W., & Chen, Z. (2014). Regulation of Androgen Receptor by E3 Ubiquitin Ligases: for More or Less. *Receptors & clinical investigation*, *1*(5), https://doi.org/10.14800/rci.122
70. Li, M., Brooks, C. L., Kon, N., & Gu, W. (2004). A Dynamic Role of HAUSP in the p53-Mdm2 Pathway. *Molecular Cell*, *13*(6), 879–886. https://doi.org/10.1016/s1097-2765(04)00157-1
71. Li, M., Chen, D., Shiloh, A., Luo, J., Nikolaev, A. Y., Qin, J., & Gu, W. (2002). Deubiquitination of p53 by HAUSP is an important pathway for p53 stabilization. *Nature*, *416*(6881), 648–653. https://doi.org/10.1038/nature737
72. Li, Y., Matsumori, H., Nakayama, Y., Osaki, M., Kojima, H., Kurimasa, A., Ito, H., Mori, S., Katoh, M., Oshimura, M., & Inoue, T. (2010). SIRT2 down-regulation in HeLa can induce p53 accumulation via p38 MAPK activation-dependent p300 decrease, eventually leading to apoptosis. *Genes to Cells*, *16*(1), 34–45. https://doi.org/10.1111/j.1365-2443.2010.01460.x
73. Lin, Z., Yang, H., Kong, Q., Li, J., Lee, S.-M., Gao, B., Dong, H., Wei, J., Song, J., Zhang, Donna D., & Fang, D. (2012). USP22 Antagonizes p53 Transcriptional Activation by Deubiquitinating Sirt1 to Suppress Cell Apoptosis and Is Required for Mouse Embryonic Development. *Molecular Cell*, *46*(4), 484–494. https://doi.org/10.1016/j.molcel.2012.03.024
74. Lin, Z., Yang, H., Tan, C., Li, J., Liu, Z., Quan, Q., Kong, S., Ye, J., Gao, B., & Fang, D. (2013). USP10 Antagonizes c-Myc Transcriptional Activation through SIRT6 Stabilization to Suppress Tumor Formation. *Cell Reports*, *5*(6), 1639–1649. https://doi.org/10.1016/j.celrep.2013.11.029
75. LindströmM. S., Jin, A., Deisenroth, C., White Wolf, G., & Zhang, Y. (2007). Cancer-Associated Mutations in the MDM2 Zinc Finger Domain Disrupt Ribosomal Protein Interaction and Attenuate MDM2-Induced p53 Degradation. *Molecular and Cellular Biology*, *27*(3), 1056–1068. https://doi.org/10.1128/mcb.01307-06
76. Linke, K., Mace, P. D., Smith, C. A., Vaux, D. L., Silke, J., & Day, C. L. (2008). Structure of the MDM2/MDMX RING domain heterodimer reveals dimerization is required for their ubiquitylation in trans. *Cell Death & Differentiation*, *15*(5), 841–848. https://doi.org/10.1038/sj.cdd.4402309
77. Liu, A., Desai, B. M., & Stoffers, D. A. (2004). Identification of PCIF1, a POZ Domain Protein That Inhibits PDX-1 (MODY4) Transcriptional Activity. *Molecular and Cellular Biology*, *24*(10), 4372–4383. https://doi.org/10.1128/MCB.24.10.4372-4383.2004
78. Liu, L., Yu, L., Zeng, C., Long, H., Duan, G., Yin, G., Dai, X., & Lin, Z. (2020). E3 Ubiquitin Ligase HRD1 Promotes Lung Tumorigenesis by Promoting Sirtuin 2 Ubiquitination and Degradation. *Molecular and Cellular Biology*, *40*(7), e00257-19. https://doi.org/10.1128/MCB.00257-19
79. Luo, J., Bao, Y.-C., Ji, X.-X., Chen, B., Deng, Q.-F., & Zhou, S.-W. (2017). SPOP promotes SIRT2 degradation and suppresses non-small cell lung cancer cell growth. *Biochemical and Biophysical Research Communications*, *483*(2), 880–884. https://doi.org/10.1016/j.bbrc.2017.01.027
80. Ma, J., Chang, K., Peng, J., Shi, Q., Gan, H., Gao, K., Feng, K., Xu, F., Zhang, H., Dai, B., Zhu, Y., Shi, G., Shen, Y., Zhu, Y., Qin, X., Li, Y., Zhang, P., Ye, D., & Wang, C. (2018). SPOP promotes ATF2 ubiquitination and degradation to suppress prostate cancer progression. *Journal of Experimental & Clinical Cancer Research*, *37*(1). https://doi.org/10.1186/s13046-018-0809-0
81. Ma, J., Shi, Q., Cui, G., Sheng, H., Botuyan, M. V., Zhou, Y., Yan, Y., He, Y., Wang, L., Wang, Y., Mer, G., Ye, D., Wang, C., & Huang, H. (2021). SPOP mutation induces replication over-firing by impairing Geminin ubiquitination and triggers replication catastrophe upon ATR inhibition. *Nature Communications*, *12*(1), 5779. https://doi.org/10.1038/s41467-021-26049-6

82. Mani, A., & Gelmann, E. P. (2005). The ubiquitin-proteasome pathway and its role in cancer. *Journal of Clinical Oncology : Official Journal of the American Society of Clinical Oncology*, *23*(21), 4776–4789. https://doi.org/10.1200/JCO.2005.05.081
83. Mani, A., & Gelmann, E. P. (2005). The ubiquitin-proteasome pathway and its role in cancer. *Journal of Clinical Oncology : Official Journal of the American Society of Clinical Oncology*, *23*(21), 4776–4789. https://doi.org/10.1200/JCO.2005.05.081
84. Mani, R.-S. (2014). The emerging role of speckle-type POZ protein (SPOP) in cancer development. *Drug Discovery Today*, *19*(9), 1498–1502. https://doi.org/10.1016/j.drudis.2014.07.009
85. Marine, J.-C. ., & Lozano, G. (2010). Mdm2-mediated ubiquitylation: p53 and beyond. *Cell Death & Differentiation*, *17*(1), 93–102. https://doi.org/10.1038/cdd.2009.68
86. Marzahn, M. R., Marada, S., Lee, J., Nourse, A., Kenrick, S., Zhao, H., … Mittag, T. (2016). Higher-order oligomerization promotes localization of SPOP to liquid nuclear speckles. *The EMBO Journal*, *35*(12), 1254–1275. https://doi.org/10.15252/embj.201593169
87. Maxwell, M. M., Tomkinson, E. M., Nobles, J., Wizeman, J. W., Amore, A. M., Quinti, L., Chopra, V., Hersch, S. M., & Kazantsev, A. G. (2011). The Sirtuin 2 microtubule deacetylase is an abundant neuronal protein that accumulates in the aging CNS. *Human Molecular Genetics*, *20*(20), 3986–3996. https://doi.org/10.1093/hmg/ddr326
88. Micel, L. N., Tentler, J. J., Smith, P. G., & Eckhardt, G. S. (2013). Role of Ubiquitin Ligases and the Proteasome in Oncogenesis: Novel Targets for Anticancer Therapies. *Journal of Clinical Oncology*, *31*(9), 1231–1238. https://doi.org/10.1200/jco.2012.44.0958
89. Momand, J., Wu, H.-H., & Dasgupta, G. (2000). MDM2 — master regulator of the p53 tumor suppressor protein. *Gene*, *242*(1-2), 15–29. https://doi.org/10.1016/s0378-1119(99)00487-4
90. Morotti, A., Panuzzo, C., Crivellaro, S., Pergolizzi, B., Familiari, U., Berger, A. H., Saglio, G., & Pandolfi, P. P. (2014). BCR-ABL disrupts PTEN nuclear-cytoplasmic shuttling through phosphorylation-dependent activation of HAUSP. *Leukemia*, *28*(6), 1326–1333. https://doi.org/10.1038/leu.2013.370
91. Murata, S., Yashiroda, H., & Tanaka, K. (2009). Molecular mechanisms of proteasome assembly. *Nature Reviews Molecular Cell Biology*, *10*(2), 104–115. https://doi.org/10.1038/nrm2630
92. Nagai, Y., Kojima, T., Muro, Y., Hachiya, T., Nishizawa, Y., Wakabayashi, T., & Hagiwara, M. (1997). Identification of a novel nuclear speckle-type protein, SPOP. *FEBS Letters*, *418*(1–2), 23–26. https://doi.org/10.1016/s0014-5793(97)01340-9
93. Nahhas, F., Dryden, S. C., Abrams, J., & Tainsky, M. A. (2007). Mutations in SIRT2 deacetylase which regulate enzymatic activity but not its interaction with HDAC6 and tubulin. *Molecular and Cellular Biochemistry*, *303*(1-2), 221–230. https://doi.org/10.1007/s11010-007-9478-6
94. Nguyen, H. C., Wang, W., & Xiong, Y. (2017). Cullin-RING E3 Ubiquitin Ligases: Bridges to Destruction. *Sub-Cellular Biochemistry*, *83*, 323–347. https://doi.org/10.1007/978-3-319-46503-6_12
95. Nininahazwe, L., Liu, B., He, C., Zhang, H., & Chen, Z.-S. (2021). The emerging nature of Ubiquitin-specific protease 7 (USP7): a new target in cancer therapy. *Drug Discovery Today*, *26*(2), 490–502. https://doi.org/10.1016/j.drudis.2020.10.028
96. North, B. J., & Verdin, E. (2007a). Mitotic Regulation of SIRT2 by Cyclin-dependent Kinase 1-dependent Phosphorylation. *Journal of Biological Chemistry*, *282*(27), 19546–19555. https://doi.org/10.1074/jbc.m702990200
97. North, B. J., & Verdin, E. (2007b). Interphase Nucleo-Cytoplasmic Shuttling and Localization of SIRT2 during Mitosis. *PLoS ONE*, *2*(8), e784. https://doi.org/10.1371/journal.pone.0000784
98. North, B. J., Marshall, B. L., Borra, M. T., Denu, J. M., & Verdin, E. (2003). The human Sir2 ortholog, SIRT2, is an NAD+-dependent tubulin deacetylase. *Molecular Cell*, *11*(2), 437–444. https://doi.org/10.1016/s1097-2765(03)00038-8
99. North, B. J., Rosenberg, M. A., Jeganathan, K. B., Hafner, A. V., Michan, S., Dai, J., Baker, D. J., Cen, Y., Wu, L. E., Sauve, A. A., van Deursen, J. M., Rosenzweig, A., & Sinclair, D. A. (2014). SIRT2 induces the checkpoint kinase BubR1 to increase lifespan. *The EMBO Journal*, *33*(13), 1438–1453. https://doi.org/10.15252/embj.201386907

100. Oh, Y. M., Yoo, S. J., & Seol, J. H. (2007). Deubiquitination of Chfr, a checkpoint protein, by USP7/HAUSP regulates its stability and activity. *Biochemical and Biophysical Research Communications*, *357*(3), 615–619. https://doi.org/10.1016/j.bbrc.2007.03.193
101. Olmos, Y., Brosens, J. J., & Lam, E. W.-F. . (2011). Interplay between SIRT proteins and tumour suppressor transcription factors in chemotherapeutic resistance of cancer. *Drug Resistance Updates*, *14*(1), 35–44. https://doi.org/10.1016/j.drup.2010.12.001
102. Ostertag, M. S., Messias, A. C., Sattler, M., & Popowicz, G. M. (2019). The Structure of the SPOP-Pdx1 Interface Reveals Insights into the Phosphorylation-Dependent Binding Regulation. *Structure*, *27*(2), 327-334.e3. https://doi.org/10.1016/j.str.2018.10.005
103. Pfoh, R., Lacdao, I. K., Georges, A. A., Capar, A., Zheng, H., Frappier, L., & Saridakis, V. (2015). Crystal Structure of USP7 Ubiquitin-like Domains with an ICP0 Peptide Reveals a Novel Mechanism Used by Viral and Cellular Proteins to Target USP7. *PLOS Pathogens*, *11*(6), e1004950. https://doi.org/10.1371/journal.ppat.1004950
104. Pickart, C. M. (2001). Mechanisms Underlying Ubiquitination. *Annual Review of Biochemistry*, *70*(1), 503–533. https://doi.org/10.1146/annurev.biochem.70.1.503
105. Pozhidaeva, A., & Bezsonova, I. (2019). USP7: Structure, substrate specificity, and inhibition. *DNA Repair*, *76*, 30–39. https://doi.org/10.1016/j.dnarep.2019.02.005
106. Priest, C., Prives, C., & Poyurovsky, M. V. (2010). Deconstructing nucleotide binding activity of the Mdm2 RING domain. *Nucleic Acids Research*, *38*(21), 7587–7598. https://doi.org/10.1093/nar/gkq669
107. Prostate Cancer Statistics: Canadian Cancer Society. (2019). Retrieved from www.cancer.ca website https://www.cancer.ca/en/cancer-information/cancer-type/prostate/statistics/?region=on
108. Qin, D., Wang, W., Lei, H., Luo, H., Cai, H., Tang, C., Wu, Y., Wang, Y., Jin, J., Xiao, W., Wang, T., Ma, C., Xu, H., Zhang, J., Gao, F., & Wu, Y.-L. (2016). CDDO-Me reveals USP7 as a novel target in ovarian cancer cells. *Oncotarget*, *7*(47), 77096–77109. https://doi.org/10.18632/oncotarget.12801
109. Rider, L., & Cramer, S. D. (2015). SPOP the mutation. *ELife*, *4*. https://doi.org/10.7554/elife.11760
110. Riley, J. F., Dao, T. P., & Castañeda, C. A. (2018). Cancer Mutations in SPOP Put a Stop to Its Inter-compartmental Hops. *Molecular Cell*, *72*(1), 1–3. https://doi.org/10.1016/j.molcel.2018.09.025
111. Ristic, G., Tsou, W.-L., & Todi, S. V. (2014). An optimal ubiquitin-proteasome pathway in the nervous system: the role of deubiquitinating enzymes. *Frontiers in Molecular Neuroscience*, *7*. https://doi.org/10.3389/fnmol.2014.00072
112. Rogina, B., & Helfand, S. L. (2004). Sir2 mediates longevity in the fly through a pathway related to calorie restriction. *Proceedings of the National Academy of Sciences of the United States of America*, *101*(45), 15998–16003. https://doi.org/10.1073/pnas.0404184101
113. Rougé, L., Bainbridge, Travis W., Kwok, M., Tong, R., Di Lello, P., Wertz, Ingrid E., Maurer, T., Ernst, James A., & Murray, J. (2016). Molecular Understanding of USP7 Substrate Recognition and C-Terminal Activation. *Structure*, *24*(8), 1335–1345. https://doi.org/10.1016/j.str.2016.05.020
114. Saridakis, V., Sheng, Y., Sarkari, F., Holowaty, M. N., Shire, K., Nguyen, T., Zhang, R. G., Liao, J., Lee, W., Edwards, A. M., Arrowsmith, C. H., & Frappier, L. (2005). Structure of the p53 Binding Domain of HAUSP/USP7 Bound to Epstein-Barr Nuclear Antigen 1. *Molecular Cell*, *18*(1), 25–36. https://doi.org/10.1016/j.molcel.2005.02.029
115. Sarkari, F., Wheaton, K., La Delfa, A., Mohamed, M., Shaikh, F., Khatun, R., Arrowsmith, C. H., Frappier, L., Saridakis, V., & Sheng, Y. (2013). Ubiquitin-specific Protease 7 Is a Regulator of Ubiquitin-conjugating Enzyme UbE2E1. *Journal of Biological Chemistry*, *288*(23), 16975–16985. https://doi.org/10.1074/jbc.m113.469262
116. Schrader, E. K., Harstad, K. G., & Matouschek, A. (2009). Targeting proteins for degradation. *Nature Chemical Biology*, *5*(11), 815–822. https://doi.org/10.1038/nchembio.250
117. Serrano, L., Martínez-Redondo, P., Marazuela-Duque, A., Vazquez, B. N., Dooley, S. J., Voigt, P., Beck, D. B., Kane-Goldsmith, N., Tong, Q., Rabanal, R. M., Fondevila, D., Muñoz, P., Krüger, M., Tischfield, J. A., & Vaquero, A. (2013). The tumor suppressor SirT2 regulates cell cycle progression and genome stability by modulating the mitotic deposition of H4K20 methylation. *Genes & Development*, *27*(6), 639–653. https://doi.org/10.1101/gad.211342.112

118. Shadfan, M., Lopez-Pajares, V., & Yuan, Z.-M. (2012). MDM2 and MDMX: Alone and together in regulation of p53. *Translational Cancer Research*, *1*(2), 88–89. https://www.ncbi.nlm.nih.gov/pmc/articles/PMC3448287/
119. Sheng, Y., Saridakis, V., Sarkari, F., Duan, S., Wu, T., Arrowsmith, C. H., & Frappier, L. (2006). Molecular recognition of p53 and MDM2 by USP7/HAUSP. *Nature Structural & Molecular Biology*, *13*(3), 285–291. https://doi.org/10.1038/nsmb1067
120. Song, M. S., Salmena, L., Carracedo, A., Egia, A., Lo-Coco, F., Teruya-Feldstein, J., & Pandolfi, P. P. (2008). The deubiquitinylation and localization of PTEN are regulated by a HAUSP–PML network. *Nature*, *455*(7214), 813–817. https://doi.org/10.1038/nature07290
121. Song, N., Cao, C., Tian, S., Long, M., & Liu, L. (2019). USP7 Deubiquitinates and Stabilizes SIRT1. *The Anatomical Record*, *303*(5), 1337–1345. https://doi.org/10.1002/ar.24252
122. Song, N., Cao, C., Tian, S., Long, M., & Liu, L. (2019). USP7 Deubiquitinates and Stabilizes SIRT1. *The Anatomical Record*, *303*(5), 1337–1345. https://doi.org/10.1002/ar.24252
123. Sun, L., & Chen, Z. J. (2004). The novel functions of ubiquitination in signaling. *Current Opinion in Cell Biology*, *16*(2), 119–126. https://doi.org/10.1016/j.ceb.2004.02.005
124. Takahashi, I., Kameoka, Y., & Hashimoto, K. (2002). MacroH2A1.2 binds the nuclear protein Spop. *Biochimica et Biophysica Acta (BBA) - Molecular Cell Research*, *1591*(1–3), 63–68. https://doi.org/10.1016/s0167-4889(02)00249-5
125. Theurillat, J.-P. P., Udeshi, N. D., Errington, W. J., Svinkina, T., Baca, S. C., Pop, M., Wild, P. J., Blattner, M., Groner, A. C., Rubin, M. A., Moch, H., Privé, G. G., Carr, S. A., & Garraway, L. A. (2014). Ubiquitylome analysis identifies dysregulation of effector substrates in SPOP-mutant prostate cancer. *Science*, *346*(6205), 85–89. https://doi.org/10.1126/science.1250255
126. Tissenbaum, H. A., & Guarente, L. (2001). Increased dosage of a sir-2 gene extends lifespan in Caenorhabditis elegans. *Nature*, *410*(6825), 227–230. https://doi.org/10.1038/35065638
127. Valles, G. J., Bezsonova, I., Woodgate, R., & Ashton, N. W. (2020). USP7 Is a Master Regulator of Genome Stability. *Frontiers in Cell and Developmental Biology*, *8*, 717. https://doi.org/10.3389/fcell.2020.00717
128. van der Horst, A., de Vries-Smits, A. M. M., Brenkman, A. B., van Triest, M. H., van den Broek, N., Colland, F., Maurice, M. M., & Burgering, B. M. T. (2006). FOXO4 transcriptional activity is regulated by monoubiquitination and USP7/HAUSP. *Nature Cell Biology*, *8*(10), 1064–1073. https://doi.org/10.1038/ncb1469
129. van Geersdaele, L. K., Stead, M. A., Harrison, C. M., Carr, S. B., Close, H. J., Rosbrook, G. O., Connell, S. D., & Wright, S. C. (2013). Structural basis of high-order oligomerization of the cullin-3 adaptor SPOP. *Acta Crystallographica Section D Biological Crystallography*, *69*(9), 1677–1684. https://doi.org/10.1107/s0907444913012687
130. Vaquero, A., Scher, M. B., Lee, D. H., Sutton, A., Cheng, H. L., Alt, F. W., Serrano, L., Sternglanz, R., & Reinberg, D. (2006). SirT2 is a histone deacetylase with preference for histone H4 Lys 16 during mitosis. *Genes & Development*, *20*(10), 1256–1261. https://doi.org/10.1101/gad.1412706
131. Wadosky, K. M., & Koochekpour, S. (2016). Molecular mechanisms underlying resistance to androgen deprivation therapy in prostate cancer. *Oncotarget*, *7*(39). https://doi.org/10.18632/oncotarget.10901
132. Wang, Q., Ma, S., Song, N., Li, X., Liu, L., Yang, S., Ding, X., Shan, L., Zhou, X., Su, D., Wang, Y., Zhang, Q., Liu, X., Yu, N., Zhang, K., Shang, Y., Yao, Z., & Shi, L. (2016). Stabilization of histone demethylase PHF8 by USP7 promotes breast carcinogenesis. *Journal of Clinical Investigation*, *126*(6), 2205–2220. https://doi.org/10.1172/jci85747
133. Wang, Z., Song, Y., Ye, M., Dai, X., Zhu, X., & Wei, W. (2020). The diverse roles of SPOP in prostate cancer and kidney cancer. *Nature Reviews Urology*, *17*(6), 339–350. https://doi.org/10.1038/s41585-020-0314-z
134. Wei, X., Fried, J., Li, Y., Hu, L., Gao, M., Zhang, S., & Xu, B. (2018). Functional roles of Speckle-Type Poz (SPOP) Protein in Genomic stability. *Journal of Cancer*, *9*(18), 3257–3262. https://doi.org/10.7150/jca.25930
135. Witting, K. F., Mulder, M., & Ovaa, H. (2017). Advancing our Understanding of Ubiquitination Using the Ub-Toolkit. *Journal of molecular biology*, *429*(22), 3388–3394. https://doi.org/10.1016/j.jmb.2017.04.002

136. Wu, F., Dai, X., Gan, W., Wan, L., Li, M., Mitsiades, N., Wei, W., Ding, Q., & Zhang, J. (2017). Prostate cancer-associated mutation in SPOP impairs its ability to target Cdc20 for poly-ubiquitination and degradation. *Cancer Letters*, *385*, 207–214. https://doi.org/10.1016/j.canlet.2016.10.021
137. Xiao, Z.-X., Chen, J., Levine, A. J., Modjtahedi, N., Xing, J., Sellers, W. R., & Livingston, D. M. (1995). Interaction between the retinoblastoma protein and the oncoprotein MDM2. *Nature*, *375*(6533), 694–698. https://doi.org/10.1038/375694a0
138. Ye, Y., & Rape, M. (2009). Building ubiquitin chains: E2 enzymes at work. *Nature Reviews Molecular Cell Biology*, *10*(11), 755–764. https://doi.org/10.1038/nrm2780
139. Yi, L., Cui, Y., Xu, Q., & Jiang, Y. (2016). Stabilization of LSD1 by deubiquitinating enzyme USP7 promotes glioblastoma cell tumorigenesis and metastasis through suppression of the p53 signaling pathway. *Oncology Reports*, *36*(5), 2935–2945. https://doi.org/10.3892/or.2016.5099
140. Zhang, C., Lu, J., Zhang, Q.-W., Zhao, W., Guo, J.-H., Liu, S.-L., Wu, Y.-L., Jiang, B., & Gao, F.-H. (2016). USP7 promotes cell proliferation through the stabilization of Ki-67 protein in non-small cell lung cancer cells. *The International Journal of Biochemistry & Cell Biology*, *79*, 209–221. https://doi.org/10.1016/j.biocel.2016.08.025
141. Zhang, P., Gao, K., Tang, Y., Jin, X., An, J., Yu, H., Wang, H., Zhang, Y., Wang, D., Huang, H., Yu, L., & Wang, C. (2014). Destruction of DDIT3/CHOP Protein by Wild-Type SPOP but Not Prostate Cancer-Associated Mutants. *Human Mutation*, *35*(9), 1142–1151. https://doi.org/10.1002/humu.22614
142. Zhang, P., Wang, D., Zhao, Y., Ren, S., Gao, K., Ye, Z., Wang, S., Pan, C.-W., Zhu, Y., Yan, Y., Yang, Y., Wu, D., He, Y., Zhang, J., Lu, D., Liu, X., Yu, L., Zhao, S., Li, Y., & Lin, D. (2017). Intrinsic BET inhibitor resistance in SPOP-mutated prostate cancer is mediated by BET protein stabilization and AKT–mTORC1 activation. *Nature Medicine*, *23*(9), 1055–1062. https://doi.org/10.1038/nm.4379
143. Zhang, X., Azhar, G., & Wei, J. Y. (2017). SIRT2 gene has a classic SRE element, is a downstream target of serum response factor and is likely activated during serum stimulation. *PloS One*, *12*(12), e0190011. https://doi.org/10.1371/journal.pone.0190011
144. Zhang, Z.-M., Rothbart, S. B., Allison, D. F., Cai, Q., Harrison, J. S., Li, L., Wang, Y., Strahl, B. D., Wang, G. G., & Song, J. (2015). An Allosteric Interaction Links USP7 to Deubiquitination and Chromatin Targeting of UHRF1. *Cell Reports*, *12*(9), 1400–1406. https://doi.org/10.1016/j.celrep.2015.07.046
145. Zhao, Y., Yu, H., & Hu, W. (2014). The regulation of MDM2 oncogene and its impact on human cancers. *Acta Biochimica et Biophysica Sinica*, *46*(3), 180–189. https://doi.org/10.1093/abbs/gmt147
146. Zheng, Q., Li, J., & Wang, X. (2009). Interplay between the ubiquitin-proteasome system and autophagy in proteinopathies. *International Journal of Physiology, Pathophysiology and Pharmacology*, *1*(2), 127–142. Retrieved from https://www.ncbi.nlm.nih.gov/pmc/articles/PMC2856956/
147. Zhuang, M., Calabrese, M. F., Liu, J., Waddell, M. B., Nourse, A., Hammel, M., Miller, D. J., Walden, H., Duda, D. M., Seyedin, S. N., Hoggard, T., Harper, J. W., White, K. P., & Schulman, B. A. (2009). Structures of SPOP-Substrate Complexes: Insights into Molecular Architectures of BTB-Cul3 Ubiquitin Ligases. *Molecular Cell*, *36*(1), 39–50. https://doi.org/10.1016/j.molcel.2009.09.022